Design of Antioxidant Encapsulated Polymeric Micro- or Nano-drug Delivery Systems for Ischemic Stroke Treatment

---

A

Thesis

Presented to

the faculty of the School of Engineering and Applied Science

University of Virginia

---

in partial fulfillment

of the requirements for the degree

Master of Science

by

Zhiqi Zhang

August 2022

APPROVAL SHEET

This

Thesis

is submitted in partial fulfillment of the requirements
for the degree of

Master of Science

Author: Zhiqi Zhang

This Thesis has been read and approved by the examing committee:

Advisor: Kyle J. Lampe

Advisor:

Committee Member: Rachel A. Letteri

Committee Member: Kyle J. Lampe

Committee Member: Nina J. Solenski

Committee Member:

Committee Member:

Committee Member:

Accepted for the School of Engineering and Applied Science:

Jennifer L. West, School of Engineering and Applied Science

August 2022

Abstract

Ischemic stroke is a leading cause of adult death and disability worldwide. However, current ischemic stroke drug treatments remain inadequate. Due to the severity of the ischemic stroke, there is an urgent need to develop effective drug delivery systems with better temporal and spatial controls of drug releases. We propose delivering antioxidant drugs, with temporal and spatial controls, via polymeric microcarriers for directly injection to the stroke lesion and via polymeric nanocarriers for an easier and less invasive intravenously injection. The delivered antioxidants that released from the polymeric micro/nanoparticles will scavenge reactive oxygen species (ROS) generated after ischemic stroke. In the thesis, we discuss the loadings and release profiles of antioxidants encapsulated polymeric microparticles (MPs) (single-wall and core-shell (in theory, the shell phase could act as a diffusive barrier to avoid the burst release of the drug encapsulated in the core phase and to support the sustained release) MPs) and dynamic light scattering (DLS) sizes of single-wall MPs sizes. We also focus on the antioxidant encapsulated polymeric nanoparticles (NPs) in this thesis. NPs were fabricated via nanoprecipitation and the sizes were measured by DLS. We control nanoparticle size via polymer concentration and molecular weight with our smallest untargeted antioxidant nanoparticles having a 106.52+/- 0.40 nm diameter. This size provides the potential for surface modification while maintaining a ~200nm target size limit. The reconstituted NPs with preserved sizes after freeze-drying steps could be achieved by adding appropriate concentration of sucrose, a cryo/lyoprotectant, before lyophilizations.

Acknowledgement

First of all, thanks for my advisor, Dr. Kyle Lampe, for all the supports during my master journey. Years 2020 and 2021 had been my though years. Without your supports, both technically and emotionally, I couldn't resume my hopes for the future. Your enthusiasm lightens up my life and your understanding makes me feel warm inside.

I would like to thank Dr. Rachel Letteri and Dr. Nina Solenski for being my thesis committee and the help your generous help during my master journey. I would like to thank past and present graduate research colleagues, Nicholas Murphy, Lauren Russell, Edi Meco, James Tang, Deniz Unal, Rachel Mazur, Jonathan Florian, Nadeesani Sirinayake and Aditi Gourishakar, for the help and support during my master time. I would say thank to my undergraduate mentees, Giberto Hermandez and Ivy Wu, and I will never forget the time spending with you.

My family and my friends, Can Liu and Chenyang Shang, thanks for your emotional support and willing to spend your time listening to my troubles and help me through every difficulties in my life.

Table of Contents

Introduction

Ischemic stroke is a severe disease that arise from the blockage of brain blood vessel and is a leading cause of worldwide adult death and disability. Ischemic stroke could cause people death every 3.5 minutes in the United States [1]. Within a few minutes of ischemic stroke, loss of blood supply can lead to permanent impairment of brain tissue [2]. The levels of ROS rapidly increase immediately after ischemic stroke, which results in the first burst of ROS generation and damage to DNA, proteins, and lipids. Additionally, when the blood supply returns to the tissue, a second burst of ROS generation occurs, which leads to reperfusion injury. These two rapid ROS generations overwhelm the antioxidant defenses in the brain and cause cell injury and death in the central nervous system (CNS) [3]. Thus, antioxidant drug delivery has the potential for ischemic stroke treatment.

In Chapter 1, we are introducing a core-shell micro-drug delivery system, encapsulating a hydrophobic antioxidant Bpin-disulfide prodrug-*N*-acetyl cysteine (BDP-NAC) in the core phase, for the sustained release of the drug. Add a shell layer could help to prevent the burst release of the core-encapsulated drug. Chapter 2 discuss an antioxidant N-acetylcysteine (NAC) micro-drug delivery system, using a modified double emulsion (water-in-oil-in-water) fabrication method, to improve loadings and characterize the properties of MPs for further studies (e.g. animal studies). Chapter 3 introduce the concept of nano-drug delivery system and discuss their advantages, potential challenges, common fabrication methods. This chapter also discuss brain drug delivery, ischemic stroke pathophysiology, up-to-date FDA-approved ischemic stroke treatments and their limitations, blood-brain barrier (BBB) crossing approaches, and stimuli-responsive polymeric nanocarriers. In Chapter 4, we are interested in developing an antioxidant BDP-NAC nano-drug delivery system, with intravenously route application, that could cross the BBB and target to the stroke affected site with targeting ligands surface modifications.

Chapter 1

Design of an antioxidant core-shell polymeric micro-drug delivery system for ischemic stroke treatment

1.1 Introduction

Ischemic stroke is a leading cause of adult death and disability worldwide that arises from the blockage of the blood vessel in the brain. Within a few minutes, the brain cells begin to die due to oxygen deprivation, resulting in permanent impairment or death [2]. Every 3.5 minutes, someone dies from stroke in the United States [1]. ROS are elevated after ischemic stroke [3]. The rapid increases of ROS after ischemic stroke produces oxidative stress and overwhelm the antioxidant defenses in the brain, which can lead cell apoptosis and cell death in the CNS, especially oligodendrocyte progenitor cells (OPCs). NAC is a small hydrophilic molecule that has both direct and indirect antioxidant properties. It has a free thiol group that can direct react with ROS. Also, NAC is a precursor of body's master antioxidant glutathione (GSH), which has future indirect antioxidant effect [4]. BDP-NAC, a small hydrophobic NAC prodrug, has a reduced burst release and a longer release time, more reduction potential compared to traditional NAC, and has antioxidant activity only under oxidative stress by generating persulfide NAC-SSH from BDP-NAC [5]. Thus, it's promising to design a drug delivery system that encapsulates with the antioxidant prodrug BDP-NAC, to relieve the OPCs from oxidative stress during the progression of ischemic stroke.

In this work, we are interested in developing a micro-drug delivery system that can be directly injected into the stroke lesion with controlled release. Thus, we developed a core-shell micro-drug delivery system encapsulated BDP-NAC using poly(lactic-co-glycolic acid) (PLGA) and poly-L-lactic acid (PLLA). Both PLGA and PLLA are FDA-approved biodegradable polymers that have highly controlled release and consistent degradation properties [6,7]. The shell phase of the core-shell drug delivery system can provide the diffusive barrier to the core-encapsulated drug, which decrease the burst release and increase the duration of release.

1.2 Materials and methods

1.2.1 BDP-NAC loaded core-shell microparticle fabrication

BDP-NAC fluorescent core-shell microparticles were fabricated via oil-in-oil-in-water double emulsion. 50:50 lactide: glycolide (50:50) 1.15 inherent viscosity (IV), 50:50 0.59IV PLGA and 100:0 1.16IV PLLA polymers were used during core-shell microparticles fabrication. 50:50 fluorescent PLGA-Fluorescein (FL) (Mn 20,000-40,000 Da) and PLLA-FPR648 (Mw~40,000Da) were the fluorescent polymers that used in core-shell microparticles fabrication and those fluorescent polymers are 1 in 25 dilution with regular PLGA/PLLA polymers. Briefly, PLLA was dissolved in dichloromethane (DCM) at a concentration of 200mg/ml in a glass test tube (0.5ml DCM for "1:1 PLGA: PLLA, 20 wt% PLGA" and "2:1 PLGA: PLLA, 20 wt% PLGA, 300rpm"; 0.4ml DCM for "2:1 PLGA: PLLA, 10 wt% PLGA, 500rpm"; 0.25ml DCM for "2:1 PLGA: PLLA, 20 wt% PLGA, 900rpm") . PLGA was dissolved in appropriate volume of DCM based on the PLGA:PLLA ratio in another glass test tube at desired concentration (e.g. 200mg PLLA/ml DCM for 20 wt% PLLA). 10wt% BDP-NAC was then dissolved in PLLA oil phase by sonication. Then, transfer PLGA solution to PLLA phase with Pasteur pipette, sonicate 10 sec twice with 10-sec break on ice at 90% amplitude to form O/O emulsion. Next, add 1ml 0.5% polyvinyl alcohol (PVA) /100mg polymer to the O/O emulsion, slowly alongside the wall of the tube. Sonicate 20 sec twice with 10-sec break on ice at 90% amplitude to form O/O/W emulsion and pour the solution into stirring 50ml 0.5% PVA /100mg polymer. Stir at 900rpm (or 500rpm, or 300rpm) for four hours for solvent evaporation. Next, collect particle suspension into 50ml conical centrifuge tubes and centrifuge 5 min at 10000rpm and 4°C. Then, wash the particles by discarding the supernatant and resuspending the particles with 40ml deionized (DI) water by vortexing. Centrifuge again at 10000rpm and 4°C for 5 min. Repeat this wash step one more time. Discard the supernatant and add 10ml of DI water to resuspend the particles via vortexing. Freeze the particles at -80°C overnight and then lyophilize for 3 days. The dry particles were stored at -20°C.

1.2.2 BDP-NAC load measurement

First, weight 2mg MPs and add 1ml of DCM to the MPs. Incubate at 37°C to fully dissolve the polymers. Prepare BDP-NAC in DMSO standards that range from 0 to 1mg BDP-NAP/ml DCM. Measure the load, with a UV-transparent 96-well plate, at absorbance of

250nm on a plate reader. The encapsulation efficiency of BDP-NAC is defined as the percentage of actual load of BDP-NAC relative to the theoretical load of BDP-NAC.

1.2.3 BDP-NAC release study assessment

To get the BDP-NAC release profiles over time, 10mg/ml of particles were suspended in phosphate-buffered saline (PBS) solution in Eppendorf tubes and incubated at 37°C. At desired time, centrifuge the particle suspensions at 10000rpm for 10mins. The supernatants were transferred to new Eppendorf tubes and stored at -20°C. Fresh PBS solutions were added to particles at the concentration of 10mg/ml to resuspend the particles. Then, the particle suspensions were incubated at 37°C. The release of BDP-NAC over time can be measured at absorbance of 250nm on a plate reader with a UV-transparent 96-well plate.

1.2.3 Statistical analysis

All errors bars are the standard error of the mean. Unpaired, two-tailed t-test was to determine the statistical significance between two conditions.

1.3 Results and Discussion

1.3.1 Loads and release profiles of BDP-NAC Encapsulated Fluorescent PLGA/PLLA Core-shell MPs

Five batches of microparticles with different PLGA: PLLA ratios, wt% PLGA, solvent evaporation stirring rates were prepared as shown in **Figure 1-1** and **Figure 1-2**. BDP-NAC was encapsulated in PLLA phases. The theoretical load of BDP-NAC 100μg/mg. Thus, the encapsulation efficiencies (or loads (ug/ml)) of BDP-NAC for "0:1 PLGA:PLLA, 20 wt% PLGA, 900rpm", "1:1 PLGA:PLLA, 20 wt% PLGA, 900rpm", "2:1 PLGA:PLLA, 20 wt% PLGA, 900rpm", "2:1 PLGA:PLLA, 10 wt% PLGA, 500rpm" and "2:1 PLGA:PLLA, 20 wt% PLGA, 300rpm" MPs are 34.76 +/- 1.94 % (or 34.76 +/- 1.94 ug/mg), 44.52 +/- 1.70 % (or 44.52 +/- 1.70 ug/mg), 89.01 +/- 2.32 % (or 89.01 +/- 2.32 ug/mg), 64.24 +/- 6.23 % (or 64.24 +/- 6.23 ug/mg) and 44.27 +/- 2.05 % (or 44.27 +/- 2.05 ug/mg), respectively **(Figure 1-1)**. At day 7, the totals of 43.85 +/- 3.37 %, 63.59 +/- 3.41 %, 18.08 +/- 1.29 %, 23.17 +/- 1.74 % and 42.30 +/- 2.27 % of BDP-NAC were released from "0:1 PLGA:PLLA, 20 wt% PLGA, 900rpm", "1:1 PLGA:PLLA, 20 wt% PLGA, 900rpm", "2:1 PLGA:PLLA, 20 wt% PLGA, 900rpm", "2:1

PLGA:PLLA, 10 wt% PLGA, 500rpm" and "2:1 PLGA:PLLA, 20 wt% PLGA, 300rpm" MPs, respectively **(Figure 1-2)**.

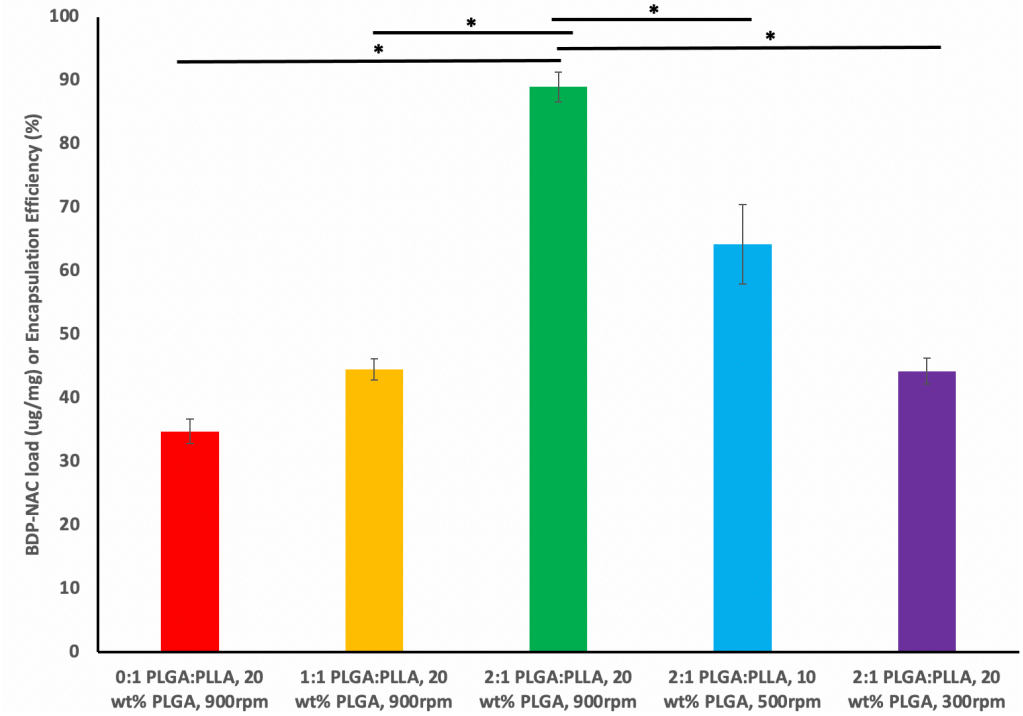

Figure 1-1. Loads or Encapsulation Efficiencies of BDP-NAC Encapsulated Core-shell MPs. 900rpm, 500rpm and 300rpm refer to the stirring rates during solvent evaporation step of MPs fabrication. * represents $p<0.05$ from unpaired, two-tail t-test.

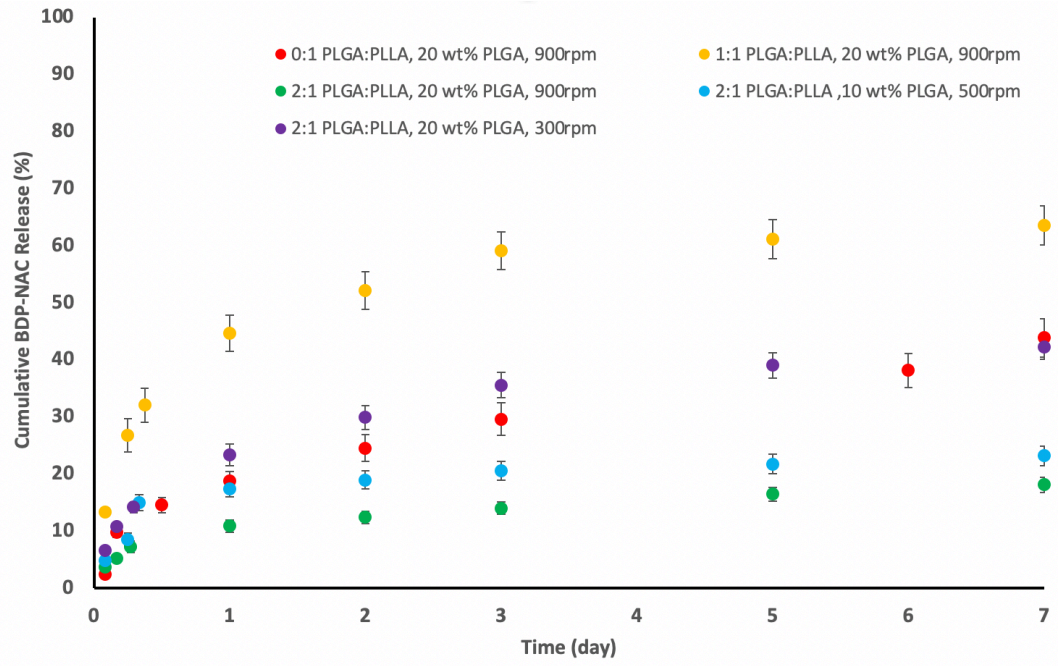

Figure 1-2. Release profiles of BDP-NAC Encapsulated Core-shell MPs. 900rpm, 500rpm and 300rpm refer to the stirring rates during solvent evaporation step of MPs fabrication.

The goal for this core-shell MPs work is to encapsulate BDP-NAC in the core phase to have a sustained release of BDP-NAC. PLGA is more hydrophilic than PLLA due to the glycolide presented in PLGA, in theory, PLLA will move to core phase and BDP-NAC is hydrophobic so it likes the PLLA phase. Thus, BDP-NAC in the PLLA core phase will release slower than single-wall MPs. However, if in practice the PLLA ended up in the shell phase with various reasons (e.g. the formation of PLLL core/PLGA shell structure hindered by the high viscosity of polymer concentrations), the release rate of BDP-NAC will be faster than single-wall MPs. Thus, the release profiles of BDP-NAC core-shell MPs is highly dependent on their structures. Previous work from our lab done by Nicholas P. Murphy, Ph.D. shows the structures of 1:1 PLGA: PLLA and 2:1 PLGA: PLLA MPs from confocal images. From **Figure 1-2**, "1:1 PLGA: PLLA, 20 wt% PLGA, 900 rpm" MPs had the highest burst release and cumulative release at 7 day in percentage compared to other core-shell and single wall MPs, which was consistent with their structures that some showed incomplete encapsulation and some other had PLLA shells (Nicholas P. Murphy, Ph.D.). Moreover, their sizes/structures are heterogenous (Nicholas P. Murphy, Ph.D.), which make them unqualified for the controlled releases purposes. The "2:1 PLGA: PLLA, 20 wt% PLGA, 300rpm" showed a middle cumulative release rate at 7 day and its release profile is similar as the "0:1 PLGA:PLLA, 20 wt% PLGA, 900rpm" (single-wall) MPs. The "2:1 PLGA: PLLA, 20 wt% PLGA, 300rpm" MPs from confocal images showed PLLA shells and some PLLA clusters disturbed across the PLGA (Nicholas P. Murphy, Ph.D.). The presence of PLLA shells (favor faster release than single-wall MPs) and PLLA clusters in PLGA (favor slower release than single-wall MPs) may balance out, which resulted in a similar effect to the release profile as the single-wall MPs. The "2:1 PLGA: PLLA, 20 wt% PLGA, 900rpm" MPs had the slowest cumulative release rate at 7 day, and from **Figure 1-1**, those MPs also had the highest encapsulation efficiency at a significance level of 0.05. Their slowest release profile consistent with their structures that some of them (with larger size, the sizes of MPs are heterogenous) had PLLA clusters in PLGA, without a PLLA shell (Nicholas P. Murphy, Ph.D.). The MPs that contribute to the slowest release profile are too large (>25μm, Nicholas P. Murphy, Ph.D.) that they are not suitable for injection and cell studies. From **Figure 1-1** and **Figure 1-2**, "2:1 PLGA: PLLA, 10 wt% PLGA, 500 rpm" MPs had similar release profile as the "2:1 PLGA: PLLA, 20 wt% PLGA, 900rpm" MPs and the second highest encapsulation efficiency. Lowering the wt% of PLGA decreases its viscosity, which could drive the formation of PLLA core/PLGA

shell structure. The slow release of the "2:1 PLGA: PLLA, 10 wt% PLGA, 500 rpm" MPs consistent with their very thin PLLA shell with PLLA clusters in PLGA structures (Nicholas P. Murphy, Ph.D.). Thus, their slow release and high encapsulation efficiency, in conjugation with their homogenous structure and relatively small size (Nicholas P. Murphy, Ph.D.), the "2:1 PLGA: PLLA, 10 wt% PLGA, 500 rpm" is most ideal among all other MPs in **Figure 1-1** and **Figure 1-2.**

1.4 Conclusions

In summary, we could get ideal slow-release of BDP-NAC and high encapsulation efficiency with 2:1 PLGA: PLLA ratio, low wt% in PLGA, and medium level of solvent evaporation stirring rate. The effects of solvent evaporation stirring rate to MPs structure formation is unclear since the structure should form during the O/O/W emulsion step, which is before the step of solvent evaporation. However, there are some invasiveness of direct injection of MPs to the stroke lesion of the patients especially their brain functions were already compromised. Thus, we proposed to design an antioxidant nano-drug delivery system for intravenously injection to minimize invasiveness (Chapter 4).

1.5 Acknowledgements

We gratefully acknowledge financial support from NIH grant R21 EB026723. We thankfully acknowledge Nicholas P. Murphy for generating ideas, performing experiments, and collecting data, Xhesika Sula for assisting in performing experiments and collecting data.

1.6 References

1. CDC. Stroke Facts | cdc.gov. Centers for Disease Control and Prevention. Published April 5, 2022. Accessed June 27, 2022. https://www.cdc.gov/stroke/facts.htm

2. Khan M, Sekhon B, Jatana M, Giri S, Gilg AG, Sekhon C, Singh I, Singh AK. Administration of N-acetylcysteine after focal cerebral ischemia protects brain and reduces inflammation in a rat model of experimental stroke. *J Neurosci Res*. 2004;76(4):519-527. doi:10.1002/jnr.20087

3. Rodrigo R, Fernandez-Gajardo R, Gutierrez R, Matamala J, Carrasco R, Miranda-Merchak A, Feuerhake W. Oxidative Stress and Pathophysiology of Ischemic Stroke: Novel Therapeutic Opportunities. *CNS Neurol Disord - Drug Targets*. 2013;12(5):698-714. doi:10.2174/18715273113120500 15

4. Sun SY. N-acetylcysteine, reactive oxygen species and beyond. *Cancer Biol Ther*. 2010;9(2):109-110.

5. Powell CR, Dillon KM, Wang Y, Carrazzone RJ, Matson JB. A Persulfide Donor Responsive to Reactive Oxygen Species: Insights into Reactivity and Therapeutic Potential. *Angew Chem Int Ed*. 2018;57(21):6324-6328. doi:10.1002/anie.201803087

6. Makadia HK, Siegel SJ. Poly Lactic-co-Glycolic Acid (PLGA) as Biodegradable Controlled Drug Delivery Carrier. *Polymers*. 2011;3(3):1377-1397. doi:10.3390/polym3031377

7. Rotunda AM, Narins RS. Poly-L-lactic acid: a new dimension in soft tissue augmentation. *Dermatol Ther*. 2006;19(3):151-158. doi:10.1111/j.1529-8019.2006.00069.x

Chapter 2

Design of an antioxidant polymeric micro-drug delivery system for ischemic stroke treatment

2.1 Introduction

Ischemic stroke, a disease due to the brain blood vessel blockage, is a leading cause of adult death and disability worldwide and could cause irreversible damage of the brain tissue only a few minutes after ischemic stroke [1]. The elevated level of ROS after ischemic stroke evoke oxidative stress and defeat the brain's native antioxidant defenses, which could injury the cells in CNS and cause necrosis [2]. NAC, a small and cheap hydrophilic molecule with a free thiol group, could scavenge the ROS efficiently. NAC is also a GSH (our native body antioxidant) precursor, which add another layer of antioxidant ability [3].

However, the hydrophilicity of NAC makes it hard to encapsulate and lead to low load. In this work, we are focused on developing a NAC loaded microcarrier with the FDA-approved biodegradable, controllable polymer PLGA for direct injection to the ischemic stroke area through a modified version of double emulsion technique [4]. From this modified fabrication technique, NAC is also added to the outer water phase, the solvent evaporation solution the and the washing solution, which protect the NAC loss due to the diffusion by minimizing the concentration gradients.

2.2 Materials and methods

2.2.1 NAC loaded microparticle fabrication

A modified version of water-in-oil-in-water double emulsion were used to fabricate NAC microparticles (MPs) [5] (**Figure 2-1**). Four different PLGA formulations with varied lactide: glycolide ratio and inherent viscosity (IV), 50:50 lactide: glycolide (50:50) 0.55-0.75 IV PLGA, 50:50 0.95-1.20IV PLGA, 85:15 0.66IV PLGA and 100:0 0.67IV PLLA polymers were used to fabricate MPs and to further assess the MPs properties with varied PLGA formulations . First, dissolve PLGA at a concertation of 150mg/ml in 2ml of DCM in a glass test tube. Next, prepare NAC solution in DI water at 100mg/ml and add 100ul to the PLGA

solution in dropwise. Sonicate 10 sec on ice at 90% amplitude twice, with a 10-break in between. W/O emulsion is formed. Then, slowly add 3ml of 3.33% NAC/ml 1% PVA to the W/O emulsion along the wall. To form W/O/W emulsion between W/O emulsion and outer aqueous phase, sonicate the solution 10 sec twice on ice, with a 10-sec break, at 90% amplitude. Pour W/O/W emulsion into 75ml of stirring 5% NAC/ml 0.3% PVA solution. Stir 4 hours at 300rpm for solvent evaporation. After solvent evaporation, collect the particles and centrifuge at 10000rpm for 5 mins at 4°C. Discard the supernatant and add 30ml of 2.5% NAC/ml DI water to resuspend the MPs. Centrifuge again for 5 mins at 10000rpm and 4°C. Repeat one more time of this wash step. Dispose of the supernatant. 10ml DI water was then added to resuspend the MPs. Put the MPs suspension at -80°C overnight for freezing. Then, lyophilize the MPs for 3 days. Store the lyophilized MPs at -20°C. A empty version of MP was made without adding NAC to inner and outer water phase, solvent evaporation stirring solution and washing solution.

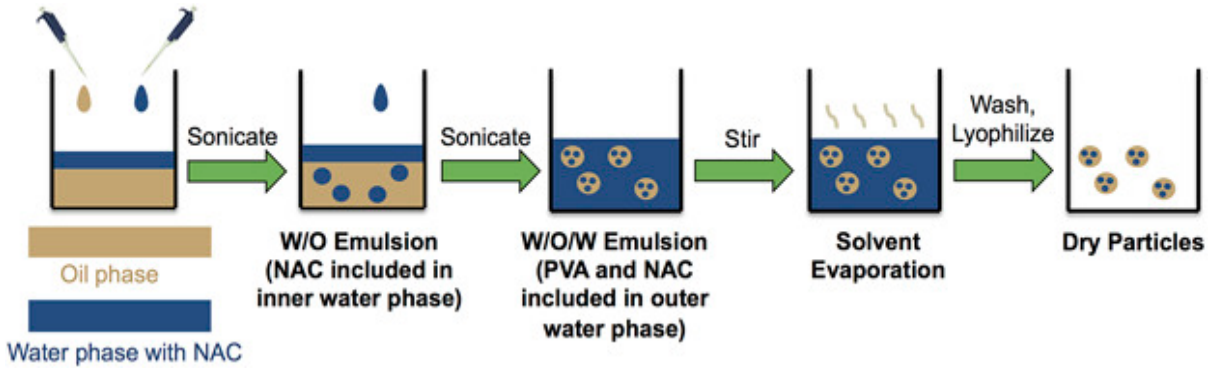

Figure 2-1. Schematic of NAC PLGA MPs fabrication via a modified water-in-oil-in-water double emulsion method. Reproduced from N.P. Murphy, etc. *Biotechnol Bioeng*. 2018 Jan;115(1):246-256.

2.2.2 Prepare the load and release samples

To prepare the load samples, weight 5mg MPs to glass vials in triplicate. Add 1ml of DCM to each vial and stir for 30 mins at 300rpm with closed lids. Then, add 2ml of 1mM ethylenediaminetetraacetic acid (EDTA)/ml phosphate buffered saline (PBS) solution to each vial, stir for 15 mins at 300 rpm. The introduction of EDTA is to prevent the metal-catalyzed oxidation of NAC thiol groups. Two phases become separated. The top phase is aqueous phase, which contains the NAC from liquid-liquid extraction, and the bottom phase is

organic phase. Take 1ml of aqueous phase to Eppendorf tube for the NAC load measurement.

To get the release samples, weight 10mg MPs to each Eppendorf tube and add 1ml of 1mM EDTA/PBS solution to them. Mix the MPs well and incubate the samples at 37°C. At each desired time point, centrifuge the samples for 10mins at 10000rpm. Prepare new Eppendorf tubes and transfer the supernatants to them. Store the release samples at -20°C. Add 1ml of 1mM EDTA/PBS to the MPs, resuspend them well, and continue incubating at 37°C.

2.2.3 NAC content measurement of load and releases samples

To measure the NAC content that contained in load and release samples, first prepare the reagent solution by dissolving 4mg/ml 5,5'-Dithiobis(2-nitrobenzoic acid) (DNTB) (Ellman's reagent), together with 0.1 M sodium phosphate monobasic and 1mM EDTA, in DI water. Adjust the pH to ~8. Then prepare the NAC standard from 0 -1000 μM in 1mM EDTA/PBS solution. Dilute the samples if necessary. Then, the NAC loads and releases could be measured at absorbance of 412nm with a clear 96-well plate on plate reader.

2.2.4 pH measurement of MPs

The pHs of both NAC and empty MPs were measured with a pH meter. Calibrate the pH probe with pH calibration solutions before measuring the samples.

2.2.5 NAC MPs size measurement

NAC MPs size distribution were measured on a Zetasizer Ultra. Prepare the samples at 2mg/ml concentration in DI water (without buffers). The temperatures setting for the size distribution measurement is 25 °C. For the measurement, set the dispersant viscosity at 0.8872 cp and the dispersant refractive index at 1.33, respectively.

2.2.6 Statistical analysis

All errors bars are the standard error of the mean. To determine the statistical significance among more than two groups, one-way or two-way ANOVA test was applied.

2.3 Results and Discussion

2.3.1 NAC Encapsulated MPs loads and release profiles

Figure 2-2 and **Figure 2-3** shows the encapsulation efficiencies and release profiles of "50:50 0.55-0.75IV, 100mg/ml", "50:50 0.95-1.20IV, 100mg/ml", "85:15 0.66IV, 100mg/ml" and "100:0 0.67IV, 100mg/ml" NAC MPs, respectively. The encapsulation efficiencies for "50:50 0.55-0.75IV, 100mg/ml", "50:50 0.95-1.20IV, 100mg/ml", "85:15 0.66IV, 100mg/ml" and "100:0 0.67IV, 100mg/ml" MPs are 117.11 +/- 18.94 %, 133.73 +/- 42.07 %, 107.23 +/- 9.60 %, and 133.49 +/- 5.03 %, respectively, which are at a similar level regardless the PLGA formulations **(Figure 2-2)**. However, it is worth to noted that even though the variances of measured loadings are decent during one single measurement (e.g, prepare loads samples for all batches and measure them together on day 1), the variance are large between different repetitions (e.g. repeat the load preparation and measure again on day 2, the results deviate from day 1). Thus, other loading samples preparation and/or measurement methods, for example, acid and base PLGA MPs degradation and/or high-performance liquid chromatography (HPLC), need to apply to affirm the load results. Moreover, the efficiency of NAC extraction from organic phase to aqueous phase during liquid-liquid extraction process need to be further assessed, since the inefficiency of NAC extraction could contribute to loading results inconsistency.

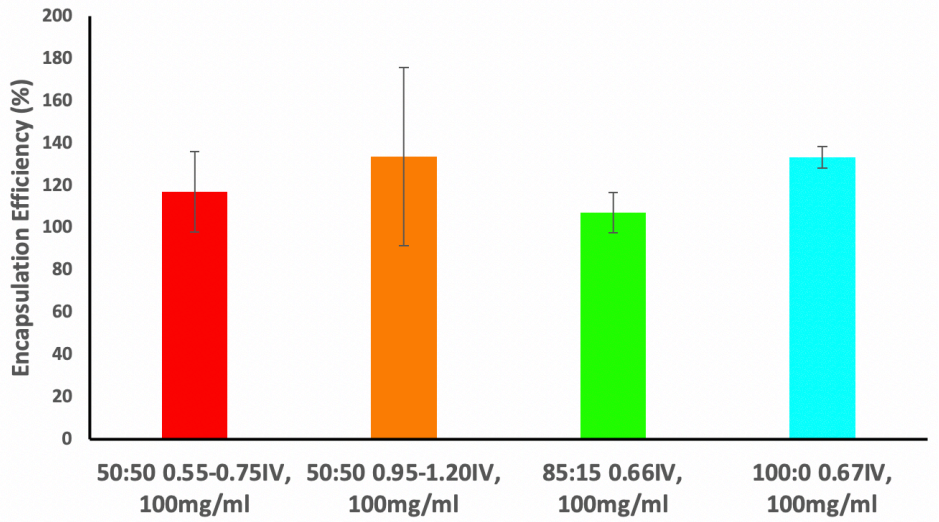

Figure 2-2. Encapsulation Efficiencies of NAC Encapsulated MPs.

From **Figure 2-3**, the cumulative releases at day 36 is 36.32 +/- 4.08 %, 41.21 +/- 7.22 %, 65.77 +/- 6.49 %, and 49.08 +/- 4.44 % of loadings for "50:50 0.55-0.75IV, 100mg/ml", "50:50 0.95-1.20IV, 100mg/ml", "85:15 0.66IV, 100mg/ml" and "100:0 0.67IV, 100mg/ml" MPs, respectively. However, there is almost no NAC release that could be measured after day 1

(even stop detecting NAC in hours (e.g., couldn't detect NAC after 4 hours and 7 hours for "50:50 0.55-0.75IV, 100mg/ml" and "50:50 0.95-1.20IV, 100mg/ml" MPs, respectively)). Thus, there are gaps between the NAC loadings and detectable NAC releases which may be due to the loss of EDTA activity. There could be trace amounts of heavy metal ions presented in PBS, and the EDTA could protect the thiol groups of NAC from metal-catalyzed oxidation. Since the loads measurements were done immediate after load samples preparation, we may neglect the effect of EDTA activity loss (not true for release samples because of the time span of each release study). Thus, another around of MPs fabrications with new EDTA is needed to assess the NAC releases from MPs.

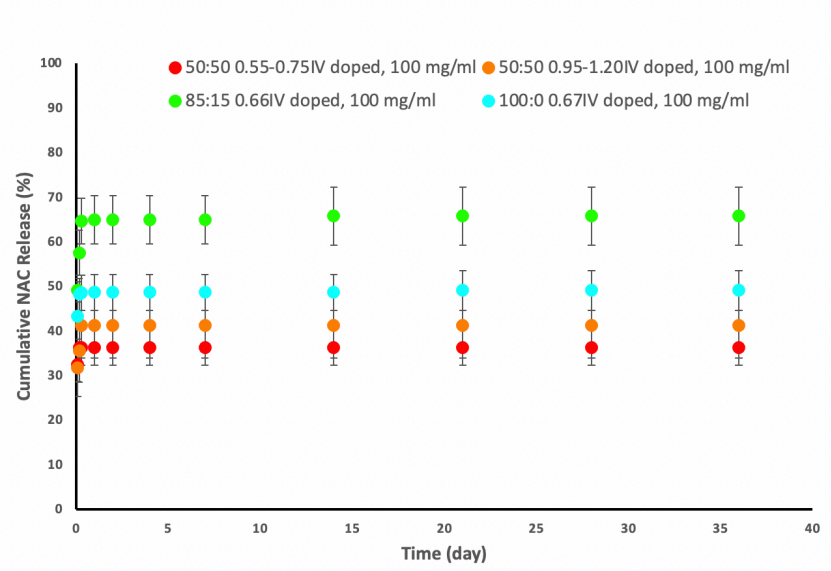

Figure 2-3. Release profiles of NAC Encapsulated MPs

2.3.2. pHs of NAC and empty MPs

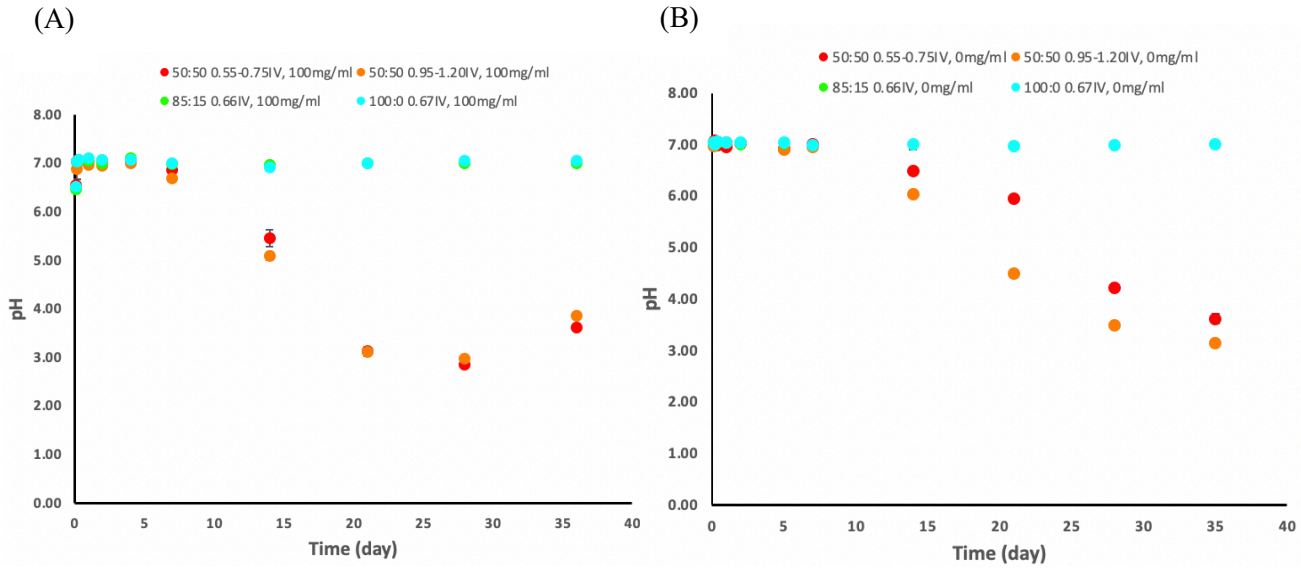

Figure 2-4. pHs for NAC and empty MPs (A) pHs of NAC MPs over 36 days. **(B)** pHs of empty MPs over 36 days

Figure 2-4 shows the pHs of NAC MPs (**Figure 2-4A**) and empty MPs (**Figure 2-4B**). Both NAC MPs with 50: 50 lactide (L): glycolide (G) ratio became acidic at and after day 7, and for the two empty (label as "PLGA formulation, 0mg/ml") MPs with 50: 50 L:G ratios, they became acidic at day 14. For all MPs with 85: 15 L:G ratio and 100: 0 L:G ratio, they stayed at ~7 for 36 days. This lowering in pH in 50:50 MPs could be due to the degradation products of the polymer (lactic and glycolic acids), which consistent of the lower L:G ratio would degrade faster. This could also indicate the effect of L:G ratio to PLGA degradation rates is larger than the IV effect (high IV will degrade slower). At 2h, the pHs for NAC MPs are around 6.5, while the pHs for empty MPs at 2h are around 7. This could result from the carboxylic acid group of NAC. It is worth to noted that from day 7 to day 28 time points, the release samples of 50:50 NAC MPs are more acidic than 50:50 empty PLGA, which could imply there are NAC presented in those release samples. The detection of the NAC is based on thiol group, which could be affected by metal-catalyzed oxidation (PBS could contains minute traces of heavy metal ions). However, the carboxylic acid group wouldn't be affected regardless the present or absent of EDTA. Even though the pHs for all 85:15 and 100:0 MPs are ~7, this could because the effect of NAC to the pH is relatively small and it is still in the buffer range of PBS. For 50:50 release samples, they were out of PBS buffer range for later time points due to polymer degradation, thus the NAC effect on the pH could be observed.

2.3.3. Sizes of NAC and empty MPs

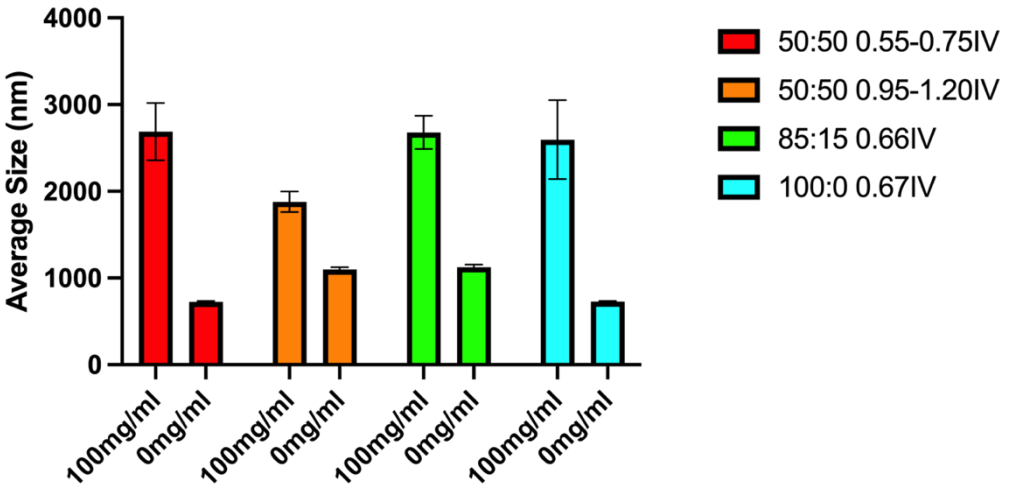

Figure 2-5. DLS average sizes of NAC (100mg/ml) and empty (0mg/ml) MPs

To examine the effects of factors, NAC encapsulating and PLGA formulation, on MPs average sizes, the average sizes of NAC and empty MPs were obtained through DLS (**Figure 2-5**). The average sizes for NAC MPs are significantly larger than the average sizes of empty MPs. The standard deviations of NAC MPs are also larger than that of the empty MPs. However, the larger sizes and standard deviations in NAC MPs could potentially come from the measurements of NAC clusters since the loadings of those MPs are high and their release rates are fast. By performing a two-way ANOVA, it was found that the PLGA formulation doesn't have main effects on size while the encapsulation of NAC has a main effect on the size at a significance level of 0.05. However, there is an interaction between PLGA formulation and NAC encapsulation. Then, two one-way ANOVA tests were performed for the PLGA formulation on NAC MPs size and the empty MPs size, respectively. For the NAC MPs, there is no main effect of PLGA formulation on the MPs size. However, there is a main effect of PLGA formulation on empty MPs at a significance level of 0.05, which means encapsulating NAC will make the PLGA formulation effect insignificant for controlling the sizes.

2.4 Conclusions

In summary, we could fabricate the MPs with high loadings with modified double emulsion method. However, the accuracy of the load results needs to be further assessed. The release profiles of the MPs show gaps between loading and measurable NAC in the release samples. Another round of fabrication of MPs with new EDTA is needed to affirm the release studies. The pH of 50:50 NAC and empty MPs became acidic over time, which is consistent of the degradation is faster for low L: G ratio. 50:50 NAC MPs are more acidic than 50:50 empty MPs from day 7 to day 28 release samples, which could imply the present of NAC in those MPs. Encalpusting NAC will increase the sizes and standard deviations of the MPs, and for the NAC MPs, the PLGA formulation don't have statistically significant effect on the MP size.

2.5 Acknowledgements

We gratefully acknowledge financial support from NIH grant R21 EB026723. We thankfully acknowledge Nadeesani Sirinayake and Ivy Wu for assisting in performing experiments and collecting data.

2.6 References

1. Khan M, Sekhon B, Jatana M, Giri S, Gilg AG, Sekhon C, Singh I, Singh AK. Administration of N-acetylcysteine after focal cerebral ischemia protects brain and reduces inflammation in a rat model of experimental stroke. *J Neurosci Res*. 2004;76(4):519-527. doi:10.1002/jnr.20087

2. Rodrigo R, Fernandez-Gajardo R, Gutierrez R, Matamala J, Carrasco R, Miranda-Merchak A, Feuerhake W. Oxidative Stress and Pathophysiology of Ischemic Stroke: Novel Therapeutic Opportunities. *CNS Neurol Disord - Drug Targets*. 2013;12(5):698-714. doi:10.2174/18715273113120500 15

3. Sun SY. N-acetylcysteine, reactive oxygen species and beyond. *Cancer Biol Ther*. 2010;9(2):109-110.

4. Makadia HK, Siegel SJ. Poly Lactic-co-Glycolic Acid (PLGA) as Biodegradable Controlled Drug Delivery Carrier. *Polymers*. 2011;3(3):1377-1397. doi:10.3390/polym3031377

5. Murphy NP, Lampe KJ. Fabricating PLGA microparticles with high loads of the small molecule antioxidant N-acetylcysteine that rescue oligodendrocyte progenitor cells from oxidative stress. *Biotechnol Bioeng*. 2018;115(1):246-256. doi:10.1002/bit.26443

Chapter 3

Multifunctional polymeric nanocarriers for targeted brain delivery

The manuscript was submitted to *Engineering Biomaterials for Neural Applications,* June 2022

3.1. Introduction

3.1.1 Drug delivery to the brain

The human brain is central, not only to normal biological function, but also to personal identity. Diseases and injuries to the brain can erase this sense of self. Delivering drugs to the brain is a critical challenge in addressing diseases and injuries that degrade human interaction. While delivering drugs to the brain can play a role in addressing a host of degenerative diseases of the central nervous system diseases like Alzheimer's disease (AD), Parkinson's disease (PD), multiple sclerosis (MS), and amyotrophic lateral sclerosis (ALS), it is perhaps closer to being broadly clinically realized in the context of acute injuries or attacks. The subsequent review examines polymeric nanocarriers as a means to deliver drugs to the brain, while using ischemic stroke as a specific example of an application (**Figure 3-1**). The explicit intravenous nature of ischemic stroke provides an opportunity to illustrate some of the opportunities and limits of nanocarrier drug delivery.

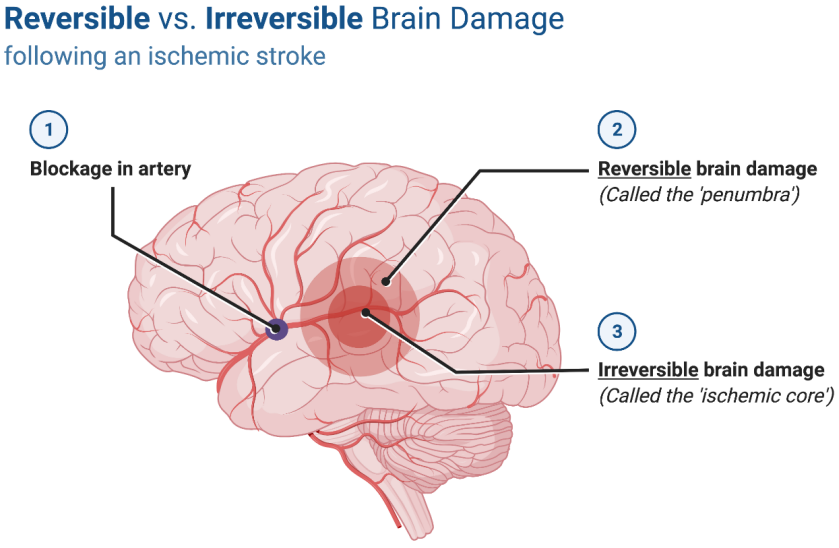

Figure 3-1. Ischemic core and penumbra formation after artery blockage. The ischemic core is the irreversibly damaged brain area that undergoes necrosis and cannot not be further salvaged. The penumbra is the tissue surrounding the ischemic core that undergoes subsequent apoptosis and may still be salvageable. Reprinted from "Reversible vs. Irreversible Brain Damage Following an Ischemic Stroke", by BioRender.com (2021). Retrieved from https://app.biorender.com/biorender-templates

3.1.2 Pathophysiology of ischemic stroke

Stroke is the third leading cause of death in the US and 20% of stroke survivors cannot walk without help [1,2]. Ischemic stroke causes the brain suffering from a transient or permanent shortage of blood supply, which leads to oxygen and glucose deprivation of the brain tissue [3,4]. The downstream effects of ischemia manifest at the molecular, cellular, and tissue scale over the course of minutes to weeks (**Figure 3-2**). The lack of oxygen and glucose supply to the brain quickly exhaust ATP, depleting energy stores. The energy failure of the brain impairs the function of ATP-dependent Na^+/K^+-ATPase, which leads to Na+ influx and membrane depolarization of the neuron [5]. This membrane depolarization activates the presynaptic voltage-sensitive Ca^{2+} channels, and the extracellular Ca^{2+} then flows into the presynaptic neuron. The sudden influx of extracellular Ca^{2+} releases excitatory amino acids, such as glutamate, to the extracellular matrix [3,4]. Besides the glutamate released due to the calcium influx, the membrane depolarization also could release the glutamate from presynaptic neuron [5]. In the meantime, the glutamate presynaptic reuptake is hindered due to energy failure, which exacerbates the glutamate accumulation in the extracellular matrix [4]. Consequently, the up-regulated extracellular glutamate activates N-methyl-D-aspartate (NMDA) and α-amino-3-hydroxy-5-methyl-4-isoxazolepropionic acid (AMPA) receptors, causing influxes of Ca^{2+} and Na^+ to the postsynaptic neuron [3–6]. The overflow of calcium ions bind and activate phospholipase and calpain protease by conformational change, which degrades cell membrane and proteins and lead to necrosis within the ischemic core [5]. Following Na^+ influx and membrane depolarization, the voltage-gated Cl- channel is activated and then the Cl- flows into the neuron down its concentration gradient [4,7]. The net increase of NaCl concentration increase the osmolarity inside the neuron, and water then flows passively to the neuron by osmosis, resulting in cell swelling and cytotoxic cerebral edema, which is the earliest marker of ischemic stroke pathophysiology. The beneficial effects of drugs that targeting early event of ischemic stroke, such as NMDA and AMPA receptors antagonist, Ca^{2+} channel blockers, are very limited to stroke patients due to their extremely narrow therapeutic windows, usually within minutes [8,9].

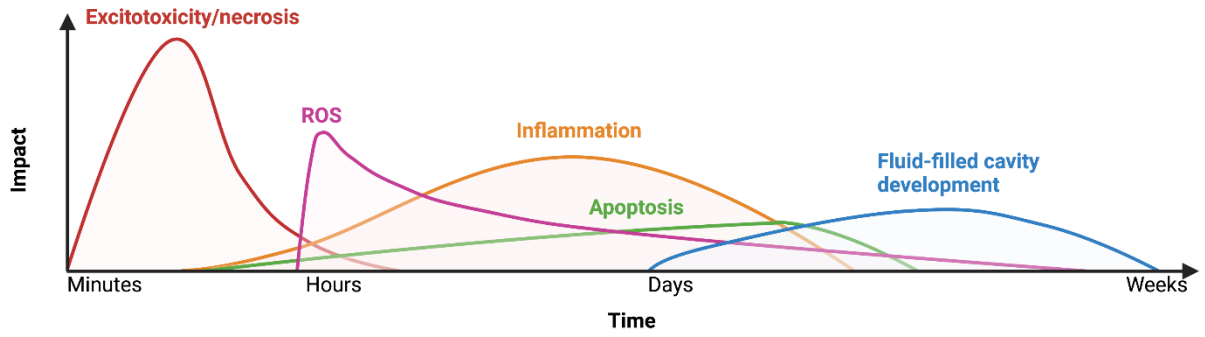

Figure 3-2. Pathophysiological cascades in ischemic tissue. At the early stage after ischemic stroke, excitotoxicity and necrosis occur in the ischemic core. In the penumbra that surrounds the ischemic core, Inflammation and apoptosis occur with a delayed timeframe. Eventually, necrosis leads to the development of fluid-filled cavity, over the course of days to weeks. The x-axis is the time after an ischemic stroke blockage. Created with BioRender.com.

The oxidative stress due to production of free radicals during ischemic stroke is an important marker for its pathophysiology. The brain is particularly vulnerable to oxidative stress because of its high polyunsaturated fatty acids contents, high demand of oxygen, scarce resource of antioxidants and high amount of iron cations Fe^{2+} [10]. There are three phases of reactive oxygen species (ROS) generations during ischemic stroke. The first and second phases of ROS generation happen immediately after ischemic onset and the third phase of ROS was generated after reperfusion [11]. During hypoxia, failure of the mitochondrial respiratory chain due to oxygen and glucose deprivation results in the first phase of reactive oxygen species (ROS) generation. The ATP depletion during hypoxia inside the cells activates xanthine oxidase (XO), which leads to second phase of ROS generation. In the meantime, the influx of Ca^{2+} to the postsynaptic neuron during hypoxia activates Ca^{2+}-stimulated enzymes cyclooxygenase (COX), which further generates ROS and exacerbates oxidative stress [3,4]. The third phase of ROS released when the blood supply returns to the brain tissue [11]. This reoxygenation, coupled with glutamate-induced high intracellular Ca^{2+} level, activates the NADPH oxidase that located in the mitochondria and cell membrane, leading to third phase of ROS generation. The main products during these three phases of ROS generations are superoxide (O^{2-}) and hydrogen peroxide (H_2O_2), and superoxide is easily converted to hydrogen peroxide by superoxide dismutases (SODs) [12]. Due to the high amount of Fe^{2+} of the brain, H_2O_2 will decompose into extremely reactive hydroxyl radicals ($OH\cdot$). Hydroxyl radicals then lead to irreversible peroxidation of polyunsaturated fatty acids and

protein and DNA damage. These three phases of ROS generations overwhelm the antioxidant defenses and cause necrosis and apoptosis in the brain [13].

The penumbra is the region that surrounding the ischemic core with reduced but nonzero blood supply [9]. Unlike cell death in the ischemic core, which is predominantly due to necrosis and occurs within minutes after ischemic stroke onset, the relatively delayed apoptosis and neuroinflammation mainly account for the damage of the tissue in the penumbra region [6,8,14]. Thus, the cells in the penumbra are still potential salvageable [15]. The ROS generated in the mitochondria during hypoxia and reperfusion signals cytochrome C release, which triggers mitochondrial apoptosis [11,13]. Additionally, H_2O_2 upregulates Fas-Fas ligand, which activates caspase-8 and downstream caspase and triggers DNA damage and H_2O_2-induced apoptosis. Although both necrosis and apoptosis are cell death processes which involve DNA damage, the apoptosis in the penumbra is more delayed than the necrosis in the core, which provides the therapeutic opportunities to salvage the penumbra. The chemokines generated during late ischemic event promote neutrophil infiltration, which leads to NO generation via inducible NOS (iNOS) [4,8,13]. The NO, together with ROS generated during hypoxia and reperfusion, activate matrix metalloproteinases (MMPs). The MMPs will degrade the structural protein of blood-brain barrier (BBB) and increase paracellular BBB permeability. Fluid in the blood vessel permeates to the brain via the leaky BBB, causing the formation of vasogenic cerebral edema. Since the impact of the pathological events in the penumbra is delayed and more gradually increases compared to the impact in the core, drugs that target penumbra ischemia are promising due to their prolonged therapeutic windows [4,6,8]. However, any of the molecular pathways involved could be potent drug targets in limiting damage and treating ischemic stroke. The delivery mechanism of such drugs is a critical engineering and design criteria for controlling their spatial and temporal presence.

One important factor that deserves attention for future CNS disease treatments is sex. Not only are the disease outcomes different on the basis of sex, but the treatment and rehabilitation regimens vary as well. An excellent review covers the sex dimorphism in ischemic stroke therapies in great detail [16]. For instance, minocycline only show significantly neuroprotective effects in males, not in females, in both preclinical and clinical stroke studies [17,18]. It is already clear that nanoparticle delivery to injured brain tissue has a sex-dependent

temporal profile [19]. Thus, when developing future CNS diseases polymeric nanocarrier treatments, it is important to include both sexes in preclinical and clinical studies, and with sufficient power to examine each group independently.

3.1.3. Current FDA-approved treatments & limitations

3.1.3.1 Tissue plasminogen activator (t-PA)

Tissue plasminogen activator (tPA) is the only the Food and Drug Administration (FDA)-approved drug treatment for ischemic stroke [20]. tPA is a serine protease that activates the zymogen plasminogen to become the fibrinolytic enzyme plasmin. Both tPA and plasminogen have high affinities to fibrin, a major structural component of blood clots [21,22]. The "clot-busting" drug tPA is administered intravenously and dissolves the blood clot lodged in an artery during ischemic stroke by activating the plasminogen into plasmin, which cleaves the fibrin component of the clot (**Figure 3-3A**). However, tPA treatment (also knowns as IV alteplase) has several limitations in clinical use [23]. There is some evidence that select patients could benefit from tPA treatment up to nine hours after ischemic onset, but the current gold standard for administration is within 4.5 hours after ischemic onset [24,25]. Thus, despite more than 690,0000 ischemic stroke cases occurring in the United States annually, only 2% to 5% of acute ischemic stroke patients could benefit from IV alteplase treatment due to the current narrow clinically approved therapeutic window [20,26,27]. The standard dose of IV alteplase for acute ischemic stroke is 0.9 mg/kg, with a 90 mg total dose limit [28]. IV alteplase is administered to patient via intravenous (IV) administration through the arm; 10% of the total dose is administered as an IV bolus dose, and the remaining 90% is infused over 60 minutes. These factors of dose and timing illustrate the potential for controlled drug delivery and release, which could prevent some of the negative side effects of tPA.

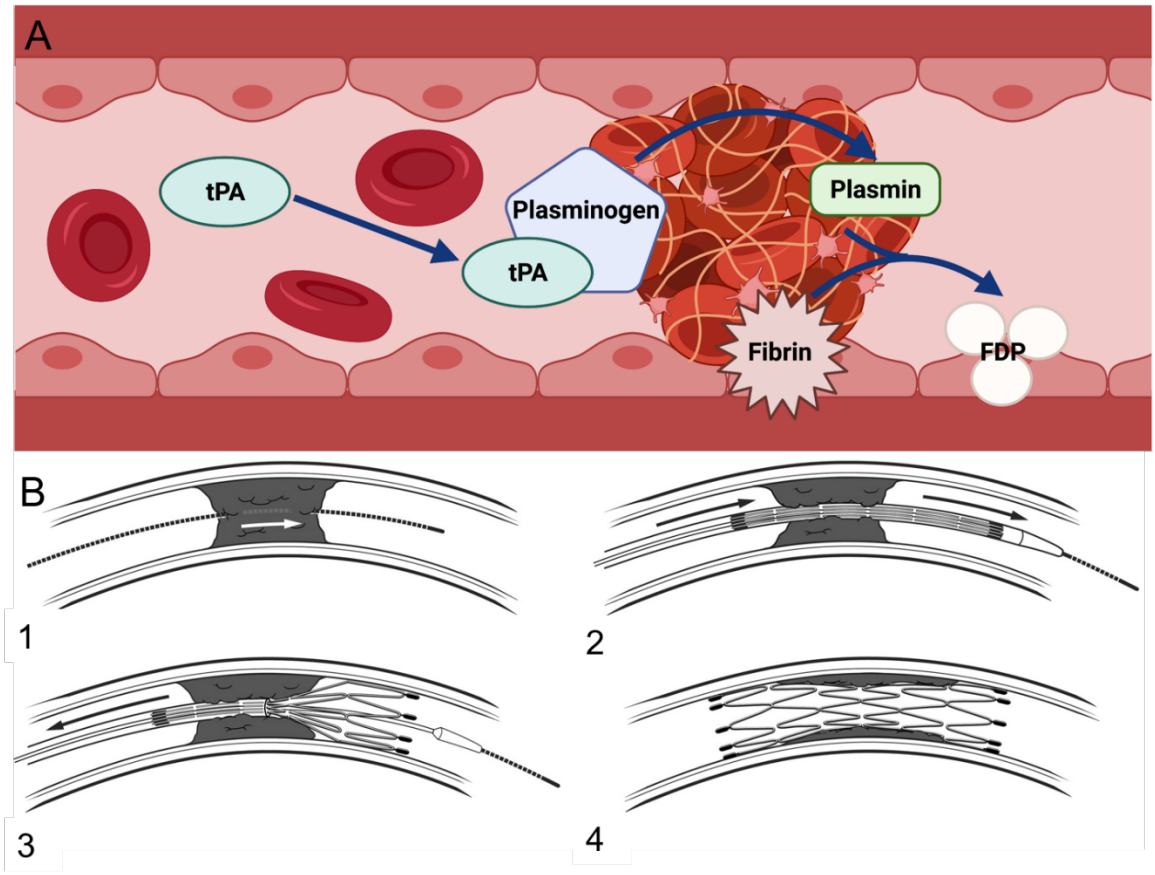

Figure 3-3. Current treatments for ischemic stoke. (A) Tissue plasminogen activator (tPA) dissolves a blood clot by activating plasminogen to plasmin. The plasmin then degrades the major blot clot structural component, fibrin, into soluble fibrin degradation products (FDP). Adapted from "Blood Vessel (Straight, Light Background)", by BioRender.com (2021). Retrieved from https://app.biorender.com/biorender-templates. **(B)** The schematic of a stent retriever for removing the blood clot and recanalize the blood vessel. Reproduced from E.I. Levy, etc. *AJNR Am J Neuroradiol*. 2007 May; 28(5): 816–822.

It's worth noting that tPA has some severe complications when it is administered to patients, such as hypoxia/reperfusion injury, inflammation, edema and hemorrhagic transformation [20,29,30]. 15% to 27% of patients who received IV alteplase treatment suffered from undesired cerebral microbleeds [23]. tPA up-regulates NMDA receptors, causing an influx of Ca^{2+} in neurons and activating Ca^{2+}-stimulated enzymes, including lipase, proteases, nucleases, and COX [3,20].

Activation of those Ca^{2+}-stimulated enzymes induces a hypoxia/reperfusion injury, which is associated with a burst of ROS release, cell injury, and cell death. tPA also up-regulates

MMPs, which degrade the tight junctions of the BBB and increase paracellular BBB permeability by allowing leakage through the intercellular space between brain endothelial cells [29]. There is also some evidence that shows tPA can, in some cases, prompt bradykinin generation [30]. tPA-induced bradykinin activates both kinin 1 (B1) and kinin 2 (B2) receptors that are up-regulated during ischemic event, causing the release of intracellular calcium, down-regulating the tight junction protein claudin-5, and increasing paracellular BBB permeability. The combination of both BBB permeability enhancement effects prompts plasma invasion through the leaky BBB to the brain parenchyma, causing a plasma-induced inflammatory response, vasogenic cerebral edema, hemorrhagic transformation and brain tissue damage [29,30].

3.1.3.2 Mechanical thrombectomy

Mechanical thrombectomy is an endovascular procedure for acute ischemic stroke that physically removes the clot [31]. This mechanical thrombectomy treatment could recanalize the occluded vessel by directly taking out the proximal large-artery blood clot that formed in the anterior circulation [32,33] (**Figure 3-3B**). The therapeutic window for mechanical thrombectomy is within 24 hours after stroke onset [23]. In clinical settings, a stent retriever device is typically used for mechanical thrombectomy surgery [23,34]. A stent retriever device resembles a tiny expandable metallic cage attached to the end of a microwire. During mechanical thrombectomy surgery, the doctor threads the microcatheter through a groin artery to the clot location in the brain. The surgeon then places the stent retriever inside the microcatheter and deploys the stent retriever across the thrombus. After the device has fully expanded (3-7 min), the doctor then pulls out the device, together with blood clot, from the artery. IV alteplase is often administrated as a pretreatment to mechanical thrombectomy surgery to help dissolve the clot and make clot retrieval easier [23]. This direct clot accessing procedure also provides an opportunity for combination therapy as the catheter is already at the local site of the ischemic core. Such access by a catheter device may allow highly controlled spatial delivery of drugs molecules and/or particles directly to the ischemic site.

Some limitations and side effects are also associated with the mechanical thrombectomy surgery. The patient accessibility to mechanical thrombectomy is relatively low due to insufficient resources in the hospital and high expertise requirement [35]. Due to the limited accessibility, IV alteplase pretreatment becomes extremely important for IV tPA-eligible patients

when they need to be transferred to another hospital to get the mechanical thrombectomy surgery [36]. Furthermore, only 19.7% of patients are eligible for mechanical thrombectomy within the 24-hour therapeutic window [37,38]. Mechanical thrombectomy surgery also poses a risk of symptomatic intracranial hemorrhage, embolism of blood vessel that are not initially affected, and intracranial stenosis [34,39].

3.2. Advantages and potential challenges of Nano-drug delivery

Disease and injury treatment, such as that within the brain, frequently require therapeutic drugs to address both symptoms and underlying causes. However, delivering these drugs can present key challenges in terms of controlling their presence with regard to space and time. Localizing drug presentation to specifically affected areas can reduce off target, systemic side effects. Controlling the concentration of drug over a period of hours, days, or weeks can reduce invasiveness of treatment and increase patient compliance. This is particularly crucial within the brain, where direct administration would require direct injections that could compromise healthy tissue and cause further damage. These challenges can be readily addressed via state of the art drug delivery technology which presents drugs within nanoparticles designed to release their payload with a tightly controlled temporal profile and spatial location (**Figure 3-4**).

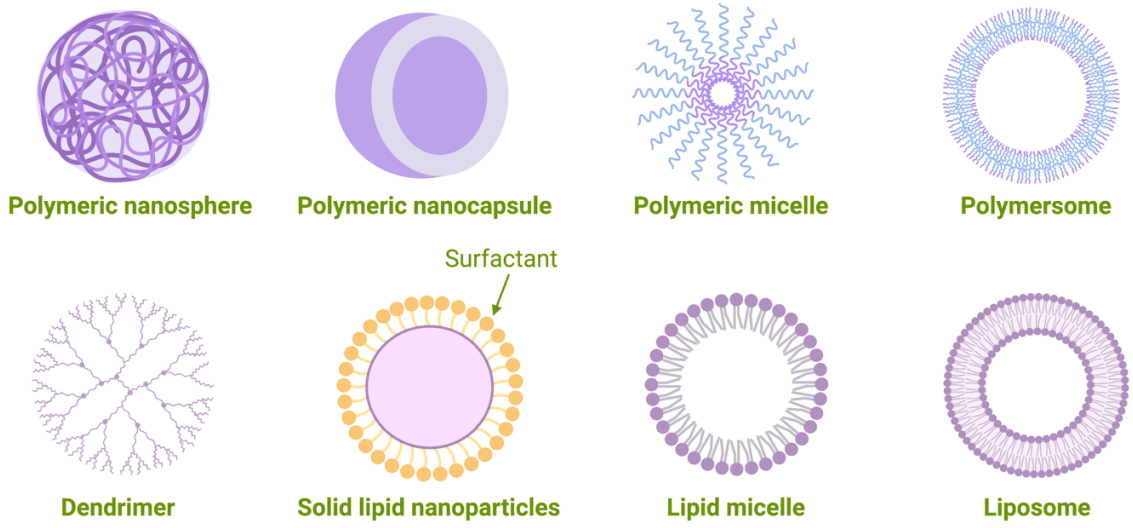

Figure 3-4. Schematic of different types of nanocarriers commonly used in drug delivery. Created with BioRender.com.

Nanocarriers, or nano-drug delivery systems, refer to materials with diameters in the range of 10-1000 nm [40]. The unique properties of nanocarriers impart several advantages for drug delivery. Due to its nano-scale size, it is suitable for less invasive, more patient accessible, intravenous delivery compared to the microcarrier counterpart. The large surface-area-to-volume ratios of nanocarriers allow multivalent surface modifications [41]. Such multivalent ligand attachment could confer nanocarriers with multiple functions, such as prolonged blood circular time and tissue-specific targeting.

Nanocarriers can controllably deliver both hydrophobic and hydrophilic drugs [41–43]. Free hydrophobic drugs have low aqueous solubility and may require solvent and/or excipients that pose safety risks to the body [44,45]. For example, Taxol®, a traditional formulation of paclitaxel, requires the excipient Cremophor EL in order to deliver this hydrophobic anticancer drug [46,47]. Cremophor EL presents potential health concerns, including life-threatening hypersensitivity, hyperlipidaemia and erythrocyte aggregation. Nano-drug delivery system could enhance hydrophobic drug solubility without introducing the toxic components that have significant health concerns. For examples, Abraxane®, a 130 nm diameter nanocarrier formulation of paclitaxel, is a FDA-approved anticancer product for delivering paclitaxel [48–50]. This paclitaxel nanocarrier is made by suspending lyophilized paclitaxel and human albumin in 0.9% sodium chloride solution and inducing noncovalent interactions via high-pressure homogenization. As opposed to Taxol®, Abraxane® doesn't require premedication since it doesn't involve Cremophor EL. This Abraxane® nano-size formulation also has a higher maximum tolerated dose compared to Taxol®.

Nanocarriers can also entrap hydrophilic drug and improve their bioavailability. For example, Lancheros et al. successfully constructed polymeric nanocarriers to deliver the hydrophilic antioxidant N-acetylcysteine (NAC) which has low bioavailability in the bloodstream [51]. NAC is prone to form disulfide bonds due to the interaction with plasma proteins when circulating in the bloodstream and resulting in a low bioavailability. Their 235.5 ±11.4 nm diameter, poly(lactic-co-glycolic acid) (PLGA) nanocarriers where synthesized via a modified version of nanoprecipitation. The specific NAC load of their nanocarriers with modified parameters in nanoprecipitation could reach to $3.14 \pm 0.33\%$, which is more than 20 times higher compared to the unmodified base case scenario. Encapsulating NAC inside a polymeric

nanocarrier helps prevent the interaction between NAC and plasma proteins, thus improving the NAC bioavailability in vivo.

Certain polymers are frequently used as drug nanocarriers as they support hydrophilic or hydrophobic drug entrapment and the subsequent slow release of entrapped drugs. PLGA, poly(lactic acid) (PLA), and polycaprolactone (PCL) are three biodegradable, tunable polymers commonly used for constructing polymeric nano-drug delivery systems [52]. Since the drug is embedded within biodegradable polymers such as these, the polymer itself is resorbed during or after the drug payload has been delivered. The preparation methods for nanocarrier are simple and efficient as further discussed in Section 3.4. The chemistry of the selected nanocarrier polymer(s) is easily tuned at the molecular level to control the release rate. In some applications, a burst release profile may be desirable, whereas in others, the goal may be to seek a more sustained release. For the latter one, Zhou et al. loaded dithiazanine iodide that could inhibit the proliferation of tumor cells in for glioblastoma treatment in PLGA polymer matrix, and the nanocarriers they fabricated achieve a sustained release of dithiazanine iodide for almost three months [53]. Another study conducted by Sánchez-López et al. successfully fabricated PEGylated PLGA nanocarriers with memantine hydrochloride for Alzheimer's disease (AD) treatment [54]. These nanocarriers deliver memantine hydrochloride in a more sustained timing compared to unencapsulated memantine hydrochloride. By taking advantage of controlled/sustained releases of drug, clinicians could lower the administration frequency and improve patient compliance [43,55].

As mentioned previously, the BBB is a biological barrier to intravenous CNS drug delivery. While intravenous delivery would generally be preferred to direct injection into the brain, getting nanocarriers across the BBB remains a challenge. BBB endothelial cells have abundances of various receptors and carriers, and their membranes are negatively charged [41]. In order to cross the BBB, the nanocarriers could utilize their large surface-area-to-volume ratios and present surface modifications with BBB-targeting ligands. BBB-targeting ligands attached to a nanocarrier can facilitate crossing the BBB by transcytosis, without requiring disruption of the tight junctions. Three specific types of transcytosis, receptor-mediated transcytosis (RMT), carrier-mediated transcytosis (CMT) and adsorptive-mediated transcytosis (AMT) will be discussed in Section 3.3.3.

One potential challenge associated with nano drug delivery is the neurotoxicity to the healthy part of the brain or other tissues and organs. In order to solve this problem, dual-targeted nanocarriers could be designed that have components of both 1) crossing the BBB and 2) targeting the disease microenvironment. For instance, Han et al. successfully fabricated dual-targeted PLGA nanocarriers with lexiscan and chlorotoxin [56] (**Figure 3-5**). The lexiscan is a BBB modulator that could transiently and reversibly open BBB and allow the nanocarriers to cross the BBB paracellularly. After crossing the BBB, the drug then needs to be targeted to the ischemic tissue. The chlorotoxin component of their nanocarriers has a high affinity to the matrix metalloproteinase 2 (MMP-2) that is upregulated under an ischemic stroke environment. As a surface moiety on the nanocarriers, the chlorotoxin acts as the ischemic microenvironment targeting ligand, localizing the nanocarriers, and their drug payload, to the stroke-affected tissue. The dual-targeted PLGA nanocarrier successfully delivered NOGO extracellular peptide, 1 to 40 (NEP1-40) to ischemic tissue in middle cerebral artery occlusion (MCAO) injured mice. Their dual-targeted nanocarrier effectively targeted the ischemic hemisphere based on IR780 fluorescent signal intensity and (NEP1-40 loaded dual-targted nanocarrier) substantially lessened the infarct volume and improved the survival rate of MCAO injured mice [Figure 2(B), Figure 2(C), and Figure 4 from reference 57]. In another example, Zhang et al. modified PEG-PLA co-polymer with two targeting ligands TGNYKALHPHNG (TGN) and QSHYRHISPAQV (QSH), to construct dual-targeted nanocarriers loaded with coumarin-6 or a near-infrared dye DiR for AD microenvironment targeting [57]. The ligand TGN acts as the BBB targeting ligand for crossing the BBB and the ligand QSH has a high affinity to the amyloid plaque $A\beta_{1-42}$ that accumulates in AD brains. The nanocarrier successfully targeted amyloid plaques in mice with AD model treatment, dependent on ligand densities on the nanoparticle surface.

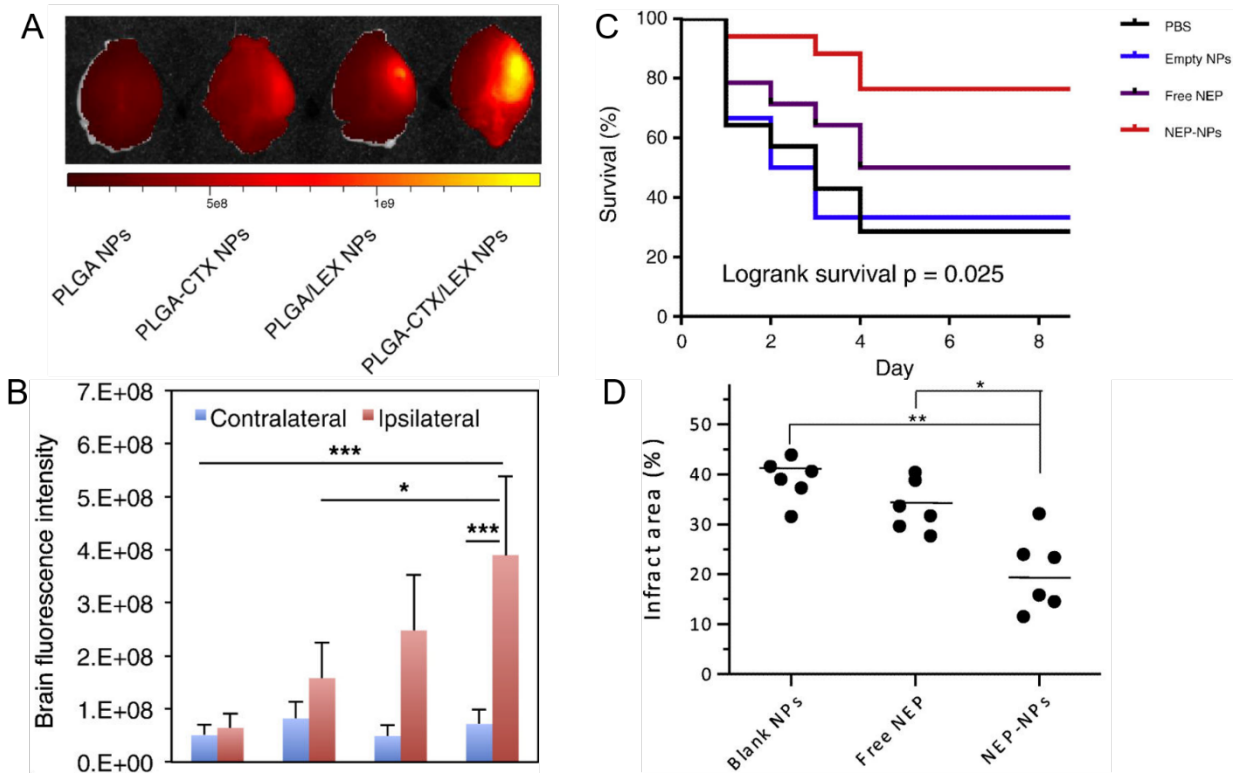

Figure 3-5. Targeting efficiency and therapeutic effects in stroked mouse brains. (A) Images of IR-780 signals in excised middle cerebral artery occlusion (MCAO) brains demonstrating high nanoparticle presence in the chlorotoxin/lexican dual-targeted system. (B) Quantitative analysis of brain IR-780 signal intensity with of contralateral and ipsilateral hemispheres of excised MCAO brains indicates clear focusing of the treatment in the stroked hemisphere. (C) Survival rate percentages of MCAO mice receiving PBS, empty NPs, free NEP1-40, and dual-targeted NEP1-40 NP treatments. (D) The infarct area percentages of MCAO mice after receiving blank NPs, free NEP1-40 and dual-targeted NEP1-40 NPs treatments. Reproduced from Liang Han, etc. *Nanomedicine.* 2016 Oct;12(7):1833-1842.

Another challenge associated with nano-drug delivery is the possibility of premature drug release before nanocarriers reach the targeted tissue. Using a passive release mechanism, this would decrease the total therapeutic amount for targeted delivery, thus reducing potential treatment efficacy. In order to solve this, stimuli-responsive nanocarriers could be constructed. Stimuli-responsive nanocarriers release the drug based on particular stimuli that is present only locally in the disease microenvironment, such as a disease-associated pH or redox-state. Four types of stimuli-responsive polymeric nanocarriers include: pH-responsive, redox-responsive, hypoxia-responsive and enzyme-responsive polymeric nanocarriers, discussed in more detail in Section 3.5.2.

When nanocarriers travel in the bloodstream, the protein corona formation around them due to the nonspecific interaction between the nanocarriers and the proteins in the bloodstream could change their properties considerably [41]. Those significant properties changes could speed up the clearance of nanocarriers via reticuloendothelial system, or lead to aggregation [41,58]. Polyethylene glycol (PEG) is a hydrophilic polymer that prevents nonspecific interactions with serum proteins due to its hydrophilicity and steric repulsion [59–62]. PEGylation increases the half-life of nanocarriers in the blood stream, minimizing the opsonization and reticuloendothelial system uptake by the immune system.

Before translating to the clinical use, there are other potential challenges that need to be considered. The nanocarriers usually have multiple components in addition to the polymers, such as ligands, excipients, or more than one type of drug in the same nanocarrier [63]. This design strategy presents opportunities as described above. However, the multiple components of the nanocarriers increases their complexities, which present challenges in regulatory approval and large-scale production of nanocarriers with good quality. New nanocarriers may include excipients never used in clinical settings before, and adding such components may also impact the biodistribution in vivo and immunotoxicity profiles [63,64]. Thus, a detailed safety and toxicity assessment need to be completed for the nanocarriers in preclinical studies, and these are not always predictive of the human results [63–65]. Sterilization is another challenge for the nanocarrier production process. Nanocarriers are sensitive to various sterilization techniques commonly used for medical equipment, such as autoclaving and γ-irradiation, which would likely disrupt the qualities of the nanocarriers [66]. Filtration, common to preparing sterile drug solutions, is a challenging choice for nanocarriers. Filtration is completed by using a membrane filter, typically with less than 220 nm pore size for removing bacteria. This size cutoff favors nanocarriers that are well below 220 nm, without significant quality changes. However, the nanocarriers that have sizes close to or larger than 220 nm could clog the filter, resulting in material loss and a lower product yield.

Despite these challenges that need to be considered before large-scale production and clinical use, nano-drug delivery is gaining large interests and promising for CNS drug therapy due to its advantageous properties. New technologies are continuing to improve the properties of

nanocarriers for drug delivery to the CNS [67]. The limitless design parameters allow a great deal of control for existing and future drugs.

3.3. Approaches of crossing BBB

As discussed elsewhere in this book, the BBB generally prevents passive diffusion into the brain. When one considers the numerous potential drug targets and extreme therapeutic need, controlled delivery's potential to controllably cross the BBB clearly makes it an attractive treatment strategy for the CNS. Although the BBB may be partially compromised after CNS disease onset, the degree of BBB opening might not be sufficient to allow polymeric nanocarrier transport, and disease-induced BBB opening is uncontrolled and thus ineffective for targeted applications. In this section, several on-demand methods that could open the BBB transiently and reversibly will be discussed. Recommended methods facilitate minimally invasive, controlled BBB opening, which helps reduce safety concerns (for example, section 3.3.1 and 3.3.3). Such approaches provide the clearest pathway for the development of targeted brain delivery polymeric nanocarrier treatments.

3.3.1 Methods to physically increase BBB permeability

3.3.1.1 Focused Ultrasound

Focused ultrasound (FUS) is a non-invasive, clinically-approved technology that can reversibly open tight junctions with high spatial control to temporarily increase blood-brain barrier (BBB) permeability [68–73] (**Figure 3-6**). A low energy mode of FUS applied to the brain opens the BBB without thermal injury or tissue damage [74,75]. Intravenously injecting pre-made pressure-sensitive microbubbles to the body, before applying FUS, lowers the input energy required for the technique since energy is not needed for FUS to create the microbubbles. These injected pre-made microbubbles have a typical diameter sizes range of 1-10 um [76–83]. An FUS transducer applied to the targeted region activates the microbubbles in the vessel to oscillate and raise the pressure at the vessel wall, physically forcing the tight junctions open [84,85]. In this case, FUS and microbubbles allows the intravenously injected payload to cross the BBB in the immediate FUS-disrupted area, and locally deliver the drug to the tissue. Magnetic resonance imaging (MRI) guides and monitors the BBB opening and drug release in a real-time manner [86]. Preclinical results demonstrated BBB opening and payload delivery of glycogen synthase kinase

3 (GSK-3) inhibitor [81], anti-alpha synuclein (a-syn) monoclonal antibodies (mAb) [83], or mesenchymal stem cells (MSCs) [82] without damaging healthy tissue. Several clinical trials of FUS have been conducted for Alzheimer's disease and Parkinson's disease [70–73]. FUS therapy for ischemic stroke is still in the early laboratory phase, but the results are promising [82,87–91]. In a recent study, the researchers applied FUS to the lateral hippocampal region of male Sprague–Dawley rats to facilitate engraftment of donor MSCs in host brain tissue [82]. Compared to the group without FUS treatment, FUS-induced BBB opening increased engraftment of intravenously delivered MSCs by more than two fold. This approach provides inspiration for potential stem cell therapy as a therapy for ischemic stroke. Furthermore, FUS itself can have neuroprotective function after ischemic stroke [87–89,91]. One study demonstrated that 20 min of Low-Intensity Focused Ultrasound (LIFU) stimulation to the lateral cerebellar nucleus once per day for two days, beginning the day after MCAO injury, could reduce brain edema and improve the survival rate of Purkinje neurons in mice [87]. To our best knowledge, the application of FUS to polymeric nanocarriers in brain delivery is still underdeveloped. Several studies indicate that FUS improves the brain tissue penetration of polymeric nanocarriers, and thus the distribution of payload such as model trangenes [92,93]. Although there is a research gap in applying FUS with polymeric nanocarriers, the reversible BBB opening created with FUS provides an opportunity for the polymeric nanocarrier to cross the BBB and localize to the targeted area. In summary, FUS can locally deliver payloads by reversibly opening the BBB without damaging brain tissue, is being investigated in several clinical trials, and shows potential for further development of CNS disease nanotechnology treatments.

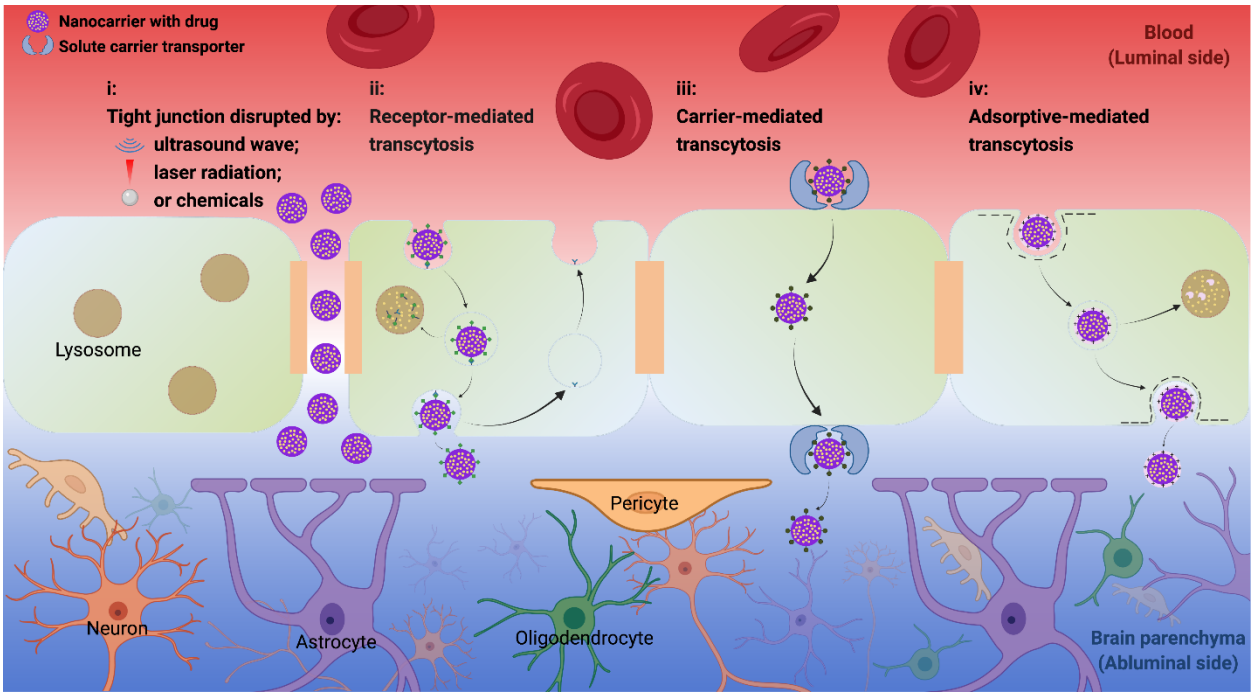

Figure 3-6. Schematic representation of several nanocarriers blood brain barrier (BBB) crossing mechanisms. i) Nanocarriers cross the BBB by transiently and reversibly disrupted tight junctions, caused by focused ultrasound waves, near-infrared femtosecond-pulsed laser irradiation, or chemicals. **ii)** Nanocarriers cross the BBB by receptor-mediated transcytosis with ligand-receptor binding and vesicle formation porting drugs to the tissue side of the endothelial cell barrier. **iii)** Nanocarriers cross the BBB by carrier-mediated transcytosis with the help of solute carrier transporters**. iv)** Nanocarriers cross the BBB via adsorptive-mediated transcytosis by utilizing the electrostatic interaction between positively charged peptides/proteins and negatively charged membranes with vesicle formation again facilitating transport through the cell to the abluminal side. Created with BioRender.com.

3.3.1.2 Near-infrared Femtosecond-pulsed Laser Irradiation

Near-infrared femtosecond-pulsed laser irradiation is a minimally invasive tool that increases BBB permeability and allows local delivery of payloads with high spatial resolution in a subcellular level [94,95]. By briefly exposing the targeted blood vessel to the femtosecond-pulsed laser, the high peak intensity irritation induces transient and reversible tight junction disruption. The plasma, together with injected payloads, extravasates through the disrupted blood vessel wall into targeted brain tissue. The technique successfully targets the blood vessels that have lumen diameters from 10um to 50um [94]. A lager lumen diameter vessel has a smaller area of plasma extravasation and a lower plasma extravasation circularity. Thus, it may have a lumen diameter limitation of blood vessel for near-infrared femtosecond-pulsed laser irradiation, which may restrict the application of this technique. In this way, near-infrared femtosecond-pulsed laser

irradiation allows large molecules, including recombinant proteins, monoclonal antibodies, and gene therapy carriers to deliver to the targeted brain tissue [94,96]. However, a large amount of drug is needed for intravenously injection due to the blood plasma dilution, which increase the cost and poses a risk of side effects due to high doses of injected drug [94]. The infiltration of some plasma components, such as albumin, may also lead to inflammation and damage the brain tissue [94,97]. Theoretically, plasma extravasation could also happen to focused ultrasound as a side effect. However, the focused ultrasound in Section 3.3.1.1 uses low intensity ultrasound energy beam, and a lower acoustic energy could reduce the inflammatory responses and brain tissue damage chances in the patient [68,69,74,75]. Thus, low-intensity focused ultrasound is more developed technique for opening BBB, and several preclinical results and clinical trials, as mentioned in previous section, show focused ultrasound could temporarily opening BBB and delivering payloads without damaging surrounding healthy tissue.

3.3.2 Chemically opening BBB approaches

In this section, four chemical substances, mannitol, lexiscan, borneol and RMP-7, that could transiently opening BBB will be discussed. The limitations of the chemically BBB disruption approaches will be discussed at the end of Section 3.3.2.

Mannitol (also known as Osmitrol) is an FDA-approved diuretic administered via intravenous infusion that relieves elevated intracranial pressure in clinical practice [98]. Mannitol rapidly poses an osmotic shock to the brain endothelial cells [99,100]. The plasma osmolarity rises within minutes after mannitol infusion, which creates an osmotic gradient across the luminal membranes of brain endothelial cells [98–100]. Water inside the brain endothelial cells flows outward to the higher osmolarity blood vessel lumen by osmosis. This water outflow causes the shrinkage of the brain endothelial cells, which opens the tight junctions and increases paracellular BBB permeability. The effect of increasing BBB permeability is transient and reversible, and will recover following mannitol excretion. For instance, the maximal duration of action on increasing BBB permeability is ~5 minutes when injected into the internal carotid artery [101].

Lexiscan (also known as Regadenoson), an FDA-approved adenosine A2A receptor agonist, also modulates BBB permeability in a transient and reversible manner [99]. Lexiscan binds

to the adenosine receptor (AR) expressed on brain endothelial cells. The activation of AR downregulates Rac1 and upregulates RhoA. Rac1 is a small GTPase important for BBB structural stability [102]. RhoA, on the other hand, is a small GTPase that disrupts tight junctions by reorganizing actin-cytoskeleton [102,103]. The actin-cytoskeleton is a dynamic structural network for cell morphological regulation. Thus, the tight junction disruptions due to the changing in cell morphology increase the BBB permeability. Additionally, lexiscan has a fast downregulation effect on P-glycoprotein (P-gp) [104]. P-gp is a membrane protein on BBB that flows out the substances, for example, the NPs and their payloads, back to the blood stream. By decreasing P-gp expression, NPs has larger probability to finally permeate brain tissue. 10kDa dextran becomes detectable in the CNS within 5 minutes of a single lexiscan intravenous injection in mice [99]. The BBB reaches the maximum permeability at 30 minutes post-treatment and recovers back to pre-treatment state 180 minutes after a single lexiscan intravenous injection in mice.

Borneol is a natural plant-derived compound extracted from Dipterocarpus aromatica Gaertn. f., or more commonly, Cinnamomum camphora (L.) Presl., and in traditional Chinese medicine, borneol is for resuscitation use [105]. The most used route to administrate borneol in clinical setting is oral route of administration. There is an increasing evidence showing that borneol may also have a temporary and reversible BBB permeability enhancement effect. Borneol enhances BBB permeability by inhibiting the efflux membrane protein P-gp that has a high expression level on the brain endothelial cell luminal membranes [104,106,107]. However, borneol upregulated intercellular adhesion molecule 1 (ICAM-1) expression on brain endothelial cells [108]. Upregulation of ICAM-1 could increase paracellular BBB permeability by promoting leukocyte infiltration and eliciting an inflammatory response [13,109,110]. L-borneol induces BBB opening 20 minutes after oral administration, and the BBB permeability enhancement effect subsides within 1h after L-borneol administration [111].

RMP-7 is a bradykinin analog that could induce a rapid, transient and reversible BBB opening by activating kinin 2 (B2) receptors, which are upregulated during ischemic events [30,112,113]. The activation of B2 receptors triggers release of intracellular calcium and downregulates the claudin-5, a key tight junction protein expressed on brain endothelial cells [30,114,115]. Downregulation of claudin-5 increases the paracellular BBB permeability. The BBB

permeability enhancement effect gradually diminished during a 60-min continuous infusion administration of RMP-7 [116].

Disrupting the BBB, even temporarily, has side effects as described in the previous section on physical disruption. One major limitation of chemically BBB opening approaches is that, the tight junctions disruptions allow plasma albumin being infiltrated to the brain tissue, which may lead to cytokines generation and brain tissue damage [97,113]. Another limitation is they are susceptible to organ damage [113]. For example, intravenous administration of lexiscan may lead to bronchospasm via activation of the adenosine receptor expressed on lung mast cells [117,118]. Mannitol could also increase the osmolality in the renal tubules, which may lead to dehydration [98]. Mannitol even could potentially cause renal damage and/or failure.

3.3.3 Transcytosis

As compared to the methods that physically (3.1) or chemically (3.2) open the BBB, transcytosis provides a newer, safer way for drugs to cross the BBB without directly disrupting the tight junctions. Transcytosis delivers the cargo from one side of a cell to the other side of a cell through endocytosis, intracellular vesicle transport or substrate diffusion, and exocytosis. Three types of transcytosis will be discussed in this section: receptor-mediated transcytosis (RMT), carrier-mediated transcytosis (CMT), and adsorptive-mediated transcytosis (AMT). Vesicles formed in RMT and AMT undergo sorting inside the cell, either sorted to the opposite side for releasing cargos, or sorted to lysosomes for degradation [119–121]. To our best knowledge, the mechanisms for vesicle sorting remain unproven. CMT doesn't involve vesicle formation, instead utilizing substrate concentration gradient to drive the cargos diffusing inside the cell [119]. Nanocarriers can be designed to take advantage of transcytosis, by specific surface modifications to help the nanocarriers cross the BBB and deliver the drugs in the brain. Among these three types of transcytosis, RMT is the most widely applied type of transcytosis in drug delivery [122].

3.3.3.1 Receptor-mediated transcytosis (RMT)

Receptor-meditated transcytosis (RMT) is successful and popular strategy for researchers to develop the methods for delivering drugs and NPs across the BBB [122]. The RMT process initiates via specific recognition of a ligand to a receptor on the luminal side (inside the vessel) , followed by vesicle formation and endocytosis, vesicle transport, vesicle fusion with the

abluminal membrane, and finally, exocytosis and release of the payloads to the abluminal side [119] (**Figure 3-6)**. The cell surface receptor is recycled back to the luminal side via vesicle, thereby maintaining the receptors needed for the next round of transcytosis. The molecular recognition between ligand, which may be presented as an attachment to a drug or NP, and receptor guarantee the high specificity of RMT [120]. Insulin, transferrin, and low-density lipoprotein receptors are three typical receptors utilized for RMT to cross the BBB [120,123–125]. One obstacle for RMT is the lysosomal degradation of the endocytosed cargo vesicles during transport inside the cell, which could reduce the delivered efficiency of therapeutic cargos to the abluminal side [119]. Another problem associated with RMT is that the endogenous substrate may compete with the exogenous ligands [126]. For example, endogenous transferrin, which has a high blood concentration, could compete for the binding of the exogenous transferrin ligands on a NP, impairing the targeting efficiency. To deal with the endogenous transferrin competition problem, an antibody OX26 with a different binding site on the transferrin receptor than the endogenous transferrin could be utilized [126,127]. Using an antibody with a different binding site than endogenous substrate provides a solution to avoid the endogenous competition, thus increasing targeting efficiency [126]. This method has been used to deliver puerarin-loaded poly(butylcyanoacrylate) nanocarriers across the BBB via low-density lipoprotein receptor-mediated transcytosis, and restore neurological functions and reduce infarct volume in MCAO rats [125].

3.3.3.2 Carrier-mediated transcytosis (CMT)

Carrier-mediated transcytosis (CMT) is another strategy to transport drugs across the BBB. The carriers, such as glucose transporters, monocarboxylate transporters (MCTs) and amino acid transporters (AATs) in CMT are natively used for transmembrane nutrient delivery to the brain [126]. The CMT process involves solute-carrier recognition at the luminal side, a conformation change of the luminal carrier from luminal-facing orientation to abluminal-facing orientation, solute diffusion, a conformation change of abluminal carrier from luminal-facing orientation back to abluminal-facing orientation, and release of drug [119] (**Figure 3-6)**. Glucose transporters are abundantly expressed on both luminal and abluminal sides of BBB. One example using glucose transporters attempted to deliver the kynurenic acid (KynA) derivative 7-chlorokynurenic acid 7ClKynA, a neuroprotective agent incapable of crossing the BBB,

severally limiting its therapeutic effects [128]. Conjugating D-glucose via the 6-hydroxyol group to esterified 7ClKynA improved anticonvulsive activity compared to unconjugated free 7ClKyn and other controls. This is because D-glucose ester 7ClKynA conjugates could cross the BBB via glucose transporter 1 (GLUT1) CMT. One study shows a glucosylated polymeric micelle could successfully cross the BBB via GLUT1 CMT and improve the accumulation in the mice brains [129].

Organic anion transporting polypeptides (OATPs) are another type of carrier that are promising for BBB CMT transcytosis. OATPs could be used for both endogenous substrates and therapeutic drug transports, including thyroid hormones, steroid hormones, bile salts, statins and anticancer drugs [119,130–132]. The expression of organic anion-transporting polypeptide 1a4 (OATP1a4) in rats increases during hypoxia/reoxygenation, which provides an opportunity for delivering drug through OATP CMT [133]. One limitation of CMT is that it may be limited by the large molecular sizes of some therapeutic drugs. Unlike RMT that allows transport of large therapeutic cargos, CMT is more applied to deliver small therapeutic cargos with molecular weights less than 600Da [134]. Another limitation is the high stereoselectivity requirement of the vector, since CMT doesn't involve vesicle formation and the carrier only bind to endogenous and/or endogenous-like substrates [119,121,135].

3.3.3.3 Adsorptive-mediated transcytosis (AMT)

Adsorptive-mediated transcytosis (AMT) is a nonspecific way that allows drugs to cross the BBB [120]. The AMT process starts with electrostatic interactions between the negatively-charged cell membrane and positively-charged peptides/proteins used to drive adsorption [120,126] (**Figure 6)**. AMT uses cationic cell-penetration peptides (CPPs) and cationic proteins to interact with the negatively-charged brain endothelial cell membranes and cross the BBB [120]. Syn-B vectors, a family of linear peptides derived from antimicrobial peptide protegrin 1 (PG-1), and trans-activator of transcription (Tat)-derived peptides are two examples of CPPs. Cationized bovine serum albumin (CBSA) is an example of a cationic protein commonly used in AMT [122]. When the peptides or proteins nonspecifically bind to the luminal cell membrane, vesicles form and undergo endocytosis [119]. The endocytosed vesicle transports the drug to the abluminal side followed by exocytosis. Unlike CMT, AMT is not limited by cargo size and not stereo-selective. Furthermore, compared to RMT and CMT, the ligand of AMT has a higher saturated

concentration at the binding site, which allows a large substrate binding capacity. A study shows the BBB permeation and brain delivery of dalargin are enhanced in mice via SynB vectors AMT [136]. One limitation of AMT is, similar to RMT, the endocytosed cargo vesicles inside the cell in AMT are also subject to lysosomal degradation, which decreases transport of therapeutic cargos to the abluminal side [120]. Another limitation of AMT is that nonspecific binding increases the chance of failure by being unable to differentiate between on-target and off-target cell membranes. This lack of specificity poses a risk of off-target side effect throughout the body. Because of the nonspecific binding, AMT is rarely applied in transporting drugs through the BBB [122].

3.4. Current polymeric nano-carrier fabrication method

3.4.1 Emulsion Evaporation

Emulsion evaporation was the first NP fabrication method developed using polymer [137,138]. The earliest application of NP synthesis via emulsion evaporation was for the development of a drug carrier using biodegradable polymers [137–140]. Commonly used polymers in emulsion evaporation include alpha hydroxyl esters like PLGA, PLA, and PCL along with their copolymers; PEG-PLGA, PEG-PLA, PEG-PCL, all of which can hydrolytically degrade in the presence of water or be biodegraded by esterases [138]. The organic solvent used to dissolve the polymer should be volatile and immiscible or partially miscible with the aqueous phase antisolvent (water) [137–139]. Dichloromethane (DCM) and chloroform were commonly used organic solvent in the past, but now ethyl acetate is gaining greater use because of its safer toxicological profile [137,138].

There are two major types of emulsions: an oil in water (O/W) single emulsion, and a water in oil in water (W/O/W) double emulsion [137]. The O/W single emulsion works well for encapsulating hydrophobic drugs. The W/O/W double emulsion further develops the O/W single emulsion further to encapsulate hydrophilic drugs. For O/W single emulsions, the polymer and the hydrophobic drug both dissolve in the organic solvent [141]. Upon addition to the aqueous phase, the organic phase forms an O/W emulsion under high shear force, such as ultrasonication or high-speed homogenization [137,141] (**Figure 3-7**). The organic solvent evaporates by continuous room temperature stirring or stirring under reduced pressure or vacuum to form the solid NPs

[137,139,141]. The NPs can then be collected by centrifugation [137,139]. For W/O/W double emulsion, the hydrophilic drug dissolves in the inner aqueous phase and emulsifies with the polymer-containing organic phase. The W/O emulsion will then be emulsified into an outer organic phase, forming a W/O/W double emulsion. The remaining organic solvent evaporations and the collection steps are the same as O/W single emulsion.

A common challenge with emulsions is the lack of stability of particle size caused by aggregation during synthesis or evaporation steps. Polyvinyl alcohol (PVA), Span 40 and pluronic F68, which have both hydrophobic and hydrophilic parts, stabilize emulsions when added to the aqueous phase [137,138]. The hydrophobic parts of the stabilizer interact with the inner oil phase, and the hydrophilic parts reach out to the outer aqueous phase to alleviate the surface tension. For single emulsions, higher PVA concentrations in the aqueous phase lead to smaller particle sizes [137,142]. For W/O/W double emulsions, increasing the PVA concentration in the inner aqueous phase will decrease the particle size, but the PVA concentration in outer aqueous phase has little effect on particle size [137,142]. The major challenges of the emulsion evaporation are during time-consuming solvent evaporation step, where there is a chance of drug loss from the nascent NPs and a risk of particle coalescence [137]. Such risks are amplified in NP synthesis, as opposed to microparticle synthesis, given the higher surface to volume ratio.

3.4.2 Nanoprecipitation

Nanoprecipitation is a simple, quick, economical and reproducible method to form NPs from polymers [137,138]. The major components of nanoprecipitation are the selected polymer, an organic solvent that dissolves the selected polymer, and an aqueous antisolvent in which the selected polymer is insoluble [137,143]. Commonly used polymers for nanoprecipitation include the alpha hydroxyl esters noted previously, PLGA, PLA and PCL. The organic solvent and aqueous antisolvent must be miscible with each other. Acetone and water are the most commonly used organic solvent:antisolvent pair [138].

The polymer is first dissolved in organic solvent. The polymer concentration in the organic solvent needs to be dilute to semi-dilute for the nanoprecipitation [138]. The organic phase is then added dropwise to the aqueous antisolvent while gently stirring [137,141] (**Figure 3-7**). When the organic solvent diffuses to the aqueous phase, the solute becomes supersaturated in the

organic phase [144]. When the solute concentration exceeds the critical supersaturation concentration, crystal nuclei form and the solute concentration decreases. Nuclei will continue to form until the solute concentration dips below the critical supersaturation concentration point. When the solute concentration is below the critical supersaturation concentration point, nuclei grow as the solute transfers from the bulk solution to the nuclei interface and then condenses. The process of condensation stops after the solute concentration reaches below the equilibrium saturation concentration.

The formation of NPs is instantaneous after adding organic phase to aqueous solvent [141]. However, when attractive forces are greater than repulsive forces, particles collide and adhesion will happen [144]. Although surfactant is not mandatory in the nanoprecipitation, it could be added to the aqueous phase to prevent particle adhesion and particle agglomeration [137,144]. The NPs formed by nanoprecipitation have a narrow size distribution [141,145]. Common factors that affect NP size are polymer concentration, drug concentration, organic phase to aqueous phase ratio and aqueous stirring rate [141,145,146]. Larger polymer concentration and/or a high drug concentration will increase the viscosity, which hinders the diffusion of organic solvent to the aqueous phase, leading to a larger NP size [145]. A high drug concentration could also form more nuclei at organic/aqueous interface, which could cause aggregate and a larger NP size. Larger stirring rate decreases the NP size by enhancing mass transfer and the solvent diffusion rate. If the organic/aqueous phase is too low, the external energy from the stirring needs to be applied to a larger amount of aqueous phase, leading to weaker breakdown of droplet and a larger NP size [146]. On the other hand, if the organic/aqueous phase is too high, viscosity will increase, and a larger NP will be formed.

Nanoprecipitation is mostly used for hydrophobic drugs, for example curcumin for anti-cancer therapy [147] and triiodothyronine for ischemic stroke treatment [148]. However, it has recently been modified to encapsulate hydrophilic drugs [141] (e.g. antibiotics ciprofloxacin [149] and the antioxidant N-acetylcysteine (NAC) [150]).

One limitation of nanoprecipitation is that the drug loadings are low in many cases [151]. Drug loadings for many hydrophobic drugs are in the range of 0.2% to 17%. The low drug loading means the small fraction of the drug relative to the total mass requires larger NP administration amounts in order to reach the targeted therapeutic drug concentration [152]. This

increase of total amount of NPs administrated may cause systemic toxicity to the body due to the great amount of non-therapeutic ingredients.

3.4.3 Emulsion Diffusion

Emulsion diffusion is an efficient way of fabricating NPs with great reproducibility and simple scale-up amenability [138,153] Emulsion diffusion requires an organic solvent that is partially miscible with aqueous antisolvent. The organic solvent and the aqueous antisolvent need to be mutually saturated with each other [138,141,153,154] (**Figure 3-7)**. Because the organic solvent and aqueous antisolvent are partially miscible, this allows the two phases to become mutually saturated with each other. To obtain mutual saturation, organic solvent and aqueous antisolvent with equal volumes are added to a separation funnel to allow the phases to separate [138]. The bottom phase is the organic solvent-saturated aqueous antisolvent, and the top is aqueous antisolvent-saturated organic solvent. Commonly used polymers include PLGA, poly(D,L-Lactic Acid) (PDLLA), and PCL [138,155]. Ethyl acetate, benzyl alcohol, methyl acetate and propylene carbonate could be used for organic solvent in emulsion diffusion and water is the most widely used aqueous antisolvent [138,153].

The organic phase that composes both the polymer and the drug in the water-saturated organic solvent is first added into the aqueous phase that composes organic solvent saturated water and surfactant [138,141]. Next, the organic phase and aqueous phase form an O/W single emulsion [138]. A probe sonicator, although it is not required, could provide high energy to emulsify the phases, and adding surfactants like PVA, pluronic F68, or sodium dodecyl sulphate (SDS) stabilize the emulsion system [138,141]. The O/W single emulsion is suitable for encapsulating hydrophobic drugs. Like the emulsion evaporation method, a W/O/W double emulsion could be also developed from the O/W single emulsion in the emulsion diffusion method for encapsulating hydrophilic drugs. After forming the emulsion, a large amount of water should be added to the aqueous phase [138]. With this aqueous phase dilution, the organic solvent diffuses from the emulsion droplet to the aqueous phase, causing local superstation, and forming the NPs in milli-seconds [138,153]. The factors that affect the NPs size are polymer concentration, organic solvent and aqueous antisolvent miscibility, stirring rate, and surfactant concentration [138]. NP size increases with higher polymer concentration and decreases with higher organic solvent and aqueous antisolvent miscibility, higher stirring rate, and higher surfactant concentration.

After the NP formation, cross-flow filtration is a useful purification method to separate the NPs from the bulk liquid [153].

3.4.4 Salting-out

Salting-out is a modified version of the emulsion diffusion method [137,139]. Like emulsion diffusion, salting out frequently uses PLGA and PDLLA polymers [137,138,155,156]. However, salting out requires miscible organic and aqueous phases and doesn't require using surfactants and chlorinated organic solvents that may pose a hazard to the body and the environment [137,139,141]. Acetone and tetrahydrofuran (THF) are commonly used as organic solvents and water is most commonly used as the aqueous phase [141].

The salting-out method is suitable for encapsulating hydrophobic drugs [139]. The polymer and the drug dissolve in the organic solvent and the electrolyte dissolves in the aqueous phase [139,141] (**Figure 3-7**). Although not required, a surfactant is typically added to the aqueous phase to stabilize the emulsion [137,138]. Magnesium chloride, magnesium acetate and calcium chloride are commonly used electrolytes to hold the water for their solubilization, thus lowers the miscibility of the organic solvent to water [137–139]. Practically, the organic phase emulsifies into the aqueous phase by using an overhead stirrer, which provides the high shear forces needed to form the emulsion [138,141]. No organic solvent diffusion occurs at this point due to the presence of electrolyte in the aqueous phase [141]. Next, a great amount of water will be added into the emulsion, and the organic solvent then diffuse from the polymer phase to the aqueous phase due to the reverse salting-out effect and NPs will be formed [137,138,141]. The electrolyte and organic solvent residue could be removed by cross-flow filtration [157]. A limitation associated with the salting-out method is the drug encapsulation efficiency of the NPs may be hindered due to the large amount of washing and purification required by the initial presence of electrolytes [139].

3.4.5 Dialysis

Dialysis is a simple fabrication method that forms small NPs with a narrow size distribution [137,139]. The mechanism of dialysis fabrication method still needs more investigation, but it is assumed to be similar to the nanoprecipitation method [137,158]. The organic phase is composed of the polymer, the drug, and an organic solvent while the aqueous phase is composed of an antisolvent miscible with the organic solvent [137]. Like the nanoprecipitation method,

dialysis works well for encapsulating hydrophobic drugs. Similar to other polymeric NPs fabrication methods, PLGA, PDLLA, and pullulan acetate (PA) are suitable polymers for dialysis [137,159]. Dimethylformamide (DMF), dimethyl sulfoxide (DMSO), N-methyl-2-pyrrolidinone (NMP) and dimethylacetamide (DMAc) are widely used for organic solvent and water is the most commonly used for antisolvent [137,139,160].

The polymer and the drug dissolves in the organic solvent, and the organic phase is put inside a dialysis tube with suitable molecular weight cut-off that sever as a physical barrier for the polymer but permeable to the organic solvent and water [137,139] (**Figure 3-7**). When placed in excess aqueous phase, the organic solvent inside the dialysis tube is displaced by the water [137,139,158]. The organic solvent displacement causes loss of polymer solubility, which precipitates into NPs [137].

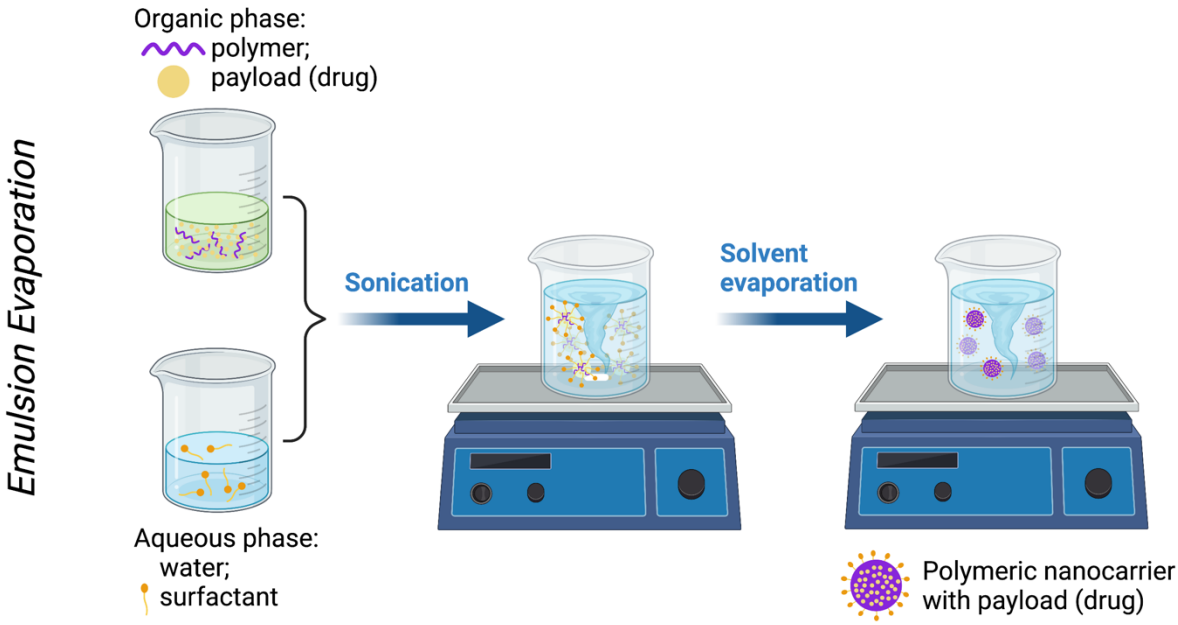

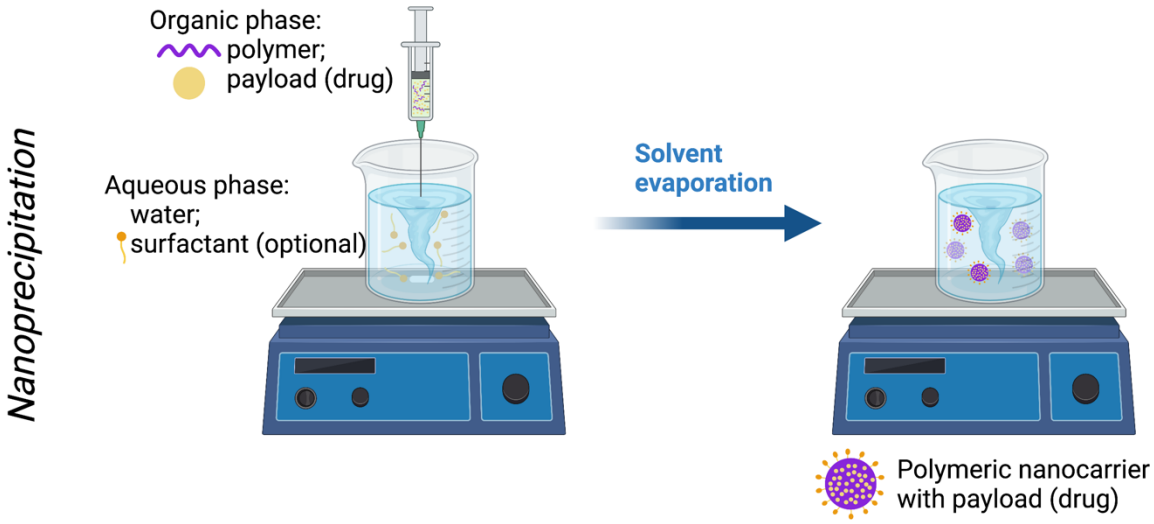
Nanoprecipitation
Organic phase:
polymer;
payload (drug)
Aqueous phase:
water;
surfactant (optional)
Solvent
evaporation
Polymeric nanocarrier
with payload (drug)

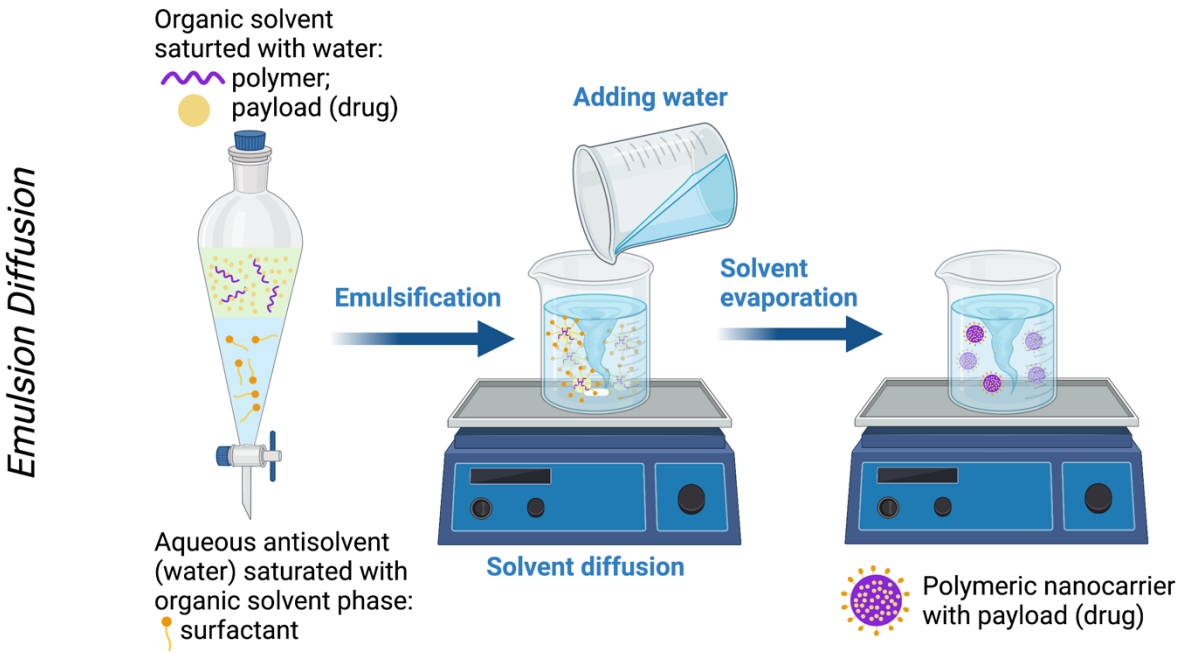
Emulsion Diffusion
Organic solvent
saturted with water:
polymer;
payload (drug)
Adding water
Emulsification
Solvent
evaporation
Aqueous antisolvent
(water) saturated with
organic solvent phase:
surfactant
Solvent diffusion
Polymeric nanocarrier
with payload (drug)

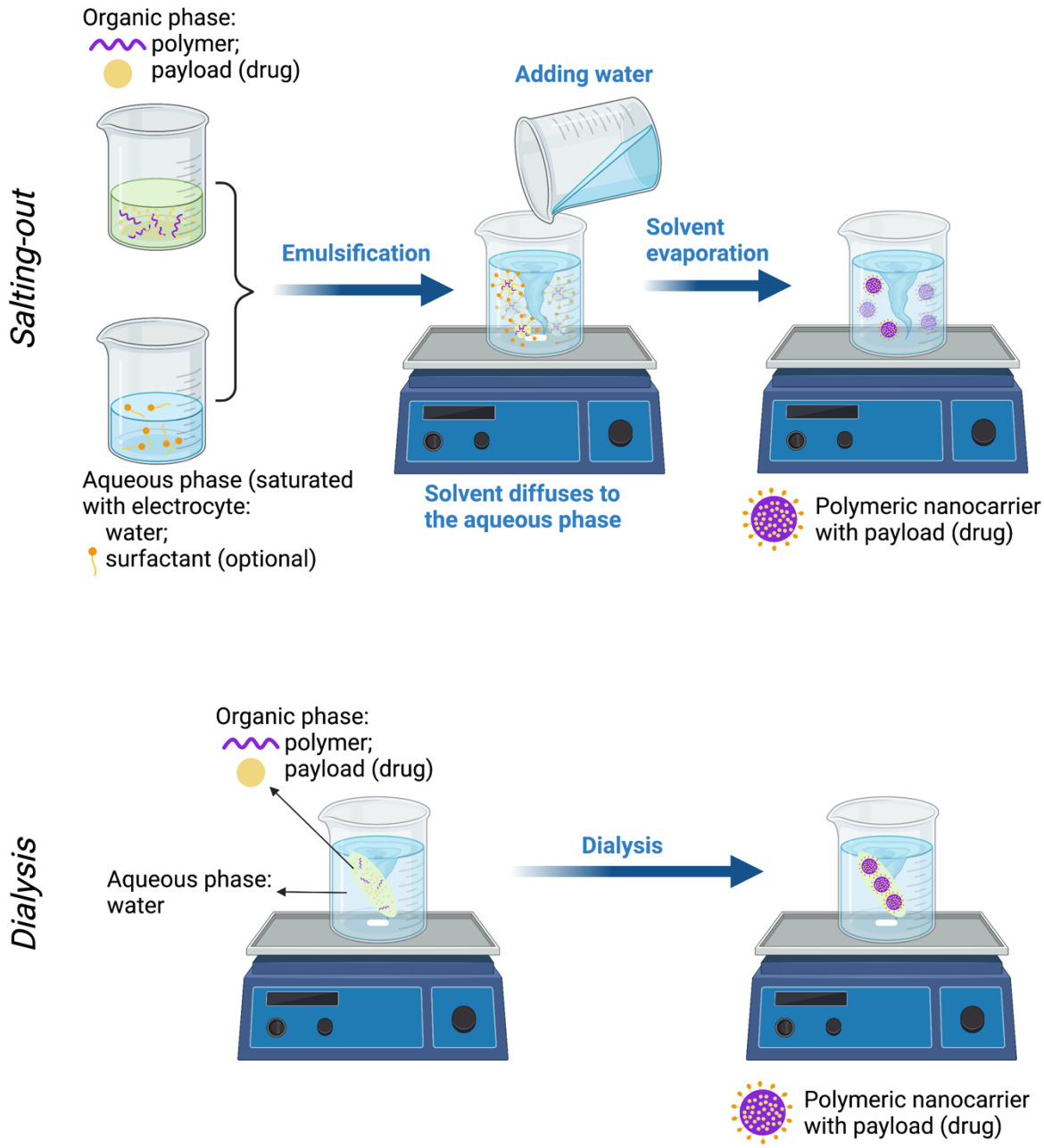

Figure 3-7. Common fabrication methods for polymeric nanocarriers. (A) Solvent evaporation method. **(B)** Nanoprecipitation method. **(C)** Emulsion diffusion method. **(D)** Salting-out method. **(E)** Dialysis method. Created with BioRender.com.

3.5. Targeted and triggered polymeric nano-drug delivery

3.5.1 (Bio)chemical strategies to functionalize nanocarriers

In this section, a non-covalent conjugation strategy, biotin-(strept)avidin interaction, and two covalent carbodiimides conjugation strategies will be discussed. Those (bio)chemical strategies are widely used to functionalize nanocarriers with multiple purposes, such as adding targeting moieties, imparting multivalent functionalities and/or modifying polymers for prolonging the circulation time of the nanocarriers in the bloodstream.

3.5.1.1 Biotin-(strept)avidin interaction

Biotin-(strept)avidin interaction is one of the strongest non-covalent interactions known, involving both hydrogen bonding and hydrophobic interaction [161,162]. The biotin-(strept)avidin interaction has high affinity with an extremely low dissociation constant, $K_{d,}$ in the order of 10^{-15} M. The biotin-(strept)avidin interaction has high resistance to extreme temperature and pH, denaturing reagents and proteolytic enzymes [162,163].

Avidin is a tetrameric protein derived from avian, reptile, and amphibian eggs [162]. A maximum of four different biotinylated ligands and/or molecules could bind to a single avidin with high affinity and specificity. Avidin has a basic PI (~10) and glycosylated, which prone to bind nonspecifically with tissue *in vivo* and elicit immune response. Streptavidin is the most commonly used avidin analogue that derived from *Streptomyces avidinii*. Streptavidin is non-glycosylated with a slightly acidic PI (~5-6), which could overcome the limitations that caused by avidin. Similar to avidin, streptavidin also has four binding sites for biotins. The multivalency of (strept)avidin gives the opportunity to employ multiple ligands with different purposes to the same (strept)avidin backbone for optimal targeting delivery.

Sumbria and coworkers employed the biotin-avidin interaction between monoclonal antibody-avidin fusion protein (HIRMAb-AV) and the biotinylated ^{125}I idolized Aβ^{1-40} peptide radiopharmaceutical to form the Aβ/HIRMAb complex for AD brain imaging [164]. This Aβ/HIRMAb complex successfully cross the BBB and deliver Aβ^{1-40} peptide radiopharmaceutical to image the AD brain amyloid plaque. The HIRMAb part acts as the molecular Trojan horse to cross the BBB via human insulin receptor (HIR)-mediated transcytosis.

3.5.1.2 Covalent Carbodiimide conjugation strategies

3.5.1.2.1 EDC/Sulfo-NHS

Carbodiimides are popular crosslinkers for conjugation of peptides and proteins to the surface of polymeric NPs, or conjugation between hydrophilic and hydrophobic polymers to form functionalized polymeric micelles [165,166]. 1-ethyl-3-(3-dimethylaminopropyl)carbodiimide hydrochloride (EDC) is a widely used zero-length crosslinker which forms an amide bond between an amine and a carboxylate group. The carboxylate group acts as the nucleophile and donates its electron pair from the oxygen to the carbon of the EDC carbodiimide group to create an O-acylisourea active-ester intermediate. However, the O-acylisourea active-ester intermediate is short-lived and prone to hydrolysis [166]. Adding water-soluble *N*-hydroxysulfosuccinimide (Sulfo-NHS) to the coupling reaction forms a sulfo-NHS ester intermediate, which is a more stable and soluble active-ester immediate. The sulfo-NHS ester intermediate then reacts with primary amines to form an amide bond [165]. The typical amine bond formation reaction time after dissolving all reagents is 2 hours. The isourea byproduct is also water soluble. Since all the reagents, intermediates, byproducts and final products in EDC/sulfo-NHS coupling reaction are water-soluble, this reaction is suitable for amide bond formation in peptide and protein-friendly aqueous environments. The final product will be purified by centrifugation, gel filtration or dialysis. EDC/Sulfo-NHS reactions can be used to bioconjugate desired peptides to any nanocarriers that have carboxylic acid group on the surface, like PLGA acid-end NPs, to impart varied function such as the targeting ability of NPs [166].

There are several practical considerations to observe when using this strategy. In order to preserve its stability for a long-term storage, both reagents EDC and Sulfo-NHS need to be stored in the dry, cool, well-ventilated places. Since EDC is moisture-sensitive, EDC needs store at -20°C with a desiccant [165]. Before using it, the container should be closed until equilibrates to the room temperature to avoid moisture condensation on EDC, thereby avoiding hydrolysis. The EDC/sulfo-NHS coupling reactions are most efficient in the range of pH 4.5-7.2, and they could be done in an adapted two-step procedure [165,167–169]. 2-(N-morpholino)ethanesulfonic acid (MES) buffer at pH of 4.7-6.0 is recommended for the first part, sulfo-NHS ester formation [165]. This is because in order to form the ester intermediate efficiently, EDC needs to be protonated [169]. In the meantime, enough carboxylate needs remain in its deprotonated form. EDC also undergoes hydrolysis at low pH, so avoid using a pH that is too low [165,168]. After that, raising the pH to >7 with sodium phosphate buffer immediately prior to the second part, the amide bond formation, allows the amine to be deprotonated in order to react effectively [165,168,169].

3.5.1.2.2 DCC

Dicyclohexyl carbodiimide (DCC) is an organic soluble coupling agent that is most widely used for water-insoluble reactions, such as peptide and copolymer synthesis that conducted in organic solvent (e.g. synthesis of PLGA-*b*-PEG-COOH copolymer) [165,170,171]. Hydrolysis is a main issue for the reactions in aqueous environments [165]. For some reactions that do not require aqueous solvent, DCC could avoid this hydrolysis issue. O-acylisourea active-ester intermediate will be formed when DCC reacts with carboxylate group. NHS could be also utilized to form NHS ester intermediate. The byproduct dicyclohexyl urea (DCU) is also water insoluble and the final product need to be purified by washing with organic solvent. PLGA-*b*-PEG-COOH copolymer could be formed via the DCC/NHS coupling reaction [171]. PLGA is first activated with DCC and N-hydroxysuccinimide (NHS) in dichloromethane solvent at room temperature for 24 hours to form PLGA-NHS. Then, the activated PLGA-NHS reacts with NH_2-PEG-COOH in chloroform solvent, with an organic soluble base N,N-diisopropylethylamine (DIPEA), at room temperature for another 24 hours to form PLGA-*b*-PEG-COOH copolymer. PLGA/PEG copolymer is frequently used to synthesize PEGylated NPs [172,173]. With combinations of other surface modification (bio)chemistries, PLGA-*b*-PEG-COOH copolymer could be used to synthesize PEGylated targeted NPs with an extended half-live when circulating in the bloodstream [59–62].

For safety considerations, both reagents DCC and NHS need to be stored in the dry, cool, well-ventilated places. DCC is recommended to be stored at -20°C and the container needs to warm to room temperature to prevent water condensation before opening it. Extra attention needs to be taken when working with DCC since its vapors are extremely dangerous to breathe in and when coming into contact with eyes [165].

3.5.2 Smart/responsive polymeric nanocarrier

3.5.2.1 pH-responsive polymeric nanocarrier

Biological differences in pH throughout the human body and in response to disease states present an opportunity for pH-responsive drug delivery [174,175]. For example, the pH in the stomach is ~2 and the pH in the intestinal tract is ~7. Intracellular pH varies greatly based on the location within the cell, for instance organelles like lysosomes have acidic pH of ~5 [176]. This is

used in some applications to release drugs inside a cell. Healthy tissue and blood have an extracellular pH of 7.4, often described as a "physiological" pH, although this characterization lacks nuance. Such a pH of 7.4 is distinctly different from a pathological pH. For instance, ischemic tissue undergoes acidosis, dropping the pH below 7 [177,178]. In a rodent model of focal ischemic stroke, the pH is 6 in the ischemic core and 6.5-6.9 in the penumbra [178]. To our best knowledge, the patterns of how the pH-responsive nanocarriers behave within the same ischemic brain with heterogenous pH remain unclear. The extracellular pH near gliomas is also below 7 due to the high glycolysis rate of cancer cells and lactic acid production [174,175,179]. Thus, a pH-responsive polymeric nanocarrier could effectively target an environment with a pathologically acidic pH, such as the acidic environment in ischemic stroke and glioma [177,179,180].

The mechanisms of pH-responsive nanocarriers for targeting acidic environments includes protonation and cleavage of acid liable bonds [174]. A pH-responsive polyion complex (PIC) nanocarrier using a positively charged poly(ethylene glycol)-b-poly[4-(2,2,6,6-tetramethylpiperidine-1-oxyl)aminomethylstyrene] (PEG-b-PMNT) copolymer and a negatively charged poly(acrylic acid) (PAAc) polymer delivered two payloads to the ischemic penumbra region in middle cerebral artery occlusion (MCAO)-injured mice [177]. The PIC nanocarrier releases the drugs inside the blood vessel when it reaches the acidic ischemic penumbra region. The nanocarrier collapses due to polyamine protonation of the PMNT segment in the acidic environment, releasing tPA and an antioxidant within the ischemic tissue. This pH-responsive nanocarrier successfully reduced infarct volume and improved locomotor function. In another designer example, PEG-poly(β-amino ester) (PBAE) was used to construct a pH-responsive micelle [181]. Under physiological pH, the PBAE segment is hydrophobic, which is on the inside of the micelle. The PEG is on the outside since it is hydrophilic. For the pH below 7, this pH-responsive micelle becomes positively charged due to protonation of the amino group of the (PBAE) segment. In an acidic environment using the MCAO model in vivo, fluorescein-labeled proteins that were originally encapsulated in micelles accumulated more than fluorescein-labeled proteins without the micelles in ischemic tissue. The fluorescein-labeled proteins are not in the healthy brain tissue, demonstrating enhanced micelle uptake and subsequent protein release from pH-responsive micelles.

3.5.2.2 Redox-responsive polymeric nanocarrier

Redox-responsive nanocarriers are increasing in popularity for intracellular drug delivery for diseases involving different redox potential, including cancer, ischemic stroke, and AD [182–185]. Reactive oxygen species (ROS) and reducing agents such as glutathione (GSH) regulate the intracellular and extracellular redox states in the body [182]. GSH is the most prominent naturally produced antioxidant. When oxidized, two GSH molecules form a disulfide-linked GSSG dimer. GSH concentration then is closely related to redox potential: high intracellular GSH concentrations provide a reducing environment inside the cell. A typical intracellular GSH concentration ranges from 2-10 mmol, much higher than the GSH concentration (approximately 2-20 umol) in the extracellular environment. Furthermore, within cancer cells, the GSH concentration is more than four times higher than healthy cells [183]. ROS play significant roles in redox homeostasis and cell signaling, but their overproduction and accumulation cause oxidative stress [182,186]. The elevated ROS levels in CNS diseases, for examples, in ischemic stroke and AD, could serve as targets for therapeutic delivery [184,187]. Thus, the differences in redox states inside the body, in physiology and/or disease pathology, makes the redox-responsive nanocarrier suitable for targeted drugs delivery to cells or tissue with elevated ROS levels.

Redox-responsive nanocarriers could be functionalized through redox-responsive drug-linking chemistry. The link is fabricated using disulfide bonds which can only be cleaved under a reducing intracellular environment. In biological tissues, such cleavage is catalyzed by enzymes such as by GSH or other antioxidant biological systems like catalase and superoxide dismutase [188]. Markoutsa et al. successfully developed a redox-responsive nanocarrier by first conjugating NAC to the poly[(2-(pyridin-2-yldisulfanyl)-co-[poly(ethylene glycol)]] (PDA-PEG) copolymer, then make nanocarrier from NAC-PDA-PEG from crosslinking reaction via disulfide bonds. The NAC releases by disulfide bond cleavage under high cytosolic GSH concentration. These NAC redox-responsive nanocarriers exert both antioxidant and anti-inflammatory effects on lipopolysaccharide (LPS)-activated murine microglial cells in vitro, an important preclinical result that could lead to benefits in CNS disease treatment, like AD. Another type of NAC-conjugated polymeric nanocarrier, hydroxyl-terminated poly(amidoamine) (PAMAM) dendrimers conjugated with NAC, presents an option for on demand NAC delivery[189]. While the neuroprotective and anti-inflammatory effects of dendrimer-N-acetyl cysteine (D-NAC) is reviewed elegantly for various brain diseases-related animal models[189], this drug nanocarrier strategy has specifically been used to treat hypoxia in neonatal mouse brains [190], mouse retina [191],

and mouse models or Rett syndrome [192]. Lu et al. applied an amphiphilic redox-responsive polymer PEG-LysB to form redox-responsive micelles for targeted AD treatment [185]. They encapsulated a hydrophobic drug curcumin within the micelle interior compartment created by the LysB hydrophobic polymer segment. The micelle exterior was decorated with amyloid beta (Aβ) protein derived peptide (KLVFFAED). This Aβ derivative targets the receptor for advanced glycation end-products (RAGE) which is highly expressed on the BBB, microglia, and neurons in AD. The hydrophobic polymer segment degrades under elevated ROS level and the amphiphilic polymer then becomes more hydrophilic. As the micelles collapse due to the change in hydrophobicity, curcumin is released. The redox-responsive micelles can modulate the overactive microglia from the early AD progression phase and are neuroprotective in a transgenic AD mouse model.

3.5.2.3 Hypoxia-responsive polymeric nanocarrier

A shortage of oxygen supply around gliomas and after ischemic stroke leads to hypoxia in the surrounding tissue [182,193]. The partial pressure of oxygen is nearly zero in ischemic stroke tissue and tumor, whereas the partial pressure of oxygen is 30 mmHg in healthy tissue [182]. Hypoxic tumor tissue also exhibits a reducing and/or acidic microenvironment due to lactate generation through anaerobic respiration. In stroke, hypoxic ischemic environment presents simultaneously with oxidative environment because of the surplus of ROS. In theory, hypoxia-responsive nanocarriers can be combined with other stimuli, i.e., redox and/or pH sensitivity, and designed for tumor or stroke targeted drug delivery. To create technologies targeted toward such an environment, researchers employ common hypoxia-responsive moieties such as nitroimidazoles, quinones, aliphatic and aromatic amine oxide, and azobenzene [194].

2-Nitroimidazoles (NIs) are the most widely used moieties in designing hypoxia-responsive nanocarriers since they are highly responsive and could convert to 2-aminoimidazoles (AIs) under hypoxia situations [182,195]. Deng et al. developed amphiphilic micelles using the hypoxia-responsive copolymers poly(ethylene glycol)-block-poly(methacrylic acid-co-2-nitroimidazole methacrylate) (PEG-b-P(MAA-co-NIMA)) to encapsulate doxorubicin (DOX), a hydrophobic cancer treatment drug, in the hydrophobic polymer segment [195]. Under hypoxia, the hydrophobic NI groups transform into hydrophilic AI groups through the reducing nicotinamide adenine dinucleotide phosphate (NADPH) catalytic reaction. The micelles then collapse,

releasing DOX. In a different approach, the azo bond group renders NPs hypoxia-responsive [196]. This hypoxia-responsive drug delivery system is composed of a hydrophobic black hole quencher 3 (BHQ3) containing an azo bond, conjugated to the hydrophilic carboxymethyl dextran (CMD) via an amide bond. The BHQ3 assembles into a hydrophobic core, loaded with the hydrophobic drug DOX, surrounded by a CMD hydrophilic shell. Under hypoxia conditions, the azo bond in BHQ3 cleaves, converting the hydrophobic BHQ3 to a hydrophilic aniline derivative, collapsing the NPs, and releasing the payload. The CMD-BHQ3 NPs loaded with Cyanine 5.5 show a higher near-infrared (NIR) fluorescence intensity in the tumor tissue of the tumor-bearing mice, compared to liver, lung, spleen, kidney, and heart, which demonstrates the effective tumor-targeting in vivo. To our best knowledge, the hypoxia-responsive concepts are not applied to the brain yet, but the preclinical successes of hypoxia-responsive nanocarriers for cancer applications shows a promising perspective for them to the future applications in the brain.

3.5.2.4 Enzyme-responsive polymeric nanocarrier

Enzyme-responsive polymeric nanocarriers could specifically release their payload at targeted disease locations where enzyme levels change. Enzymes, such as proteases, lipases, phospholipases and glycosidases, perform highly selective and specific reactions under mild, physiological conditions [175]. In some disease states, such as in ischemic stroke, cancer and inflammation, certain enzyme levels are overexpressed [175,197]. For example, the levels of MMPs, a group of endopeptidases, are elevated in the brain after ischemic stroke and during glioma invasion and metastasis [197,198]. Engineered materials can be designed to take advantage of this upregulated activity to feature tunable, on demand, release where and when it is needed. However, the substrates may overlap with enzymes of similarly connected families, emphasizing the need for researchers to pay careful attention to substrate diversity and selection [182].

Enzyme-responsive nanocarrier systems rely on enzyme-cleavable peptides. The peptide cleavage of the nanocarrier could reveal its functions that were previously protected and/or confer structural changes to it. Guo et al. successfully developed an enzyme-responsive nanocarrier systems that utilize size changes to better deliver payload to the ischemic stroke area [197]. The nanocarrier system decreases in size after enzymatic cleavage (resulting in “size-shrinkable” NPs). Size-shrinkable NPs include two PEG regions, one protease-responsive

peptide section, one PCL section, and a stroke targeting ligand section. Upon reaching the ischemic microenvironment, thrombin cleaves the protease-responsive peptide, causing NP size to decrease, facilitating BBB penetration. The size-shrinkable NPs had better targeting efficiency than nonresponsive control NPs and "size-expandable" NPs. Therapeutically, the size-shrinkable NPs upregulated the release of glyburide in the presence of thrombin, affording acontrolled release strategy. Gao et al. incorporated a MMP-2 activatable cell-penetrating peptide (ACP) composed of a series of 8 glutamic acid residues (E8) linked to an MMP2-cleavable PLGLAG sequence, followed by a series of 8 arginine (R8) residues in constructing an enzyme-responsive PEG-PLC nanocarrier system for glioma treatment [198]. They also conjugated an angiopep-2 ligand to their PEG-PLC nanocarrier, for crossing BBB and targeting to the glioma area. The angiopep-2 has high affinity for the low-density lipoprotein receptor-related protein 1 (LRP1), which is overexpressed on both the BBB and glioma cells. Before MMP-2 cleavage of PLGLAG linker, the positively charged arginine residues were protected in the blood circulation by the negatively charged glutamic acid residues. After reaching the glioma area, the elevated local MMP-2 cleaved the PLGLAG linker, allowing R8 to regain its cell penetrating function. The dual-targeted NPs with both ACP and angiopep-2 showed strong MMP-2 responsiveness, and had the highest targeting efficiency compared to single-targeted and non-targeted NPs. For NPs with the anticancer drug docetaxel, the dual-targeted NPs had the improved the survival rates the most in glioma-bearing model mice compared to other single-targeted and non-targeted NPs.

3.6. Concluding Remarks

Polymeric nanocarriers have several advantages in encapsulating both hydrophobic and hydrophilic drugs, making them promising for drug delivery to the CNS system. Their nano-scale size and large surface-area-to-volume ratios give them great potential of 1) crossing the BBB and 2) locally targeting the desired area via minimally invasive intravenous administration. Furthermore, the methods for constructing polymeric nanocarriers are quick, simple, efficient, and scalable. Adding stimuli-responsive components to the polymeric nanocarriers can improve upon passive release methods by preventing undesired release before reaching to targeted area. While we have focused on polymeric nanocarriers, numerous other forms of non-polymeric nanoparticles are useful in understanding and treating brain disease. A more rigorous review of

the broad classes and applications of nanoparticles in health and disease can be found in an excellent text edited by Chung, Leon, and Rinaldi-Ramos [199].

Core-shell nanocarriers are of great interest in developing better drug delivery systems because they allow a more controlled and sustained release of the drug in the core due to the additional shell layer. While challenging to synthesize as the nanoscale, the concept is common in the polymeric microparticle field. If you want to deliver both hydrophobic and hydrophilic drugs or deliver two different drugs at different release rates, adding the hydrophilic drug or the desired rapid release drugs to the shell layer could achieved this. The additional shell layer could be either polymer-based or lipid-based. For example, Tahir et al. constructed lipid polymer hybrid nanoparticles (LPHNPs), which have PLGA polymer cores and lecithin shells to delivery both hydrophobic drug doxorubicin and hydrophilic drug doxorubicin hydrochloride to the cancer cells in a controlled manner [200]. These core-shell concepts in targeted polymeric nanocarriers may be a critical technology for next-generation CNS treatment.

As mentioned in Section 3.2, sterilization is still a challenge for nanocarriers before transforming to the clinical settings. Building a strategy to prevent viral, bacterial, and/or fungal contamination into the nanoparticle itself could play a role in prolonging shelf life or minimizing drug or particle degradation due to high energy sterilization procedures. For instance, silver nanoparticles have antibacterial ability with safe toxicity in vivo [201]. Thus, we could potentially encapsulate sliver nanoparticles inside polymeric nanocarriers, to give them self-sterilizing properties. Alternatively, a silver-ion immobilized film could also potentially add the self-sterilizing properties to a drug delivery system [202]. Thus, we could potentially apply the sliver nanoparticles inside the polymer matrix or coat nanocarriers with silver ions for clinical use.

Other strategies can modulate the physical form of nanoparticles. For instance, modifying the deformability of a particle may potentially enhance vascular targeting [203]. Another physical feature is the shape factor – creating non-spherical particles has historically been challenging at the nanoscale. However, sub-micron rod-shaped particles can be produced via a modified solvent evaporation method [204].

Several of the recently developed strategies noted in this section “improve” upon the polymeric nanocarriers by adding components. This clearly adds complexity for large-scale

production and could potentially have safety issues both because the newly added components are new to the clinical setting before, or the new components could change the particle or drug properties [63,64]. To combat this tendency, novel polymerization strategies are synthesizing materials that are both the carrier and drug in one component. For instance, recent work has demonstrated the usefulness of a thioether-based polymeric nanocarrier in attenuating ROS-initiated damage after traumatic brain injury [205]. Drug delivery developers must be cautious in adding more components to existing one, and only added them if they could provide necessary benefits to the nanocarrier performance. This goal could be rephrased as promoting the maximum efficacy with the minimal amount of complexity. Simple or complicated materials may be able to get the job done, however, the whole life cycle of synthesis, drug loading, carrier storage, and delivery must be taken into account.

3.7 Acknowledgements

We gratefully acknowledge financial support from NIH grant R21 EB026723.

3.8 References

1. Fact Sheets | National Institute of Neurological Disorders and Stroke. Accessed August 19, 2021. https://www.ninds.nih.gov/Disorders/Patient-Caregiver-Education/Fact-Sheets

2. White BC, Sullivan JM, DeGracia DJ, O'Neil BJ, Neumar RW, Grossman LI, Rafols JA, Krause GS. Brain ischemia and reperfusion: molecular mechanisms of neuronal injury. *J Neurol Sci*. 2000;179(S 1-2):1-33. doi:10.1016/s0022-510x(00)00386-5

3. Cherubini A, Ruggiero C, Polidori MC, Mecocci P. Potential markers of oxidative stress in stroke. *Free Radic Biol Med*. 2005;39(7):841-852. doi:10.1016/j.freeradbiomed.2005.06.025

4. Dirnagl U, Iadecola C, Moskowitz MA. Pathobiology of ischaemic stroke: an integrated view. *Trends Neurosci*. 1999;22(9):391-397. doi:10.1016/S0166-2236(99)01401-0

5. Smith WS. Pathophysiology of Focal Cerebral Ischemia: a Therapeutic Perspective. *J Vasc Interv Radiol*. 2004;15(1):S3-S12. doi:10.1097/01.RVI.0000108687.75691.0C

6. Moskowitz MA, Lo EH, Iadecola C. The Science of Stroke: Mechanisms in Search of Treatments. *Neuron*. 2010;67(2):181-198. doi:10.1016/j.neuron.2010.07.002

7. Rungta RL, Choi HB, Tyson JR, Malik A, Dissing-Olesen L, Lin PJC, Cain SM, Cullis PR, Snutch TP, MacVicar BA. The Cellular Mechanisms of Neuronal Swelling Underlying Cytotoxic Edema. *Cell*. 2015;161(3):610-621. doi:10.1016/j.cell.2015.03.029

8. Candelario-Jalil E. Injury and repair mechanisms in ischemic stroke: considerations for the development of novel neurotherapeutics. *Curr Opin Investig Drugs Lond Engl 2000*. 2009;10(7):644-654.

9. Arai K, Lok J, Guo S, Hayakawa K, Xing C, Lo EH. Cellular mechanisms of neurovascular damage and repair after stroke. *J Child Neurol*. 2011;26(9):1193-1198. doi:10.1177/0883073811408610

10. Saeed SA, Shad KF, Saleem T, Javed F, Khan MU. Some new prospects in the understanding of the molecular basis of the pathogenesis of stroke. *Exp Brain Res*. 2007;182(1):1-10. doi:10.1007/s00221-007-1050-9

11. Abramov AY, Scorziello A, Duchen MR. Three Distinct Mechanisms Generate Oxygen Free Radicals in Neurons and Contribute to Cell Death during Anoxia and Reoxygenation. *J Neurosci*. 2007;27(5):1129-1138. doi:10.1523/JNEUROSCI.4468-06.2007

12. Schieber M, Chandel NS. ROS Function in Redox Signaling and Oxidative Stress. *Curr Biol*. 2014;24(10):R453-R462. doi:10.1016/j.cub.2014.03.034

13. Rodrigo R, Fernandez-Gajardo R, Gutierrez R, Matamala J, Carrasco R, Miranda-Merchak A, Feuerhake W. Oxidative Stress and Pathophysiology of Ischemic Stroke: Novel Therapeutic Opportunities. *CNS Neurol Disord - Drug Targets*. 2013;12(5):698-714. doi:10.2174/18715273113120500 15

14. Xing C, Arai K, Lo EH, Hommel M. Pathophysiologic Cascades in Ischemic Stroke. *Int J Stroke*. 2012;7(5):378-385. doi:10.1111/j.1747-4949.2012.00839.x

15. Hong HY, Choi JS, Kim YJ, Lee HY, Kwak W, Yoo J, Lee JT, Kwon TH, Kim IS, Han HS. Detection of apoptosis in a rat model of focal cerebral ischemia using a homing peptide selected from in vivo phage display. *J Controlled Release*. 2008;131(3):167-172. doi:10.1016/j.jconrel.2008.07.020

16. Sohrabji F, Park MJ, Mahnke AH. Sex Differences in Stroke Therapies. *J Neurosci Res*. 2017;95(1-2):681-691. doi:10.1002/jnr.23855

17. Li J, McCullough LD. Sex Differences in Minocycline-Induced Neuroprotection after Experimental Stroke. *J Cereb Blood Flow Metab*. 2009;29(4):670-674. doi:10.1038/jcbfm.2009.3

18. Amiri-Nikpour MR, Nazarbaghi S, Hamdi-Holasou M, Rezaei Y. An open-label evaluator-blinded clinical study of minocycline neuroprotection in ischemic stroke: gender-dependent effect. *Acta Neurol Scand*. 2015;131(1):45-50. doi:10.1111/ane.12296

19. Bharadwaj VN, Copeland C, Mathew E, Newbern J, Anderson TR, Lifshitz J, Kodibagkar VD, Stabenfeldt SE. Sex-Dependent Macromolecule and Nanoparticle Delivery in Experimental Brain Injury. *Tissue Eng Part A*. 2020;26(13-14):688-701. doi:10.1089/ten.tea.2020.0040

20. Brzica H, Abdullahi W, Ibbotson K, Ronaldson PT. Role of Transporters in Central Nervous System Drug Delivery and Blood-Brain Barrier Protection: Relevance to Treatment of Stroke. *J Cent Nerv Syst Dis*. 2017;9. doi:10.1177/1179573517693802

21. Mican J, Toul M, Bednar D, Damborsky J. Structural Biology and Protein Engineering of Thrombolytics. *Comput Struct Biotechnol J*. 2019;17:917-938. doi:10.1016/j.csbj.2019.06.023

22. Heit JA. 14 - Thrombophilia: Clinical and Laboratory Assessment and Management. In: Kitchens CS, Kessler CM, Konkle BA, eds. *Consultative Hemostasis and Thrombosis (Third Edition)*. W.B. Saunders; 2013:205-239. doi:10.1016/B978-1-4557-2296-9.00014-2

23. Powers William J., Rabinstein Alejandro A., Ackerson Teri, Adeoye Opeolu M., Bambakidis Nicholas C., Becker Kyra, Biller José, Brown Michael, Demaerschalk Bart M., Hoh Brian, Jauch Edward C., Kidwell Chelsea S., Leslie-Mazwi Thabele M., Ovbiagele Bruce, Scott Phillip A., Sheth Kevin N., Southerland Andrew M., Summers Deborah V., Tirschwell David L., null null. Guidelines for the Early Management of Patients With Acute Ischemic Stroke: 2019 Update to the 2018 Guidelines for the Early Management of Acute Ischemic Stroke: A Guideline for Healthcare Professionals From the American Heart Association/American Stroke Association. *Stroke*. 2019;50(12):e344-e418. doi:10.1161/STR.0000000000000211

24. Ma H, Campbell BCV, Parsons MW, Churilov L, Levi CR, Hsu C, Kleinig TJ, Wijeratne T, Curtze S, Dewey HM, Miteff F, Tsai CH, Lee JT, Phan TG, Mahant N, Sun MC, Krause M, Sturm J, Grimley R, Chen CH, Hu CJ, Wong AA, Field D, Sun Y, Barber PA, Sabet A, Jannes J, Jeng JS, Clissold B, Markus R, Lin CH, Lien LM, Bladin CF, Christensen S, Yassi N, Sharma G, Bivard A, Desmond PM, Yan B, Mitchell PJ, Thijs V, Carey L, Meretoja A, Davis SM, Donnan GA, EXTEND Investigators. Thrombolysis Guided by Perfusion Imaging up to 9 Hours after Onset of Stroke. N *Engl J Med*. 2019;380(19):1795-1803. doi:10.1056/NEJMoa1813046

25. Leira EC, Muir KW. EXTEND Trial. *Stroke*. 2019;50(9):2637-2639. doi:10.1161/STROKEAHA.119.026249

26. Miller DJ, Simpson JR, Silver B. Safety of Thrombolysis in Acute Ischemic Stroke: A Review of Complications, Risk Factors, and Newer Technologies. *The Neurohospitalist*. 2011;1(3):138-147. doi:10.1177/1941875211408731

27. Virani Salim S., Alonso Alvaro, Benjamin Emelia J., Bittencourt Marcio S., Callaway Clifton W., Carson April P., Chamberlain Alanna M., Chang Alexander R., Cheng Susan, Delling Francesca N., Djousse Luc, Elkind Mitchell S.V., Ferguson Jane F., Fornage Myriam, Khan Sadiya S., Kissela Brett M., Knutson Kristen L., Kwan Tak W., Lackland Daniel T., Lewis Tené T., Lichtman Judith H., Longenecker Chris T., Loop Matthew Shane, Lutsey Pamela L., Martin Seth S., Matsushita Kunihiro, Moran Andrew E., Mussolino Michael E., Perak Amanda Marma, Rosamond Wayne D., Roth Gregory A., Sampson Uchechukwu K.A., Satou Gary M., Schroeder Emily B., Shah Svati H., Shay Christina M., Spartano Nicole L., Stokes Andrew, Tirschwell David L., VanWagner Lisa B., Tsao Connie W., null null. Heart Disease and Stroke Statistics—2020 Update: A Report From the American Heart Association. *Circulation*. 2020;141(9):e139-e596. doi:10.1161/CIR.0000000000000757

28. Hughes RE, Tadi P, Bollu PC. TPA Therapy. In: *StatPearls*. StatPearls Publishing; 2021. Accessed March 10, 2021. http://www.ncbi.nlm.nih.gov/books/NBK482376/

29. Tsuji Kiyoshi, Aoki Toshiaki, Tejima Emiri, Arai Ken, Lee Sun-Ryung, Atochin Dmitriy N., Huang Paul L., Wang Xiaoying, Montaner Joan, Lo Eng H. Tissue Plasminogen Activator Promotes Matrix Metalloproteinase-9 Upregulation After Focal Cerebral Ischemia. *Stroke*. 2005;36(9):1954-1959. doi:10.1161/01.STR.0000177517.01203.eb

30. Gauberti M, Potzeha F, Vivien D, Martinez de Lizarrondo S. Impact of Bradykinin Generation During Thrombolysis in Ischemic Stroke. *Front Med*. 2018;5. doi:10.3389/fmed.2018.00195

31. Ilyas A, Chen CJ, Ding D, Foreman PM, Buell TJ, Ironside N, Taylor DG, Kalani MY, Park MS, Southerland AM, Worrall BB. Endovascular Mechanical Thrombectomy for Acute Ischemic Stroke Under General Anesthesia Versus Conscious Sedation: A Systematic Review and Meta-Analysis. *World Neurosurg*. 2018;112:e355-e367. doi:10.1016/j.wneu.2018.01.049

32. Levy EI, Mehta R, Gupta R, Hanel RA, Chamczuk AJ, Fiorella D, Woo HH, Albuquerque FC, Jovin TG, Horowitz MB, Hopkins LN. Self-Expanding Stents for Recanalization of Acute Cerebrovascular Occlusions. *AJNR Am J Neuroradiol*. 2007;28(5):816-822.

33. OHTA T, MORIMOTO M, OKADA K, FUKUDA M, ONISHI H, MASAHIRA N, MATSUOKA T, TSUNO T, TAKEMURA M. Mechanical Thrombectomy in Anterior Circulation Occlusion Could Be More Effective than Medical Management Even in Low DWI-ASPECTS Patients. *Neurol Med Chir (Tokyo)*. 2018;58(4):156-163. doi:10.2176/nmc.oa.2017-0203

34. Gascou G, Lobotesis K, Machi P, Maldonado I, Vendrell JF, Riquelme C, Eker O, Mercier G, Mourand I, Arquizan C, Bonafé A, Costalat V. Stent Retrievers in Acute Ischemic Stroke: Complications and Failures during the Perioperative Period. *Am J Neuroradiol*. 2014;35(4):734-740. doi:10.3174/ajnr.A3746

35. Josephson SA, Kamel H. The Acute Stroke Care Revolution: Enhancing Access to Therapeutic Advances. *JAMA*. 2018;320(12):1239-1240. doi:10.1001/jama.2018.11122

36. Sheth Kevin N., Smith Eric E., Grau-Sepulveda Maria V., Kleindorfer Dawn, Fonarow Gregg C., Schwamm Lee H. Drip and Ship Thrombolytic Therapy for Acute Ischemic Stroke. *Stroke*. 2015;46(3):732-739. doi:10.1161/STROKEAHA.114.007506

37. Vanacker Peter, Lambrou Dimitris, Eskandari Ashraf, Mosimann Pascal J., Maghraoui Ali, Michel Patrik. Eligibility and Predictors for Acute Revascularization Procedures in a Stroke Center. *Stroke*. 2016;47(7):1844-1849. doi:10.1161/STROKEAHA.115.012577

38. Jadhav Ashutosh P., Desai Shashvat M., Kenmuir Cynthia L., Rocha Marcelo, Starr Matthew T., Molyneaux Bradley J., Gross Bradley A., Jankowitz Brian T., Jovin Tudor G. Eligibility for Endovascular Trial Enrollment in the 6- to 24-Hour Time Window. *Stroke*. 2018;49(4):1015-1017. doi:10.1161/STROKEAHA.117.020273

39. Zhang Xiaohao, Xie Yi, Wang Huaiming, Yang Dong, Jiang Teng, Yuan Kang, Gong Pengyu, Xu Pengfei, Li Yunzi, Chen Jingjing, Wu Min, Sheng Lei, Liu Dezhi, Liu Xinfeng, Xu Gelin. Symptomatic Intracranial Hemorrhage After Mechanical Thrombectomy in Chinese Ischemic Stroke Patients. *Stroke*. 2020;51(9):2690-2696. doi:10.1161/STROKEAHA.120.030173

40. Singh R, Lillard JW. Nanoparticle-based targeted drug delivery. *Exp Mol Pathol*. 2009;86(3):215-223. doi:10.1016/j.yexmp.2008.12.004

41. Masserini M. Nanoparticles for Brain Drug Delivery. *ISRN Biochem*. 2013;2013:1-18. doi:10.1155/2013/238428

42. Petkar KC, Chavhan SS, Agatonovik-Kustrin S, Sawant K. Nanostructured Materials in Drug and Gene Delivery: A Review of the State of the Art. *Crit Rev Ther Drug Carr Syst*. 2011;28(2). doi:10.1615/CritRevTherDrugCarrierSyst.v28.i2.10

43. Gelperina S, Kisich K, Iseman MD, Heifets L. The Potential Advantages of Nanoparticle Drug Delivery Systems in Chemotherapy of Tuberculosis. *Am J Respir Crit Care Med*. 2005;172(12):1487-1490. doi:10.1164/rccm.200504-613PP

44. Mudshinge SR, Deore AB, Patil S, Bhalgat CM. Nanoparticles: Emerging carriers for drug delivery. *Saudi Pharm J*. 2011;19(3):129-141. doi:10.1016/j.jsps.2011.04.001

45. Narvekar M, Xue HY, Eoh JY, Wong HL. Nanocarrier for Poorly Water-Soluble Anticancer Drugs—Barriers of Translation and Solutions. *AAPS PharmSciTech*. 2014;15(4):822-833. doi:10.1208/s12249-014-0107-x

46. Weiss RB, Donehower RC, Wiernik PH, Ohnuma T, Gralla RJ, Trump DL, Baker JR, Van Echo DA, Von Hoff DD, Leyland-Jones B. Hypersensitivity reactions from taxol. *J Clin Oncol Off J Am Soc Clin Oncol*. 1990;8(7):1263-1268. doi:10.1200/JCO.1990.8.7.1263

47. Gelderblom H, Verweij J, Nooter K, Sparreboom A. Cremophor EL: the drawbacks and advantages of vehicle selection for drug formulation. *Eur J Cancer*. 2001;37(13):1590-1598. doi:10.1016/S0959-8049(01)00171-X

48. Gradishar WJ. Albumin-bound paclitaxel: a next-generation taxane. *Expert Opin Pharmacother*. 2006;7(8):1041-1053. doi:10.1517/14656566.7.8.1041

49. Ibrahim NK, Desai N, Legha S, Soon-Shiong P, Theriault RL, Rivera E, Esmaeli B, Ring SE, Bedikian A, Hortobagyi GN, Ellerhorst JA. Phase I and Pharmacokinetic Study of ABI-007, a Cremophor-free, Protein-stabilized, Nanoparticle Formulation of Paclitaxel. *Clin Cancer Res*. 2002;8(5):1038-1044.

50. Desai N. Nanoparticle Albumin-Bound Paclitaxel (Abraxane®). In: Otagiri M, Chuang VTG, eds. *Albumin in Medicine: Pathological and Clinical Applications*. Springer; 2016:101-119. doi:10.1007/978-981-10-2116-9_6

51. Lancheros R, Guerrero CA, Godoy-Silva RD. Improvement of N-Acetylcysteine Loaded in PLGA Nanoparticles by Nanoprecipitation Method. *J Nanotechnol*. 2018;2018:e3620373. doi:10.1155/2018/3620373

52. Gagliardi A, Giuliano E, Venkateswararao E, Fresta M, Bulotta S, Awasthi V, Cosco D. Biodegradable Polymeric Nanoparticles for Drug Delivery to Solid Tumors. *Front Pharmacol*. 2021;12:601626. doi:10.3389/fphar.2021.601626

53. Zhou J, Patel TR, Sirianni RW, Strohbehn G, Zheng MQ, Duong N, Schafbauer T, Huttner AJ, Huang Y, Carson RE, Zhang Y, Sullivan DJ, Piepmeier JM, Saltzman WM. Highly penetrative, drug-loaded nanocarriers improve treatment of glioblastoma. *Proc Natl Acad Sci*. 2013;110(29):11751-11756. doi:10.1073/pnas.1304504110

54. Sánchez-López E, Ettcheto M, Egea MA, Espina M, Cano A, Calpena AC, Camins A, Carmona N, Silva AM, Souto EB, García ML. Memantine loaded PLGA PEGylated nanoparticles for Alzheimer's disease: in vitro and in vivo characterization. *J Nanobiotechnology*. 2018;16(1):32. doi:10.1186/s12951-018-0356-z

55. Singh S, Pandey VK, Agarwal RPT and V. Nanoparticle based drug delivery system: Advantages and applications. *Indian Journal of Science and Technology*. Published March 3, 2011. Accessed February 20, 2021. https://indjst.org/

56. Han L, Cai Q, Tian D, Kong DK, Gou X, Chen Z, Strittmatter SM, Wang Z, Sheth KN, Zhou J. Targeted drug delivery to ischemic stroke via chlorotoxin-anchored, lexiscan-loaded nanoparticles. *Nanomedicine Nanotechnol Biol Med*. 2016;12(7):1833-1842. doi:10.1016/j.nano.2016.03.005

57. Zhang C, Wan X, Zheng X, Shao X, Liu Q, Zhang Q, Qian Y. Dual-functional nanoparticles targeting amyloid plaques in the brains of Alzheimer's disease mice. *Biomaterials*. 2014;35(1):456-465. doi:10.1016/j.biomaterials.2013.09.063

58. Nie S. Understanding and overcoming major barriers in cancer nanomedicine. *Nanomed*. 2010;5(4):523-528. doi:10.2217/nnm.10.23

59. Suk JS, Xu Q, Kim N, Hanes J, Ensign LM. PEGylation as a strategy for improving nanoparticle-based drug and gene delivery. *Adv Drug Deliv Rev*. 2016;99(Pt A):28-51. doi:10.1016/j.addr.2015.09.012

60. Saraiva C, Praça C, Ferreira R, Santos T, Ferreira L, Bernardino L. Nanoparticle-mediated brain drug delivery: Overcoming blood–brain barrier to treat neurodegenerative diseases. *J Controlled Release*. 2016;235:34-47. doi:10.1016/j.jconrel.2016.05.044

61. Bharadwaj VN, Nguyen DT, Kodibagkar VD, Stabenfeldt SE. Nanoparticle-Based Therapeutics for Brain Injury. *Adv Healthc Mater*. 2018;7(1):1700668. doi:10.1002/adhm.201700668

62. Swierczewska M, Lee KC, Lee S. What is the future of PEGylated therapies? *Expert Opin Emerg Drugs*. 2015;20(4):531-536. doi:10.1517/14728214.2015.1113254

63. Hua S, de Matos MBC, Metselaar JM, Storm G. Current Trends and Challenges in the Clinical Translation of Nanoparticulate Nanomedicines: Pathways for Translational Development and Commercialization. *Front Pharmacol*. 2018;9. doi:10.3389/fphar.2018.00790

64. Metselaar JM, Lammers T. Challenges in nanomedicine clinical translation. *Drug Deliv Transl Res*. 2020;10(3):721-725. doi:10.1007/s13346-020-00740-5

65. Anselmo AC, Mitragotri S. Nanoparticles in the clinic: An update post COVID-19 vaccines. *Bioeng Transl Med*. n/a(n/a):e10246. doi:10.1002/btm2.10246

66. Vetten MA, Yah CS, Singh T, Gulumian M. Challenges facing sterilization and depyrogenation of nanoparticles: effects on structural stability and biomedical applications. *Nanomedicine Nanotechnol Biol Med*. 2014;10(7):1391-1399. doi:10.1016/j.nano.2014.03.017

67. Joseph A, Nance E. Nanotherapeutics and the Brain. *Annu Rev Chem Biomol Eng*. Published online February 23, 2022. doi:10.1146/annurev-chembioeng-092220-030853

68. Konofagou EE, Tung YS, Choi J, Deffieux T, Baseri B, Vlachos F. Ultrasound-Induced Blood-Brain Barrier Opening. *Curr Pharm Biotechnol*. 2012;13(7):1332-1345.

69. Etame AB, Diaz RJ, Smith CA, Mainprize TG, Kullervo HH, Rutka JT. Focused ultrasound disruption of the blood brain barrier: a new frontier for therapeutic delivery in molecular neuro-oncology. *Neurosurg Focus*. 2012;32(1):E3. doi:10.3171/2011.10.FOCUS11252

70. Lipsman N, Meng Y, Bethune AJ, Huang Y, Lam B, Masellis M, Herrmann N, Heyn C, Aubert I, Boutet A, Smith GS, Hynynen K, Black SE. Blood–brain barrier opening in Alzheimer's disease using MR-guided focused ultrasound. *Nat Commun*. 2018;9(1):2336. doi:10.1038/s41467-018-04529-6

71. Mehta RI, Carpenter JS, Mehta RI, Haut MW, Ranjan M, Najib U, Lockman P, Wang P, D'haese PF, Rezai AR. Blood-Brain Barrier Opening with MRI-guided Focused Ultrasound Elicits Meningeal Venous Permeability in Humans with Early Alzheimer Disease. *Radiology*. 2021;298(3):654-662. doi:10.1148/radiol.2021200643

72. Martínez-Fernández R, Máñez-Miró JU, Rodríguez-Rojas R, Del Álamo M, Shah BB, Hernández-Fernández F, Pineda-Pardo JA, Monje MHG, Fernández-Rodríguez B, Sperling SA, Mata-Marín D, Guida P, Alonso-Frech F, Obeso I, Gasca-Salas C, Vela-Desojo L, Elias WJ, Obeso JA. Randomized Trial of Focused Ultrasound Subthalamotomy for Parkinson's Disease. *N Engl J Med*. 2020;383(26):2501-2513. doi:10.1056/NEJMoa2016311

73. Bond AE, Shah BB, Huss DS, Dallapiazza RF, Warren A, Harrison MB, Sperling SA, Wang XQ, Gwinn R, Witt J, Ro S, Elias WJ. Safety and Efficacy of Focused Ultrasound Thalamotomy for Patients With Medication-Refractory, Tremor-Dominant Parkinson Disease. *JAMA Neurol*. 2017;74(12):1412-1418. doi:10.1001/jamaneurol.2017.3098

74. Rezai AR, Ranjan M, D'Haese PF, Haut MW, Carpenter J, Najib U, Mehta RI, Chazen JL, Zibly Z, Yates JR, Hodder SL, Kaplitt M. Noninvasive hippocampal blood−brain barrier opening in Alzheimer's disease with focused ultrasound. *Proc Natl Acad Sci*. 2020;117(17):9180-9182. doi:10.1073/pnas.2002571117

75. Alonso A. Ultrasound-Induced Blood-Brain Barrier Opening for Drug Delivery. *Transl Neurosonology*. 2015;36:106-115. doi:10.1159/000366242

76. Dauba A, Delalande A, Kamimura HAS, Conti A, Larrat B, Tsapis N, Novell A. Recent Advances on Ultrasound Contrast Agents for Blood-Brain Barrier Opening with Focused Ultrasound. *Pharmaceutics*. 2020;12(11):1125. doi:10.3390/pharmaceutics12111125

77. D'Haese PF, Ranjan M, Song A, Haut MW, Carpenter J, Dieb G, Najib U, Wang P, Mehta RI, Chazen JL, Hodder S, Claassen D, Kaplitt M, Rezai AR. β-Amyloid Plaque Reduction in the Hippocampus After Focused Ultrasound-Induced Blood–Brain Barrier Opening in Alzheimer's Disease. *Front Hum Neurosci*. 2020;14:593672. doi:10.3389/fnhum.2020.593672

78. Kinoshita M, McDannold N, Jolesz FA, Hynynen K. Targeted delivery of antibodies through the blood–brain barrier by MRI-guided focused ultrasound. *Biochem Biophys Res Commun*. 2006;340(4):1085-1090. doi:10.1016/j.bbrc.2005.12.112

79. Lin CY, Hsieh HY, Pitt WG, Huang CY, Tseng IC, Yeh CK, Wei KC, Liu HL. Focused ultrasound-induced blood-brain barrier opening for non-viral, non-invasive, and targeted gene delivery. *J Controlled Release*. 2015;212:1-9. doi:10.1016/j.jconrel.2015.06.010

80. Lynch M, Heinen S, Markham-Coultes K, O'Reilly M, Van Slyke P, Dumont DJ, Hynynen K, Aubert I. Vasculotide restores the blood-brain barrier after focused ultrasound-induced permeability in a mouse model of Alzheimer's disease. *Int J Med Sci*. 2021;18(2):482-493. doi:10.7150/ijms.36775

81. Hsu PH, Lin YT, Chung YH, Lin KJ, Yang LY, Yen TC, Liu HL. Focused Ultrasound-Induced Blood-Brain Barrier Opening Enhances GSK-3 Inhibitor Delivery for Amyloid-Beta Plaque Reduction. *Sci Rep*. 2018;8(1):12882. doi:10.1038/s41598-018-31071-8

82. Lee J, Chang WS, Shin J, Seo Y, Kong C, Song BW, Na YC, Kim BS, Chang JW. Non-invasively enhanced intracranial transplantation of mesenchymal stem cells using focused ultrasound mediated by overexpression of cell-adhesion molecules. *Stem Cell Res*. 2020;43:101726. doi:10.1016/j.scr.2020.101726

83. Zhang H, Sierra C, Kwon N, Karakatsani ME, Jackson-Lewis VR, Przedborski S, Konofagou E. Focused-ultrasound Mediated Anti-Alpha-Synuclein Antibody Delivery for the Treatment of Parkinson's Disease. In: *2018 IEEE International Ultrasonics Symposium (IUS)*. ; 2018:1-4. doi:10.1109/ULTSYM.2018.8579677

84. Tung YS, Vlachos F, Feshitan JA, Borden MA, Konofagou EE. The mechanism of interaction between focused ultrasound and microbubbles in blood-brain barrier opening in mice. *J Acoust Soc Am*. 2011;130(5):3059-3067. doi:10.1121/1.3646905

85. Pouliopoulos AN, Wu SY, Burgess MT, Karakatsani ME, Kamimura HAS, Konofagou EE. A Clinical System for Non-invasive Blood–Brain Barrier Opening Using a Neuronavigation-Guided Single-Element Focused Ultrasound Transducer. *Ultrasound Med Biol*. 2020;46(1):73-89. doi:10.1016/j.ultrasmedbio.2019.09.010

86. Burgess A, Hynynen KH. Drug delivery across the blood-brain barrier using focused ultrasound. *Expert Opin Drug Deliv*. 2014;11(5):711-721. doi:10.1517/17425247.2014.897693

87. Baek H, Sariev A, Kim MJ, Lee H, Kim J, Kim H. A neuroprotective brain stimulation for vulnerable cerebellar Purkinje cell after ischemic stroke: a study with low-intensity focused ultrasound. In: *2018 40th Annual International Conference of the IEEE Engineering in Medicine and Biology Society (EMBC)*. ; 2018:4744-4747. doi:10.1109/EMBC.2018.8513138

88. Wang J, Li G, Deng L, Mamtilahun M, Jiang L, Qiu W, Zheng H, Sun J, Xie Q, Yang GY. Transcranial Focused Ultrasound Stimulation Improves Neurorehabilitation after Middle Cerebral Artery Occlusion in Mice. *Aging Dis*. 2021;12(1):50-60. doi:10.14336/AD.2020.0623

89. Baek H, Pahk KJ, Kim MJ, Youn I, Kim H. Modulation of Cerebellar Cortical Plasticity Using Low-Intensity Focused Ultrasound for Poststroke Sensorimotor Function Recovery. *Neurorehabil Neural Repair*. 2018;32(9):777-787. doi:10.1177/1545968318790022

90. Lee TH, Yeh JC, Tsai CH, Yang JT, Lou SL, Seak CJ, Wang CY, Wei KC, Liu HL. Improved thrombolytic effect with focused ultrasound and neuroprotective agent against acute carotid artery thrombosis in rat. *Sci Rep*. 2017;7(1):1638. doi:10.1038/s41598-017-01769-2

91. Baek H, Sariev A, Lee S, Dong SY, Royer S, Kim H. Deep Cerebellar Low-Intensity Focused Ultrasound Stimulation Restores Interhemispheric Balance after Ischemic Stroke in Mice. *IEEE Trans Neural Syst Rehabil Eng*. 2020;28(9):2073-2079. doi:10.1109/TNSRE.2020.3002207

92. Mead BP, Curley CT, Kim N, Negron K, Garrison WJ, Song J, Rao D, Miller GW, Mandell JW, Purow BW, Suk JS, Hanes J, Price RJ. Focused Ultrasound Preconditioning for Augmented Nanoparticle Penetration and Efficacy in the Central Nervous System. *Small Weinh Bergstr Ger*. 2019;15(49):e1903460. doi:10.1002/smll.201903460

93. Curley CT, Mead BP, Negron K, Kim N, Garrison WJ, Miller GW, Kingsmore KM, Thim EA, Song J, Munson JM, Klibanov AL, Suk JS, Hanes J, Price RJ. Augmentation of brain tumor interstitial flow via focused ultrasound promotes brain-penetrating nanoparticle dispersion and transfection. *Sci Adv*. 2020;6(18):eaay1344. doi:10.1126/sciadv.aay1344

94. Choi M, Ku T, Chong K, Yoon J, Choi C. Minimally invasive molecular delivery into the brain using optical modulation of vascular permeability. *Proc Natl Acad Sci*. 2011;108(22):9256-9261. doi:10.1073/pnas.1018790108

95. Yoon J, Choi C. Application of Ultrashort-Pulsed Lasers for Optical Manipulation of Biological Functions. In: Ho AHP, Kim D, Somekh MG, eds. *Handbook of Photonics for Biomedical Engineering*. Springer Netherlands; 2017:717-729. doi:10.1007/978-94-007-5052-4_15

96. Appelboom G, Detappe A, LoPresti M, Kunjachan S, Mitrasinovic S, Goldman S, Chang SD, Tillement O. Stereotactic modulation of blood-brain barrier permeability to enhance drug delivery. *Neuro-Oncol*. 2016;18(12):1601-1609. doi:10.1093/neuonc/now137

97. LeVine SM. Albumin and multiple sclerosis. *BMC Neurol*. 2016;16:47. doi:10.1186/s12883-016-0564-9

98. Tenny S, Patel R, Thorell W. Mannitol. In: *StatPearls*. StatPearls Publishing; 2021. Accessed March 10, 2021. http://www.ncbi.nlm.nih.gov/books/NBK470392/

99. Carman AJ, Mills JH, Krenz A, Kim DG, Bynoe MS. Adenosine Receptor Signaling Modulates Permeability of the Blood–Brain Barrier. *J Neurosci*. 2011;31(37):13272-13280. doi:10.1523/JNEUROSCI.3337-11.2011

100. Bálint Z, Krizbai IA, Wilhelm I, Farkas AE, Párducz A, Szegletes Z, Váró G. Changes induced by hyperosmotic mannitol in cerebral endothelial cells: an atomic force microscopic study. *Eur Biophys J EBJ*. 2007;36(2):113-120. doi:10.1007/s00249-006-0112-4

101. Cosolo WC, Martinello P, Louis WJ, Christophidis N. Blood-brain barrier disruption using mannitol: time course and electron microscopy studies. *Am J Physiol*. 1989;256(2 Pt 2):R443-447. doi:10.1152/ajpregu.1989.256.2.R443

102. Spindler V, Schlegel N, Waschke J. Role of GTPases in control of microvascular permeability. *Cardiovasc Res*. 2010;87(2):243-253. doi:10.1093/cvr/cvq086

103. Kim DG, Bynoe MS. A2A adenosine receptor regulates the human blood brain barrier permeability. *Mol Neurobiol*. 2015;52(1):664-678. doi:10.1007/s12035-014-8879-2

104. Kim DG, Bynoe MS. A2A adenosine receptor modulates drug efflux transporter P-glycoprotein at the blood-brain barrier. *J Clin Invest*. 126(5):1717-1733. doi:10.1172/JCI76207

105. Zhang QL, Fu BM, Zhang ZJ. Borneol, a novel agent that improves central nervous system drug delivery by enhancing blood-brain barrier permeability. *Drug Deliv*. 2017;24(1):1037-1044. doi:10.1080/10717544.2017.1346002

106. Zheng Q, Chen ZX, Xu MB, Zhou XL, Huang YY, Zheng GQ, Wang Y. Borneol, a messenger agent, improves central nervous system drug delivery through enhancing blood-brain barrier permeability: a preclinical systematic review and meta-analysis. *Drug Deliv*. 2018;25(1):1617-1633. doi:10.1080/10717544.2018.1486471

107. Yu B, Ruan M, Dong X, Yu Y, Cheng H. The mechanism of the opening of the blood-brain barrier by borneol: a pharmacodynamics and pharmacokinetics combination study. *J Ethnopharmacol*. 2013;150(3):1096-1108.

108. Wu T, Zhang A, Lu H, Cheng Q. The Role and Mechanism of Borneol to Open the Blood-Brain Barrier. *Integr Cancer Ther*. 2018;17(3):806-812. doi:10.1177/1534735418767553

109. Huber JD, Campos CR, Mark KS, Davis TP. Alterations in blood-brain barrier ICAM-1 expression and brain microglial activation after lambda-carrageenan-induced inflammatory pain. *Am J Physiol Heart Circ Physiol*. 2006;290(2):H732-740. doi:10.1152/ajpheart.00747.2005

110. Müller N. The Role of Intercellular Adhesion Molecule-1 in the Pathogenesis of Psychiatric Disorders. *Front Pharmacol*. 2019;10. doi:10.3389/fphar.2019.01251

111. Yin Y, Cao L, Ge H, Duanmu W, Tan L, Yuan J, Tunan C, Li F, Hu R, Gao F, Feng H. L-Borneol induces transient opening of the blood–brain barrier and enhances the therapeutic effect of cisplatin. *NeuroReport*. 2017;28(9):506-513. doi:10.1097/WNR.0000000000000792

112. Bartus RT, Elliott P, Hayward N, Dean R, McEwen EL, Fisher SK. Permeability of the blood brain barrier by the bradykinin agonist, RMP-7: evidence for a sensitive, auto-regulated, receptor-mediated system. *Immunopharmacology*. 1996;33(1-3):270-278. doi:10.1016/0162-3109(96)00070-7

113. Liangran G, Jinfeng R, Xinguo J. Perspectives on Brain-Targeting Drug Delivery Systems. *Current Pharmaceutical Biotechnology*. Published August 31, 2012. Accessed March 10, 2021. https://www.eurekaselect.com/103501/article

114. Nokkari A, Abou-El-Hassan H, Mechref Y, Mondello S, Kindy MS, Jaffa AA, Kobeissy F. Implication of the Kallikrein-Kinin System in Neurological Disorders: Quest for Potential Biomarkers and Mechanisms. *Prog Neurobiol*. 2018;165-167:26-50. doi:10.1016/j.pneurobio.2018.01.003

115. Jia W, Lu R, Martin TA, Jiang WG. The role of claudin-5 in blood-brain barrier (BBB) and brain metastases (review). *Mol Med Rep*. 2014;9(3):779-785. doi:10.3892/mmr.2013.1875

116. Bartus RT, Elliott PJ, Dean RL, Hayward NJ, Nagle TL, Huff MR, Snodgrass PA, Blunt DG. Controlled modulation of BBB permeability using the bradykinin agonist, RMP-7. *Exp Neurol*. 1996;142(1):14-28. doi:10.1006/exnr.1996.0175

117. Polosa R. Adenosine-receptor subtypes: their relevance to adenosine-mediated responses in asthma and chronic obstructive pulmonary disease. *Eur Respir J*. 2002;20(2):488-496. doi:10.1183/09031936.02.01132002

118. Anderson KM, Murphy DL, Balaji M. Essentials of noninvasive cardiac stress testing. *J Am Assoc Nurse Pract*. 2014;26(2):59-69. doi:https://doi.org/10.1002/2327-6924.12096

119. Abdul Razzak R, Florence GJ, Gunn-Moore FJ. Approaches to CNS Drug Delivery with a Focus on Transporter-Mediated Transcytosis. *Int J Mol Sci*. 2019;20(12). doi:10.3390/ijms20123108

120. Hervé F, Ghinea N, Scherrmann JM. CNS Delivery Via Adsorptive Transcytosis. *AAPS J*. 2008;10(3):455-472. doi:10.1208/s12248-008-9055-2

121. Herda LM, Polo E, Kelly PM, Rocks L, Hudecz D, Dawson KA. Designing the future of nanomedicine: current barriers to targeted brain therapeutics. *Eur J Nanomedicine*. 2014;6(3):127-139. doi:10.1515/ejnm-2014-0022

122. Gao H. Progress and perspectives on targeting nanoparticles for brain drug delivery. *Acta Pharm Sin B*. 2016;6(4):268-286. doi:10.1016/j.apsb.2016.05.013

123. Wu D, Yang J, Pardridge WM. Drug targeting of a peptide radiopharmaceutical through the primate blood-brain barrier in vivo with a monoclonal antibody to the human insulin receptor. *J Clin Invest*. 1997;100(7):1804-1812.

124. Zhang Yun, Pardridge William M. Neuroprotection in Transient Focal Brain Ischemia After Delayed Intravenous Administration of Brain-Derived Neurotrophic Factor Conjugated to a Blood-Brain Barrier Drug Targeting System. *Stroke*. 2001;32(6):1378-1384. doi:10.1161/01.STR.32.6.1378

125. Zhao L xia, Liu A chang, Yu S wen, Wang Z xin, Lin X qian, Zhai G xi, Zhang Q zhu. The Permeability of Puerarin Loaded Poly(butylcyanoacrylate) Nanoparticles Coated with Polysorbate 80 on the Blood–Brain Barrier and Its Protective Effect against Cerebral Ischemia/Reperfusion Injury. *Biol Pharm Bull*. 2013;36(8):1263-1270. doi:10.1248/bpb.b12-00769

126. Guo L, Ren J, Jiang X. Perspectives on Brain-Targeting Drug Delivery Systems. *Curr Pharm Biotechnol*. 2012;13(12):2310-2318. doi:10.2174/138920112803341770

127. Pang Z, Lu W, Gao H, Hu K, Chen J, Zhang C, Gao X, Jiang X, Zhu C. Preparation and brain delivery property of biodegradable polymersomes conjugated with OX26. *J Controlled Release*. 2008;128(2):120-127. doi:10.1016/j.jconrel.2008.03.007

128. Battaglia G, La Russa M, Bruno V, Arenare L, Ippolito R, Copani A, Bonina F, Nicoletti F. Systemically administered d-glucose conjugates of 7-chlorokynurenic acid are centrally available and exert anticonvulsant activity in rodents. *Brain Res*. 2000;860(1):149-156. doi:10.1016/S0006-8993(00)01962-4

129. Anraku Y, Kuwahara H, Fukusato Y, Mizoguchi A, Ishii T, Nitta K, Matsumoto Y, Toh K, Miyata K, Uchida S, Nishina K, Osada K, Itaka K, Nishiyama N, Mizusawa H, Yamasoba T, Yokota T, Kataoka K. Glycaemic control boosts glucosylated nanocarrier crossing the BBB into the brain. *Nat Commun*. 2017;8:1001. doi:10.1038/s41467-017-00952-3

130. Albekairi TH, Vaidya B, Patel R, Nozohouri S, Villalba H, Zhang Y, Lee YS, Al-Ahmad A, Abbruscato TJ. Brain Delivery of a Potent Opioid Receptor Agonist, Biphalin during Ischemic Stroke: Role of Organic Anion Transporting Polypeptide (OATP). *Pharmaceutics*. 2019;11(9):467. doi:10.3390/pharmaceutics11090467

131. Thakkar N, Lockhart AC, Lee W. Role of Organic Anion-Transporting Polypeptides (OATPs) in Cancer Therapy. *AAPS J*. 2015;17(3):535-545. doi:10.1208/s12248-015-9740-x

132. Stieger B, Hagenbuch B. Organic Anion Transporting Polypeptides. *Curr Top Membr*. 2014;73:205-232. doi:10.1016/B978-0-12-800223-0.00005-0

133. Thompson BJ, Sanchez-Covarrubias L, Slosky LM, Zhang Y, Laracuente M li, Ronaldson PT. Hypoxia/reoxygenation stress signals an increase in organic anion transporting polypeptide 1a4 (Oatp1a4) at the blood–brain barrier: relevance to CNS drug delivery. *J Cereb Blood Flow Metab*. 2014;34(4):699-707. doi:10.1038/jcbfm.2014.4

134. Pavan B, Dalpiaz A, Ciliberti N, Biondi C, Manfredini S, Vertuani S. Progress in Drug Delivery to the Central Nervous System by the Prodrug Approach. *Molecules*. 2008;13(5):1035-1065. doi:10.3390/molecules13051035

135. Lajoie JM, Shusta EV. Targeting Receptor-Mediated Transport for Delivery of Biologics Across the Blood-Brain Barrier. *Annu Rev Pharmacol Toxicol*. 2015;55(1):613-631. doi:10.1146/annurev-pharmtox-010814-124852

136. Rousselle C, Clair P, Smirnova M, Kolesnikov Y, Pasternak GW, Gac-Breton S, Rees AR, Scherrmann JM, Temsamani J. Improved brain uptake and pharmacological activity of dalargin using a peptide-vector-mediated strategy. *J Pharmacol Exp Ther*. 2003;306(1):371-376. doi:10.1124/jpet.102.048520

137. Rao JP, Geckeler KE. Polymer nanoparticles: Preparation techniques and size-control parameters. *Prog Polym Sci*. 2011;36(7):887-913. doi:10.1016/j.progpolymsci.2011.01.001

138. Vauthier C, Bouchemal K. Methods for the Preparation and Manufacture of Polymeric Nanoparticles. *Pharm Res*. 2009;26(5):1025-1058. doi:10.1007/s11095-008-9800-3

139. Rauta PR, Mohanta YK, Nayak D. *Nanotechnology in Biology and Medicine: Research Advancements & Future Perspectives*. CRC Press; 2019.

140. Gurny R, Peppas NA, Harrington DD, Banker GS. Development of Biodegradable and Injectable Latices for Controlled Release of Potent Drugs. *Drug Dev Ind Pharm*. 1981;7(1):1-25. doi:10.3109/03639048109055684

141. Wang Y, Li P, Truong-Dinh Tran T, Zhang J, Kong L. Manufacturing Techniques and Surface Engineering of Polymer Based Nanoparticles for Targeted Drug Delivery to Cancer. *Nanomaterials*. 2016;6(2). doi:10.3390/nano6020026

142. Lemoine D, Préat V. Polymeric nanoparticles as delivery system for influenza virus glycoproteins. *J Controlled Release*. 1998;54(1):15-27. doi:10.1016/S0168-3659(97)00241-1

143. Fessi H, Puisieux F, Devissaguet JPh, Ammoury N, Benita S. Nanocapsule formation by interfacial polymer deposition following solvent displacement. *Int J Pharm*. 1989;55(1):R1-R4. doi:10.1016/0378-5173(89)90281-0

144. Martínez Rivas CJ, Tarhini M, Badri W, Miladi K, Greige-Gerges H, Nazari QA, Galindo Rodríguez SA, Román RÁ, Fessi H, Elaissari A. Nanoprecipitation process: From encapsulation to drug delivery. *Int J Pharm*. 2017;532(1):66-81. doi:10.1016/j.ijpharm.2017.08.064

145. M. J. Ansari. FACTORS AFFECTING PREPARATION AND PROPERTIES OF NANOPARTICLES BY NANOPRECIPITATION METHOD. *Indo Am J Pharm Sci*. 2018;04(12):4854-4858. doi:10.5281/zenodo.1134425

146. Sharma N, Madan P, Lin S. Effect of process and formulation variables on the preparation of parenteral paclitaxel-loaded biodegradable polymeric nanoparticles: A co-surfactant study. *Asian J Pharm Sci*. 2016;11(3):404-416. doi:10.1016/j.ajps.2015.09.004

147. Yallapu MM, Gupta BK, Jaggi M, Chauhan SC. Fabrication of curcumin encapsulated PLGA nanoparticles for improved therapeutic effects in metastatic cancer cells. *J Colloid Interface Sci*. 2010;351(1):19-29. doi:10.1016/j.jcis.2010.05.022

148. Mdzinarishvili A, Sutariya V, Talasila PK, Geldenhuys WJ, Sadana P. Engineering triiodothyronine (T3) nanoparticle for use in ischemic brain stroke. *Drug Deliv Transl Res*. 2013;3(4):309-317. doi:10.1007/s13346-012-0117-8

149. Xu J, Chen Y, Jiang X, Gui Z, Zhang L. Development of Hydrophilic Drug Encapsulation and Controlled Release Using a Modified Nanoprecipitation Method. *Processes*. 2019;7(6):331. doi:10.3390/pr7060331

150. Lancheros R, Guerrero CA, Godoy-Silva RD. Improvement of N-Acetylcysteine Loaded in PLGA Nanoparticles by Nanoprecipitation Method. *Journal of Nanotechnology*. doi:https://doi.org/10.1155/2018/3620373

151. Liu Y, Yang G, Zou D, Hui Y, Nigam K, Middelberg APJ, Zhao CX. Formulation of Nanoparticles Using Mixing-Induced Nanoprecipitation for Drug Delivery. *Ind Eng Chem Res*. 2020;59(9):4134-4149. doi:10.1021/acs.iecr.9b04747

152. Liu D, Zhang H, Cito S, Fan J, Mäkilä E, Salonen J, Hirvonen J, Sikanen TM, Weitz DA, Santos HA. Core/Shell Nanocomposites Produced by Superfast Sequential Microfluidic Nanoprecipitation. *Nano Lett*. 2017;17(2):606-614. doi:10.1021/acs.nanolett.6b03251

153. Quintanar-Guerrero D, Allémann E, Doelker E, Fessi H. A mechanistic study of the formation of polymer nanoparticles by the emulsification-diffusion technique. *Colloid Polym Sci*. 1997;275(7):640-647. doi:10.1007/s003960050130

154. LEROUX JC, ALLEMANN E, DOELKER E, GURNY R. New approach for the preparation of nanoparticles by an emulsification-diffusion method. *New Approach Prep Nanoparticles Emuls-Diffus Method*. 1995;41(1):14-18.

155. Quintanar-Guerrero D, Ganem-Quintanar A, Allémann E, Fessi H, Doelker E. Influence of the stabilizer coating layer on the purification and freeze-drying of poly(D, L-lactic acid) nanoparticles prepared by an emulsion-diffusion technique. *J Microencapsul*. Published online September 27, 2008. doi:10.3109/02652049809006840

156. Leroux JC, Allémann E, De Jaeghere F, Doelker E, Gurny R. Biodegradable nanoparticles — From sustained release formulations to improved site specific drug delivery. *J Controlled Release*. 1996;39(2):339-350. doi:10.1016/0168-3659(95)00164-6

157. Krishnamoorthy K, Mahalingam M. Selection of a Suitable Method for the Preparation of Polymeric Nanoparticles: Multi-Criteria Decision Making Approach. *Adv Pharm Bull*. 2015;5(1):57-67. doi:10.5681/apb.2015.008

158. Patil SS, Misra RDK. The significance of macromolecular architecture in governing structure-property relationship for biomaterial applications: an overview. *Mater Technol*. 2018;33(5):364-386. doi:10.1080/10667857.2018.1447266

159. Park KH, Song HC, Na K, Bom HS, Lee KH, Kim S, Kang D, Lee DH. Ionic strength-sensitive pullulan acetate nanoparticles (PAN) for intratumoral administration of radioisotope: Ionic strength-dependent aggregation behavior and 99mTechnetium retention property. *Colloids Surf B Biointerfaces*. 2007;59(1):16-23. doi:10.1016/j.colsurfb.2007.04.010

160. Akagi T, Kaneko T, Kida T, Akashi M. Preparation and characterization of biodegradable nanoparticles based on poly(γ-glutamic acid) with l-phenylalanine as a protein carrier. *J Controlled Release*. 2005;108(2):226-236. doi:10.1016/j.jconrel.2005.08.003

161. Egli S, Schlaad H, Bruns N, Meier W. Functionalization of Block Copolymer Vesicle Surfaces. *Polymers*. 2011;3(1):252-280. doi:10.3390/polym3010252

162. Jain A, Cheng K. The principles and applications of avidin-based nanoparticles in drug delivery and diagnosis. *J Controlled Release*. 2017;245:27-40. doi:10.1016/j.jconrel.2016.11.016

163. González M, Argaraña CE, Fidelio GD. Extremely high thermal stability of streptavidin and avidin upon biotin binding. *Biomol Eng*. 1999;16(1):67-72. doi:10.1016/S1050-3862(99)00041-8

164. Sumbria RK, Boado RJ, Pardridge WM. Imaging Amyloid Plaque in Alzheimer's Disease Brain with a Biotinylated Aβ Peptide Radiopharmaceutical Conjugated to an IgG-Avidin Fusion Protein. *Bioconjug Chem*. 2012;23(6):1318-1321. doi:10.1021/bc3001744

165. Hermanson GT. Chapter 4 - Zero-Length Crosslinkers. In: Hermanson GT, ed. *Bioconjugate Techniques (Third Edition)*. Academic Press; 2013:259-273. doi:10.1016/B978-0-12-382239-0.00004-2

166. Mehta TA, Shah N, Parekh K, Dhas N, Patel JK. Surface-Modified PLGA Nanoparticles for Targeted Drug Delivery to Neurons. In: Pathak YV, ed. *Surface Modification of Nanoparticles for Targeted Drug Delivery*. Springer International Publishing; 2019:33-71. doi:10.1007/978-3-030-06115-9_3

167. Khashayar P, Amoabediny G, Larijani B, Hosseini M, Vanfleteren J. Fabrication and Verification of Conjugated AuNP-Antibody Nanoprobe for Sensitivity Improvement in Electrochemical Biosensors. *Sci Rep*. 2017;7(1):16070. doi:10.1038/s41598-017-12677-w

168. Nakajima N, Ikada Y. Mechanism of Amide Formation by Carbodiimide for Bioconjugation in Aqueous Media. *Bioconjug Chem*. 1995;6(1):123-130. doi:10.1021/bc00031a015

169. Madison SA, Carnali JO. pH Optimization of Amidation via Carbodiimides. *Ind Eng Chem Res*. 2013;52(38):13547-13555. doi:10.1021/ie401724m

170. Sheehan JC, Hess GP. A New Method of Forming Peptide Bonds. *J Am Chem Soc*. 1955;77(4):1067-1068. doi:10.1021/ja01609a099

171. Locatelli E, Comes Franchini M. Biodegradable PLGA-b-PEG polymeric nanoparticles: synthesis, properties, and nanomedical applications as drug delivery system. *J Nanoparticle Res*. 2012;14(12):1316. doi:10.1007/s11051-012-1316-4

172. Joseph A, Nyambura CW, Bondurant D, Corry K, Beebout D, Wood TR, Pfaendtner J, Nance E. Formulation and Efficacy of Catalase-Loaded Nanoparticles for the Treatment of Neonatal Hypoxic-Ischemic Encephalopathy. *Pharmaceutics*. 2021;13(8):1131. doi:10.3390/pharmaceutics13081131

173. Nance E, Timbie K, Miller GW, Song J, Louttit C, Klibanov AL, Shih TY, Swaminathan G, Tamargo RJ, Woodworth GF, Hanes J, Price RJ. Noninvasive delivery of stealth, brain-penetrating nanoparticles across the blood-brain barrier using MRI-guided focused ultrasound. *J Control Release Off J Control Release Soc*. 2014;189:123-132. doi:10.1016/j.jconrel.2014.06.031

174. Das A, Gupta NV, Gowda DV, Bhosale RR. A Review on pH -Sensitive Polymeric Nanoparticles for Cancer Therapy. *Int J ChemTech Res*. Published online 2017:14.

175. Liu D, Yang F, Xiong F, Gu N. The Smart Drug Delivery System and Its Clinical Potential. *Theranostics*. 2016;6(9):1306-1323. doi:10.7150/thno.14858

176. Cooper GM. Lysosomes. *Cell Mol Approach 2nd Ed*. Published online 2000. Accessed August 20, 2021. https://www.ncbi.nlm.nih.gov/books/NBK9953/

177. Mei T, Kim A, Vong LB, Marushima A, Puentes S, Matsumaru Y, Matsumura A, Nagasaki Y. Encapsulation of tissue plasminogen activator in pH-sensitive self-assembled antioxidant nanoparticles for ischemic stroke treatment – Synergistic effect of thrombolysis and antioxidant –. *Biomaterials*. 2019;215:119209. doi:10.1016/j.biomaterials.2019.05.020

178. M. Tóth O, Menyhárt Á, Frank R, Hantosi D, Farkas E, Bari F. Tissue Acidosis Associated with Ischemic Stroke to Guide Neuroprotective Drug Delivery. *Biology*. 2020;9(12). doi:10.3390/biology9120460

179. Rao JU, Coman D, Walsh JJ, Ali MM, Huang Y, Hyder F. Temozolomide arrests glioma growth and normalizes intratumoral extracellular pH. *Sci Rep*. 2017;7(1):7865. doi:10.1038/s41598-017-07609-7

180. Zhao Y, Ren W, Zhong T, Zhang S, Huang D, Guo Y, Yao X, Wang C, Zhang WQ, Zhang X, Zhang Q. Tumor-specific pH-responsive peptide-modified pH-sensitive liposomes containing doxorubicin for enhancing glioma targeting and anti-tumor activity. *J Controlled Release*. 2016;222:56-66. doi:10.1016/j.jconrel.2015.12.006

181. Gao GH, Park MJ, Li Y, Im GH, Kim JH, Kim HN, Lee JW, Jeon P, Bang OY, Lee JH, Lee DS. The use of pH-sensitive positively charged polymeric micelles for protein delivery. *Biomaterials*. 2012;33(35):9157-9164. doi:10.1016/j.biomaterials.2012.09.016

182. Gulfam M, Sahle FF, Lowe TL. Design strategies for chemical-stimuli-responsive programmable nanotherapeutics. *Drug Discov Today*. 2019;24(1):129-147. doi:10.1016/j.drudis.2018.09.019

183. Wen HY, Dong HQ, Xie W juan, Li YY, Wang K, M. Pauletti G, Shi DL. Rapidly disassembling nanomicelles with disulfide-linked PEG shells for glutathione-mediated intracellular drug delivery. *Chem Commun*. 2011;47(12):3550-3552. doi:10.1039/C0CC04983B

184. Olmez I, Ozyurt H. Reactive oxygen species and ischemic cerebrovascular disease. *Neurochem Int*. 2012;60(2):208-212. doi:10.1016/j.neuint.2011.11.009

185. Lu Y, Guo Z, Zhang Y, Li C, Zhang Y, Guo Q, Chen Q, Chen X, He X, Liu L, Ruan C, Sun T, Ji B, Lu W, Jiang C. Microenvironment Remodeling Micelles for Alzheimer's Disease Therapy by Early Modulation of Activated Microglia. *Adv Sci*. 2019;6(4):1801586. doi:https://doi.org/10.1002/advs.201801586

186. He L, He T, Farrar S, Ji L, Liu T, Ma X. Antioxidants Maintain Cellular Redox Homeostasis by Elimination of Reactive Oxygen Species. *Cell Physiol Biochem*. 2017;44(2):532-553. doi:10.1159/000485089

187. Tönnies E, Trushina E. Oxidative Stress, Synaptic Dysfunction, and Alzheimer's Disease. *J Alzheimers Dis*. 57(4):1105-1121. doi:10.3233/JAD-161088

188. Markoutsa E, Xu P. Redox potential sensitive N-acetyl cysteine-prodrug nanoparticles inhibit the activation of microglia and improve neuronal survival. *Mol Pharm*. 2017;14(5):1591-1600. doi:10.1021/acs.molpharmaceut.6b01028

189. Smith ES, Porterfield JE, Kannan RM. Leveraging the interplay of nanotechnology and neuroscience: Designing new avenues for treating central nervous system disorders. *Adv Drug Deliv Rev*. 2019;148:181-203. doi:10.1016/j.addr.2019.02.009

190. Nemeth CL, Drummond GT, Mishra MK, Zhang F, Carr P, Garcia MS, Doman S, Fatemi A, Johnston MV, Kannan RM, Kannan S, Wilson MA. Uptake of dendrimer-drug by different cell types in the hippocampus after hypoxic–ischemic insult in neonatal mice: Effects of injury, microglial activation and hypothermia. *Nanomedicine Nanotechnol Biol Med*. 2017;13(7):2359-2369. doi:10.1016/j.nano.2017.06.014

191. Iezzi R, Guru BR, Glybina IV, Mishra MK, Kennedy A, Kannan RM. Dendrimer-based targeted intravitreal therapy for sustained attenuation of neuroinflammation in retinal degeneration. *Biomaterials*. 2012;33(3):979-988. doi:10.1016/j.biomaterials.2011.10.010

192. Nance E, Kambhampati SP, Smith ES, Zhang Z, Zhang F, Singh S, Johnston MV, Kannan RM, Blue ME, Kannan S. Dendrimer-mediated delivery of N-acetyl cysteine to microglia in a mouse model of Rett syndrome. *J Neuroinflammation*. 2017;14(1):252. doi:10.1186/s12974-017-1004-5

193. Biswal MR, Prentice HM, Blanks JC. Hypoxia Responsive Vectors Targeting Astrocytes in Glioma. *Nov Ther Concepts Target Glioma*. Published online April 4, 2012. doi:10.5772/24711

194. Wang Y, Shang W, Niu M, Tian J, Xu K. Hypoxia-active nanoparticles used in tumor theranostic. *Int J Nanomedicine*. 2019;14:3705-3722. doi:10.2147/IJN.S196959

195. Deng Y, Yuan H, Yuan W. Hypoxia-responsive micelles self-assembled from amphiphilic block copolymers for the controlled release of anticancer drugs. *J Mater Chem B*. 2019;7(2):286-295. doi:10.1039/C8TB02505C

196. Son S, Rao NV, Ko H, Shin S, Jeon J, Han HS, Nguyen VQ, Thambi T, Suh YD, Park JH. Carboxymethyl dextran-based hypoxia-responsive nanoparticles for doxorubicin delivery. *Int J Biol Macromol*. 2018;110:399-405. doi:10.1016/j.ijbiomac.2017.11.048

197. Guo X, Deng G, Liu J, Zou P, Du F, Liu F, Chen AT, Hu R, Li M, Zhang S, Tang Z, Han L, Liu J, Sheth KN, Chen Q, Gou X, Zhou J. Thrombin-Responsive, Brain-Targeting Nanoparticles for Improved Stroke Therapy. *ACS Nano*. 2018;12(8):8723-8732. doi:10.1021/acsnano.8b04787

198. Gao H, Zhang S, Cao S, Yang Z, Pang Z, Jiang X. Angiopep-2 and Activatable Cell-Penetrating Peptide Dual-Functionalized Nanoparticles for Systemic Glioma-Targeting Delivery. *Mol Pharm*. 2014;11(8):2755-2763. doi:10.1021/mp500113p

199. Chung EJ, Leon L, Rinaldi C, eds. Front Matter. In: *Nanoparticles for Biomedical Applications*. Micro and Nano Technologies. Elsevier; 2020:iii. doi:10.1016/B978-0-12-816662-8.01001-8

200. Tahir N, Madni A, Correia A, Rehman M, Balasubramanian V, Khan MM, Santos HA. Lipid-polymer hybrid nanoparticles for controlled delivery of hydrophilic and lipophilic doxorubicin for breast cancer therapy. *Int J Nanomedicine*. 2019;14:4961-4974. doi:10.2147/IJN.S209325

201. Escárcega-González CE, Garza-Cervantes JA, Vázquez-Rodríguez A, Montelongo-Peralta LZ, Treviño-González MT, Díaz Barriga Castro E, Saucedo-Salazar EM, Chávez Morales RM, Regalado Soto DI, Treviño González FM, Carrazco Rosales JL, Cruz RV, Morones-Ramírez JR. In vivo antimicrobial activity of silver nanoparticles produced via a green chemistry synthesis using Acacia rigidula as a reducing and capping agent. *Int J Nanomedicine*. 2018;13:2349-2363. doi:10.2147/IJN.S160605

202. Ishihama H, Ishii K, Nagai S, Kakinuma H, Sasaki A, Yoshioka K, Kuramoto T, Shiono Y, Funao H, Isogai N, Tsuji T, Okada Y, Koyasu S, Toyama Y, Nakamura M, Aizawa M, Matsumoto M. An antibacterial coated polymer prevents biofilm formation and implant-associated infection. *Sci Rep*. 2021;11(1):3602. doi:10.1038/s41598-021-82992-w

203. Fish MB, Fromen CA, Lopez-Cazares G, Golinski AW, Scott TF, Adili R, Holinstat M, Eniola-Adefeso O. Exploring Deformable Particles in Vascular-Targeted Drug Delivery: Softer is Only Sometimes Better. *Biomaterials*. 2017;124:169. doi:10.1016/j.biomaterials.2017.02.002

204. Safari H, Adili R, Holinstat M, Eniola-Adefeso O. Modified two-step emulsion solvent evaporation technique for fabricating biodegradable rod-shaped particles in the submicron size range. *J Colloid Interface Sci*. 2018;518:174-183. doi:10.1016/j.jcis.2018.02.030

205. Tarudji AW, Gee CC, Romereim SM, Convertine AJ, Kievit FM. Antioxidant thioether core-crosslinked nanoparticles prevent the bilateral spread of secondary injury to protect spatial learning and memory in a controlled cortical impact mouse model of traumatic brain injury. *Biomaterials*. 2021;272:120766. doi:10.1016/j.biomaterials.2021.120766

Chapter 4

Design of an Antioxidant Polymeric Nano-drug Delivery System for Ischemic Stroke Treatment

4.1 Introduction

Nanoparticles (NPs), with a size of 10-1000nm, has noticeable advantages over microparticles counterpart for delivering drugs for the ischemic treatment [1]. Ischemic stroke is a leading cause of adult death and disability worldwide, and every 3.5 minutes, someone in the United States dies from a stroke [2]. The nano size of these drug delivery system makes it suitable for intravenous delivery, which is more patient-friendly and easier than direct injection of microparticles counterpart to the brain, and could minimize invasiveness for stroke patients who already suffer from compromised brain function. The major challenges for delivering the drug to the brain via the intravenous (i.v.) route is the existence of the BBB and lack of tissue specificity. The nano-scale drug delivery system could overcome those challenges since it' high surface-area-to-volumes ratio give it ability to be engineered with functional moieties to impart the properties of crossing the BBB and targeting to the ischemic tissue [3].

In this work, we are using an antioxidant NAC prodrug, BDP-NAC, to developing antioxidant PLGA NPs via a simple, quick, and economical nanoprecipitation technique. The particle size is inversely correlated with the BBB penetration efficiency, and the target sizes for these PLGA BDP-NAC NPs after surface modifications with targeting moieties are below ~200nm to effectively cross the BBB [4]. Zeta potential determines the stability of the NP in aqueous suspension. The target zeta potentials for those NPs are between -1mV and -40mV to avoid quick MPS uptake, serum protein aggregation and BBB disruption [4,5]. However, during lyophilization, stresses that are produced during freezing and drying stages could damage the NP structure, and the size preservation after lyophilization becomes a frequent issue that compromises the NP quality [6,7]. Sucrose is a cryo/lyoprotectant that could protect the NPs during both freezing and drying stages [6–9]. In this work, we are using sucrose to preserve the sizes and quality.

4.2 Materials and methods

4.2.1 PLGA nanoparticles fabrication

First, PLGA was dissolved in acetone at a desired concentration (eg. 5mg PLGA/ml acetone). For PLAG BDP-NAC NPs **(Figure 4-1)**, 10wt % BDP-NAC was added to PLGA/acetone solution, and then vortexed to mix the cargo well. 1ml PLGA/BDP/acetone solution was transferred dropwise with a gel-loading pipette tip to 3ml DI water which is stirring at 800rpm. After 2 hours of solvent evaporation, NPs was washed by centrifuging in 10kDa MWCO filters at 4000 rpm for 30 mins. The wash step was repeated again with ~3ml of DI water. For PLGA empty MPs, no BDP-NAC was added into the PLGA/acetone solution. To obtain a higher mass product of NPs, the process could be upscaled. The NPs were collected with DI water and lyophilized for three days. The lyophilized NPs were stored at -20°C.

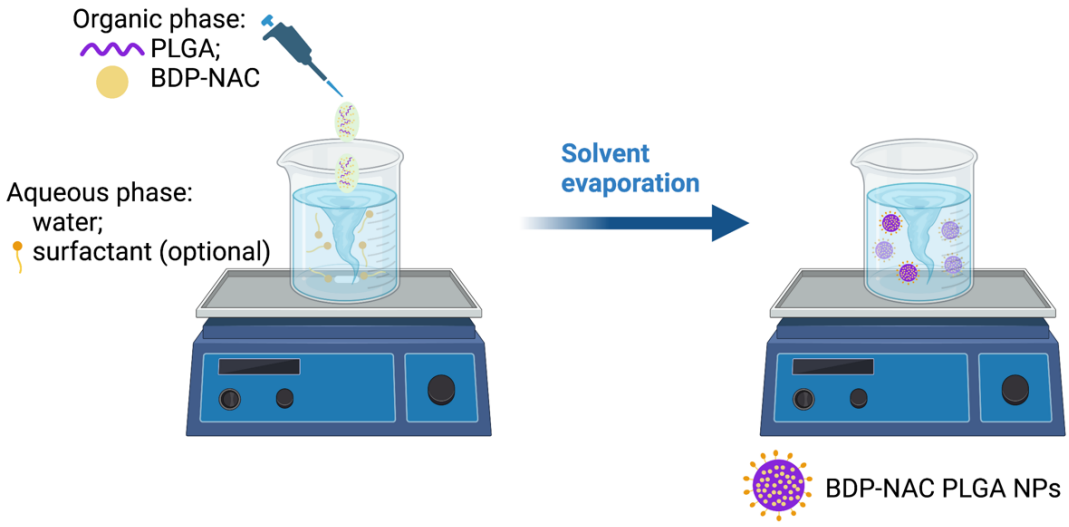

Figure 4-1. Schematic of BDP-NAC PLGA NPs fabrication via nanoprecipitation method. Figure is not drawn to scale. Created with BioRender.com.

4.2.2 Size and zeta potential measurement for PLGA nanoparticles

Size distribution and zeta potential of PLGA NPs were measured on a Zetasizer Nano ZSP or Zetasizer Ultra. Samples were measured in DI water (without buffers) at a concentration of 0.2mg/ml. The temperatures were set at 25 °C for the measurements. The dispersant refractive index and the viscosity for the measurements were set at 1.33 and 0.8872cp, respectively.

4.2.3 PLGA nanoparticles sizes preservation study

Desired amount of sucrose (e.g. 2 w/v% of sucrose/ml NPs suspension) was added to the NPs suspension before lyophilization. Size distribution of PLGA NPs were measured on a Zetasizer Ultra after adding the sucrose and before lyophilization (S_i). After lyophilization, reconstitute the lyophilized NPs with DI water at 0.2mg/ml. Measure the size distribution again (S_f). The ratio of S_f to S_i (S_f/S_i) characterizes how efficiently the sucrose persevering the size during lyophilization. Measure the size distribution again (S_f). The ratio of S_f to S_i (S_f/S_i) characterizes how efficiently the sucrose persevering the size during lyophilization.

4.2.4 Statistical analysis

All errors bars are the standard error of the mean. The statistical significance between two conditions was determined by the unpaired, two-tailed t-test. The statistical significance among more than two groups was determined by one-way ANOVA test.

4.3 Results and Discussion

4.3.1 Factors that impact PLGA NPs sizes

Several factors that could impact PLGA NPs sizes, such as drug, stabilizer type, stabilizer concentration, aqueous to organic phase ratio, stirring rate, and PLGA concentration, were tested. In this work, we only apply the statistical tests to the sizes, not zeta potentials, because the target range of the zeta potentials (-1mV and -40mV) is wide that all the zeta potentials in **Figure 4-2 to Figure 4-6** are in this target range. All the NPs in **Figure 4-2 to Figure 4-5** were made with 50:50 0.59 inherent viscosity (IV) PLGA in a concentration of 8mg PLGA/ml acetone (8mg/ml). Higher IV correlates with higher molecular weight of the polymer.

The average sizes and average zeta potentials for 8mg/ml 50:50 0.59IV without and with BDP-NAC are shown in **Figure 4-2**. No stabilizer was added for the NPs in **Figure 4-2**. For the NPs without the BDP-NAC (empty NPs), the average size is 100.6 +/- 0.2 nm and for the NPs with BDP-NAC, the average size is 154.6 +/- 0.7 nm. Thus, encapsulating BDP-NAC will increase the size at a significance level of 0.01 and there was ~50% increase in size when encapsulating with BDP-NAC. The zeta potentials of empty NPs and BDP-NAC NPs are -30.2 +/- 0.3 mV and -27.3 +/- 0.5 mV, respectively, which meet the target zeta potentials criteria.

(A) (B)

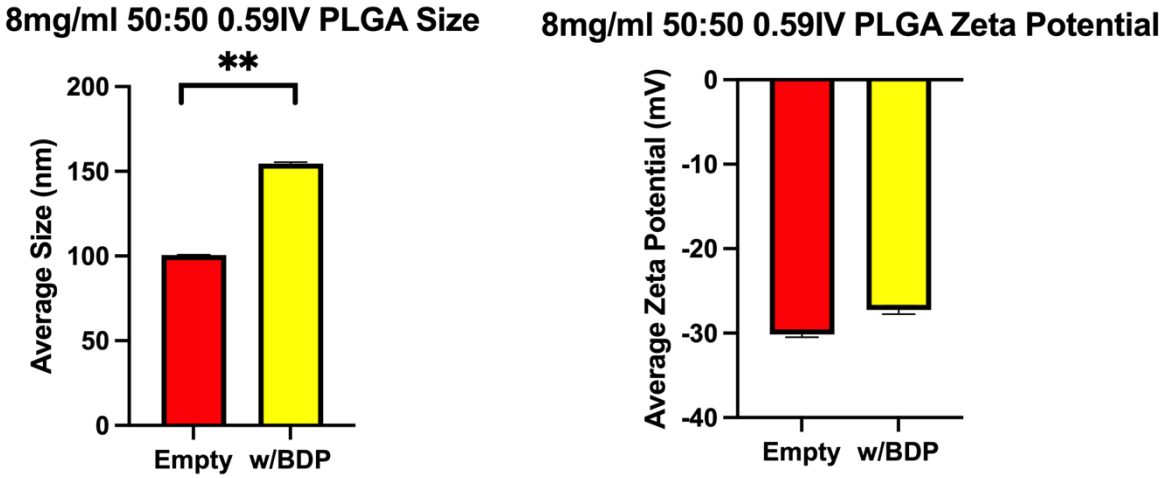

Figure 4-2. Drug effect on PLGA NPs size. (A) Average sizes of PLGA NPs without and with BDP-NAC. **(B)** Average zeta potentials of PLGA NPs without and with BDP-NAC. ** represents $p<0.01$ between two conditions from unpaired, two-tailed t-test

Figure 4-3 shows the NPs sizes and zeta potentials with two different stabilizers and varied stabilizer concentrations. Two stabilizers, polyoxyethylene-polyoxypropylene block copolymer (PF68) and poly(vinyl alcohol) (PVA) were tested in this work. The average sizes for 0% PF68, 0.1% PF68, 0.5% PF68 and 1% PF68 are 154.6 +/- 0.7 nm, 168.3 +/- 0.3 nm, 170.4 +/- 0.8 nm and 180.5 +/- 0.8 nm, respectively. The average sizes are 154.6 +/- 0.7 nm, 192.9 +/- 0.5 nm, 210.7 +/- 0.8 nm and 219.7 +/- 0.7 nm for 0% PVA, 0.1% PVA, 0.5% PVA and 1% PVA, respectively. The p values from one-way ANOVA test for both factors, PF68 concentration and PVA concentration, on NPs size are <0.0001, which means increasing PF68 or PVA concentrations will increase the size at a significance level of 0.0001. However, for the same stabilizer concentration, fabricating with PVA will produce a larger NP size than with PF68 at a significance level of 0.01. Thus, to decrease the size of PLGA NPs that's suitable for delivering the drug to the brain, PF68 with lower concentration will be used (but the concentration may not be too low since it may lose the stability effect). Since the increase in sizes from 0.1% PF68 to 0.5% PF68 condition is very limited, 0.5% PF68 will be selected for the NPs in **Figure 4-6** and **Figure 4-7** to make sure the stabilizer concentration is in the effective working range. The average zeta potentials for 0% PF68 (0% PVA), 0.1% PF68, 0.5% PF68, 1% PF68, 0.1% PVA, 0.5% PVA and 1% PVA are -27.3 +/- 0.5 mV, -33.0 +/- 0.3 mV, -32.3 +/- 0.2

mV, -30.7 +/- 0.1 mV, -23.1 +/- 0.3 mV, -21.6 +/- 0.4 mV and -21.5 +/- 0.1 mV, respectively, which are all in the target zeta potential range.

(A) (B)

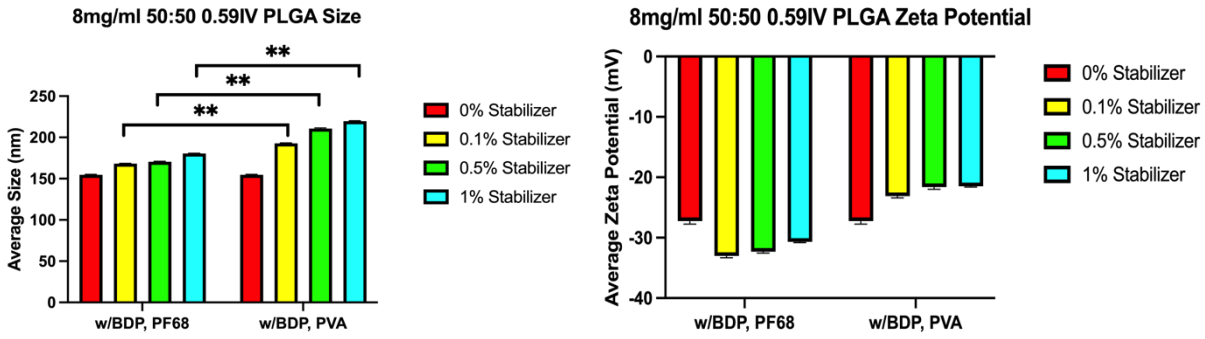

Figure 4-3. The effects of stabilizer type and stabilizer concentration on PLGA NPs sizes. **(A)** Average sizes of BDP-NAC PLGA NPs with PF68 and PVA with varied stabilizers concentrations. **(B)** Average zeta potentials of BDP-NAC PLGA NPs with PF68 and PVA with varied stabilizers concentrations. ** represents $p<0.01$ between two conditions from unpaired, two-tailed t-test

In this work, we also tested the effects of stirring rate and aqueous to organic phase volume ratio on the NPs sizes **(Figure 4-4 and Figure 4-5)**. In **Figure 4-4**, the average size for BDP-NAC PLGA NPs with a stirring rate of 800rpm during fabrication is 154.6 +/- 0.7 nm and the average size with increased rpm (1200rpm) is 154.6 +/- 0.5 nm. Thus, there is no statistically significant difference between 800rpm and 1200rpm BDP-NAC PLGA NPs, which means 800rpm stirring rate is high enough for NPs fabrication process. The average zeta potentials of 800rpm BDP-NAC PLGA NPs (27.3 +/- 0.5 mV) and 1200rpm BDP-NAC PLGA NPs (-26.7 +/- 0.3 mV) are both in target zeta potential range.

For BDP-NAC PLGA NPs in **Figure 4-5**, the average sizes are 204.9 +/- 0.5 nm, 202.6 +/- 0.5 nm and 209.6 +/- 0.5 nm for 4:1 aqueous: organic ratio, 3:1 aqueous: organic ratio and 2:1 aqueous: organic ratio, respectively. Although there are differences in sizes between different aqueous to organic volume ratio at a significance level of 0.01, the effect of aqueous to organic volume ratio on NP size is limited. Furthermore, the average size for 3:1 aqueous: organic ratio BDP-NAC PLGA NPs is smallest, we will keep the 3:1 aqueous to organic volume ratio for the NP fabrication. The average zeta potentials of BDP-NAC PLGA NPs with 4:1 aqueous: organic

ratio (-20.4 +/- 0.2 mV), 3:1 aqueous: organic ratio (-16.9 +/- 0.1 mV) and 2:1 aqueous: organic ratio (-24.0 +/- 0.2 mV) are all in the target range of zeta potential.

(A) (B)

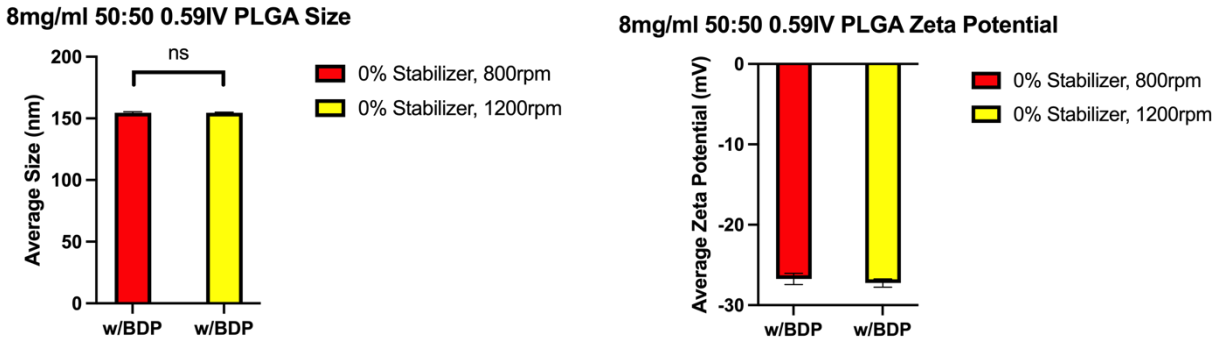

Figure 4-4. The effect of stirring rate on PLGA NPs size. (A) Average sizes of BDP-NAC PLGA NPs with 800rpm and 1200rpm stirring rates during fabrication. **(B)** Average zeta potentials of BDP-NAC PLGA NPs with 800rpm and 1200rpm stirring rates during fabrication. ns represents there is not a statistically significant difference between the two conditions from unpaired, two-tailed t-test

(A) (B)

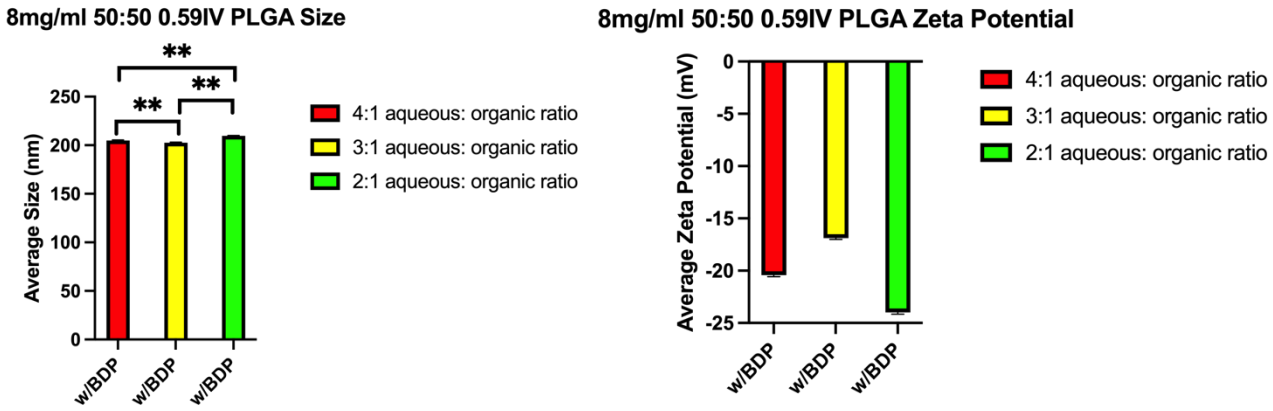

Figure 4-5. The effect of aqueous to organic ratio on PLGA NPs size. (A) Average sizes of BDP-NAC PLGA NPs with varied aqueous to organic volume ratio. **(B)** Average zeta potentials of BDP-NAC PLGA NPs with varied aqueous to organic volume ratio. ** represents $p<0.01$ between two conditions from unpaired, two-tailed t-test

Increasing the molecular weight of PLGA increases the viscosity of the organic phase, which is prone to produce larger NPs. Thus, we selected the PLGA with a low IV (Polymer IV is positively related to polymer molecular weight), 0.20IV, for studying the effect of PLGA

concentration (in acetone) on NPs size while controlling the NP size. From **Figure 4-6**, decreasing the PLGA concentration decreases the NPs size in a linear fashion. The smallest untargeted BDP-NAC loaded PLGA NPs fabricated were 106.5 +/- 0.4 nm using 50:50 0.20IV with a PLGA concentration of 1.5mg/ml. This small size provides the potential to further modify the NP surface to give targeting functionality. The average sizes for 6mg/ml, 4mg/ml, 3mg/ml and 2mg/ml are 158.3 +/- 0.8 nm, 138.1 +/- 0.3 nm, 128.3 +/- 0.2 nm and 117.1 +/- 0.4 nm, respectively. The average zeta potentials of BDP-NAC in **Figure 4-6** with 6mg/ml (-34.3 +/- 0.2 mV), 4mg/ml (-30.0 +/- 0.3 mV), 3mg/ml (-33.6 +/- 0.4 mV), 2mg/ml (-29.9 +/- 0.5 mV) and 1.5mg/ml (-33.1 +/- 0.3 mV) all met the zeta potential requirements.

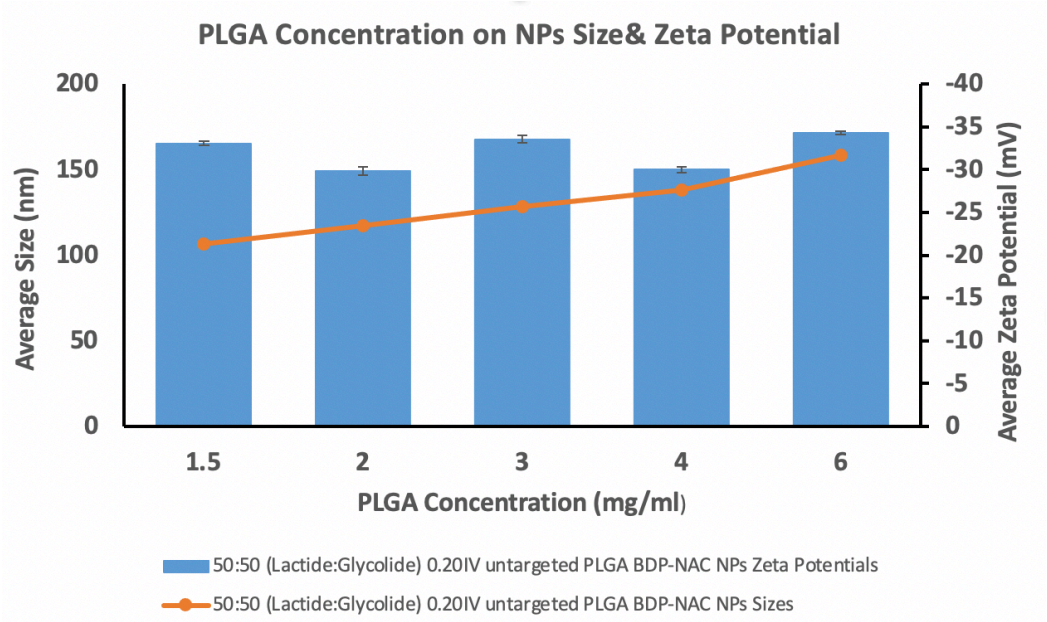

Figure 4-6. The effect of PLGA concentration on PLGA NPs size.

Figure 4-7 shows the stabilities of the NPs in **Figure 4-6** in DI water in 37°C water bath. All the BDP-NAC PLGA NPs except the 4mg/ml NPs could be stabilized in DI water for up to or over a week. The 4mg/ml BDP-NAC PLGA NPs were stabilized until 5 days, but from 5-day to 7-day data points, the average size increased from 139.0 +/- 0.4 nm to 156.0 +/- 2.7 nm. This may be due to the batch-to-batch variabilities. Thus, the stability test of NP needs to be done before further modifications.

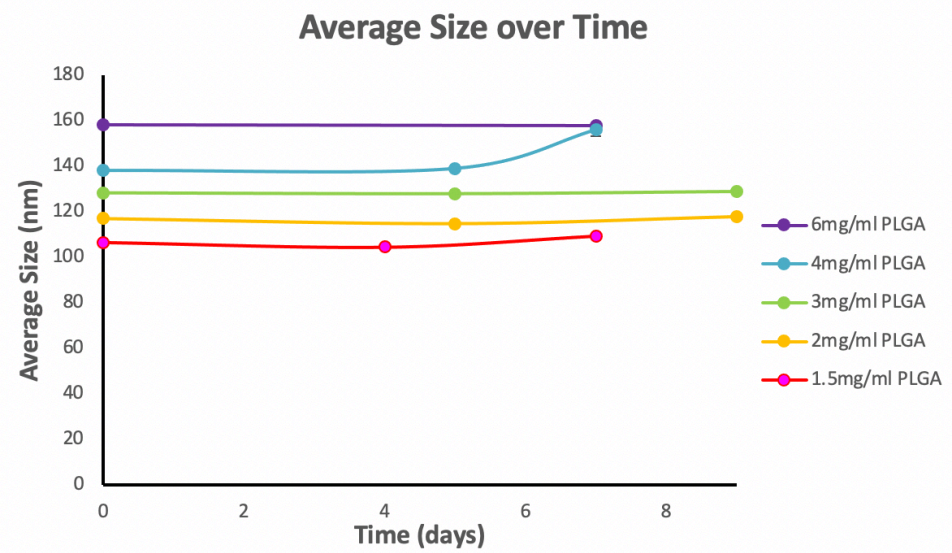

Figure 4-7. The stability tests of the BDP-NAC PLGA NPs with varied PLGA concentration.

4.3.2 Adding sucrose for persevering the NP size after lyophilization

	0 w/v% sucrose	1 w/v% sucrose	2 w/v% sucrose	5 w/v% sucrose	10 w/v% sucrose
Size before lyophilization (nm)	96.91 +/- 0.45	98.43 +/- 0.67	101.0 +/- 0.2	93.52 +/- 0.10	98.92 +/- 0.42
Size after lyophilization (nm)	124.6 +/- 0.5	121.4 +/- 1.1	108.6 +/- 0.5	99.49 +/- 0.30	103.7 +/- 0.6
S_f/S_i	**1.285**	**1.233**	**1.075**	**1.064**	**1.048**

Table 4-1. The size preservation effect of sucrose on 5mg/ml 50:50 0.66IV PLGA empty NPs.

From **Table 4-1**, for the empty NPs without adding sucrose, the size changed from 96.91 +/- 0.45 nm to 124.6 +/- 0.5 nm and the ratio of the size after lyophilization to the size before lyophilization (S_f/S_i) is 1.285. The ideal value for the S_f/S_i is close to 1. Adding the sucrose with a concentration equal to or higher than 2 w/v% before lyophilization could perverse the size effectively. However, from experimental practices, adding sucrose with a high concentration

could result in a collapsed cake, which is generally not acceptable. Thus, there is a trade-off between size preservation effect and avoiding collapsed cake when considering the desired concentration of sucrose added to the system. It is worth to noted that the yields of the NPs in **Table 4-1** are >100% (**Table C-1**), which probably due to the excipients added during the fabrication processes.

4.4 Conclusions and Future Work

In this work, we investigated several factors that could affect NP size. Encapsulating the BDP-NAC will increase the size by ~1.5 times of the empty NPs. Adding PVA during the fabrication produces larger NP than adding PF68, and the size is increased with a higher stabilizer concentration for both PVA and PF68 conditions. There is no significant difference between the NPs that have a stirring rate of 800rpm and 1200rpm during fabrication, meaning that 800rpm is suitable for the fabrication. Although there is a size difference with varied aqueous to organic phase volume, the effect of aqueous to organic ratio is limited to the NP size. Decreasing the PLGA concentration could reduce the NP size in a liner manner, and the smallest BDP-NAC PLGA NPs we could get had an average size of 106.5 +/- 0.4 nm, fabricated with 1.5mg/ml 50:50 0.20IV PLGA. All the NPs in **Figure 4-6** except the one with 4mg/ml PLGA concentration passed the one-week (up to or more than 7 days) stability tests. All the NPs in Chapter 4 met the zeta potential requirements of NPs for brain delivery. Adding the sucrose with desired concentration (>= 2 w/v% based on **Table 4-1**) to the system before the lyophilization could protect the NPs from the stresses produced during freeze-drying process.

The future direction of this work is to develop a nano-drug delivery system modifying its surface with two types of targeting ligands, one for penetrating the BBB via receptor-mediated transcytosis and one for delivering specifically to the infarct site by targeting ischemic microenvironment, to rehabilitate the stroke victims. To impart the property of crossing the BBB, NPs will be coated with the surfactant polysorbate 80 **(Figure 4-8)**. Polysorbate 80 can adsorb apolipoprotein E/B, the serum proteins, from the blood, and then bind to the low density lipoprotein receptor (LDLR) that is over-expressed on the BBB. As a result, the polysorbate 80-coated nanoparticles can cross the BBB through LDL receptor-mediated transcytosis [4,10,11]. Since polysorbate 80 is a surfactant, it is easily incorporated onto the NPs to impart the property of

crossing the BBB. Polysorbate 80 will be added into the oil phase during nanoprecipitation to allow it to adsorb onto the surface of PLGA NPs [10].

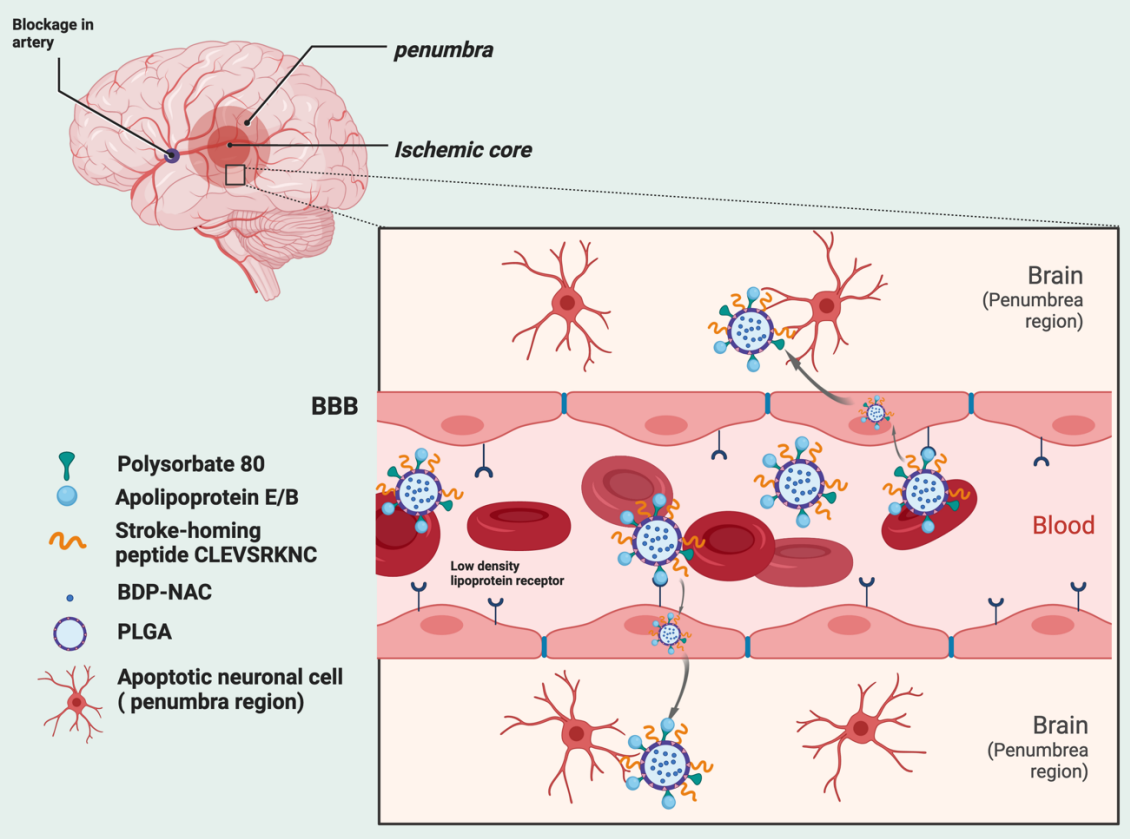

Figure 4-8. Schematic of BDP-NAC PLGA NPs that have been surface modified with two targeting moieties. Created with BioRender.com.

After crossing the BBB, the antioxidants need to be delivered specifically to the infarct site without accumulating in healthy tissue. To reach this goal, we will conjugate a stroke-homing peptide with the sequence of Cys-Leu-Glu-Val-Ser-Arg-Lys-Asn-Cys (CLEVSRKNC) to our antioxidant NPs. CLEVSRKNC has a high binding specificity and affinity to apoptotic neuronal cells at the penumbra region, where the cells are ischemic but still potentially salvageable [12]. The stroke-homing peptide CLEVSRKNC will be conjugated to PLGA NPs through EDC/Sulfo-NHS coupling reaction. EDC is a widely used zero-length crosslinker which can form the amide bond between CLEVSRKNC peptide and the carboxylate group of PLGA without inserting a linking group, and adding the Sulfo-NHS to the coupling reaction increases the solubility and stability of the active immediate that reacts with the primary amine. By incorporating these two types of targeting ligands, one for penetrating the BBB via receptor-mediated transcytosis and one for delivering specifically to the infarct site, this work aims to design a dual-targeted nano-drug delivery system with temporal and spatial control over the release of antioxidant drugs to efficiently and non-invasively treat ischemic stroke.

4.5 Acknowledgements

We gratefully acknowledge financial support from NIH grant R21 EB026723. We thankfully acknowledge Gilberto Hernandez for assisting in performing experiments and collecting data.

4.6 Reference

1. Singh R, Lillard JW. Nanoparticle-based targeted drug delivery. *Exp Mol Pathol*. 2009;86(3):215-223. doi:10.1016/j.yexmp.2008.12.004

2. CDC. Stroke Facts | cdc.gov. Centers for Disease Control and Prevention. Published April 5, 2022. Accessed June 27, 2022. https://www.cdc.gov/stroke/facts.htm

3. Masserini M. Nanoparticles for Brain Drug Delivery. *ISRN Biochem*. 2013;2013:1-18. doi:10.1155/2013/238428

4. Saraiva C, Praça C, Ferreira R, Santos T, Ferreira L, Bernardino L. Nanoparticle-mediated brain drug delivery: Overcoming blood–brain barrier to treat neurodegenerative diseases. *J Controlled Release*. 2016;235:34-47. doi:10.1016/j.jconrel.2016.05.044

5. Bharadwaj VN, Nguyen DT, Kodibagkar VD, Stabenfeldt SE. Nanoparticle-Based Therapeutics for Brain Injury. *Adv Healthc Mater*. 2018;7(1):1700668. doi:10.1002/adhm.201700668

6. Fonte P, Reis S, Sarmento B. Facts and evidences on the lyophilization of polymeric nanoparticles for drug delivery. *J Controlled Release*. 2016;225:75-86. doi:10.1016/j.jconrel.2016.01.034

7. Abdelwahed W, Degobert G, Stainmesse S, Fessi H. Freeze-drying of nanoparticles: Formulation, process and storage considerations. *Adv Drug Deliv Rev*. 2006;58(15):1688-1713. doi:10.1016/j.addr.2006.09.017

8. Kannan V, Balabathula P, Thoma LA, Wood GC. Effect of sucrose as a lyoprotectant on the integrity of paclitaxel-loaded liposomes during lyophilization. *J Liposome Res*. 2015;25(4):270-278. doi:10.3109/08982104.2014.992023

9. Rodrigues JP, Paraguassú-Braga FH, Carvalho L, Abdelhay E, Bouzas LF, Porto LC. Evaluation of trehalose and sucrose as cryoprotectants for hematopoietic stem cells of umbilical cord blood. *Cryobiology*. 2008;56(2):144-151. doi:10.1016/j.cryobiol.2008.01.003

10. Zhao L xia, Liu A chang, Yu S wen, Wang Z xin, Lin X qian, Zhai G xi, Zhang Q zhu. The Permeability of Puerarin Loaded Poly(butylcyanoacrylate) Nanoparticles Coated with Polysorbate 80 on the Blood–Brain Barrier and Its Protective Effect against Cerebral Ischemia/Reperfusion Injury. *Biol Pharm Bull*. 2013;36(8):1263-1270. doi:10.1248/bpb.b12-00769

11. Wohlfart S, Khalansky AS, Gelperina S, Begley D, Kreuter J. Kinetics of transport of doxorubicin bound to nanoparticles across the blood-brain barrier. *J Control Release Off J Control Release Soc*. 2011;154(1):103-107. doi:10.1016/j.jconrel.2011.05.010

12. Hong HY, Choi JS, Kim YJ, Lee HY, Kwak W, Yoo J, Lee JT, Kwon TH, Kim IS, Han HS. Detection of apoptosis in a rat model of focal cerebral ischemia using a homing peptide selected from in vivo phage display. *J Controlled Release*. 2008;131(3):167-172. doi:10.1016/j.jconrel.2008.07.020

Appendix A Chapter 1 supplementary material

1. PLGA BDP-NAC core-shell microparticle fabrication protocol (use 2:1 PLGA:PLLA, 20 wt% PLGA, 900rpm PLGA BDP-NAC MPs in Figure 1-1 as an example)

1. Dissolve 50:50 fluorescent PLGA-FL (Mn 20,000-40,000 Da and 50:50 1.15 IV PLGA in 0.5ml of DCM at a total concentration of 200mg/ml in a glass test tube. The ratio of regular PLGA to fluorescent PLGA-FL is 24:1
2. Dissolve fluorescent PLLA-FPR648 (Mw~40,000Da) and 100:0 1.16 IV PLGA in 0.25ml of DCM at a total concentration of 200mg/ml in another glass test tube. The ratio of regular PLLA to fluorescent PLLA-FPR648 is 24:1
3. Wait the PLGA and PLLA solutions to be fully dissolved
4. Prepare >76.5ml of 0.5% PVA, and stir 75ml of 0.5% PVA in a 400ml beaker at 900rpm with a ~5cm pill-shaped stir bar on a stir plate
5. Add 10wt% BDP-NAC to the PLLA solution, and dissolve the BDP-NAC by sonication
6. Transfer PLGA solution to PLLA/BDP-NAC solution with Pasteur pipette, to form O/O emulsion, sonicate 20 sec twice, with a 10-sec break, on ice at 90% amplitude
7. Slowly add 1.5ml of 0.5% PVA to O/O emulsion along the wall, sonicate 20 sec twice on ice with a 10-sec break at 90% amplitude to form O/O/W emulsion
8. Pour the O/O/W emulsion into the center of 75ml stirring 0.5% PVA solution, wait 4 hours for solvent evaporation
9. Collect the MPs suspension in 50ml conical tubes, centrifuge them for 5 mins at 10000rpm and 4°C to wash the MPs, discard the supernatant
10. Vortex to resuspend the MPs with 40ml DI water, and centrifuge again at 10000rpm and 4°C for 5mins, discard the supernatant
11. Repeat the wash step one more time, and discard the supernatant
12. Add 10ml DI water and vortex to resuspend the MPs
13. For the further usage, freeze the MPs suspension overnight at -80°C, lyophilize the MPs for three days and store the lyophilized MPs at -20°C for long-term storage.

Appendix B Chapter 2 supplementary material

1. PLGA NAC microparticle fabrication protocol (use 50:50 0.55-0.75IV PLGA NAC MPs in Figure 2-1 as an example)

1. Dissolve 50:50 0.55-0.75IV PLGA in 2ml acetone at 150mg PLGA/ml acetone concentration in a glass test tube, wait for it to be fully dissolved
2. Prepare >100ul NAC in DI water at 100mg/ml, 3ml of 3.33% NAC/ml 1% PVA and 75ml of stirring 5% NAC/ml 0.3% PVA solutions
3. Stir the 75ml of stirring 5% NAC/ml 0.3% PVA solution in a 400ml beaker at 300rpm on a stir plate with a ~5cm pill-shaped stir bar
4. Add 100ul NAC/DI water solution to PLGA solution in dropwise, sonicate 10 sec on ice at 90% amplitude twice, with a 10-break in between to form W/O emulsion
5. Slowly add the 3ml of 3.33% NAC/ml 1% PVA solution to the formed W/O emulsion along the wall, sonicate 10 sec on ice twice, with a 10-sec break, at 90% amplitude to for, W/O/W emulsion
6. Pour the W/O/W emulsion into the center of 75ml stirring 5% NAC/ml 0.3% PVA solution, stir 4 hours for solvent evaporation
7. Prepare >60ml of 2.5% NAC/ml DI water for washing steps
8. Collect the MPs in 50ml conical tubes, centrifuge them at 10000rpm for 5 mins at 4°C to wash the MPs, discard the supernatant
9. Add 30ml of 2.5% NAC/ml DI water to resuspend the MPs, and centrifuge again at 10000rpm and 4°C for 5 mins, discard the supernatant
10. Repeat the wash step one more time, and discard the supernatant
11. Add 10ml DI water to resuspend the MPs
12. For long-term storage and further usage, freeze the MPs suspension at -80°C overnight, lyophilize the MPs for three days and store the dry MPs at -20°C

Appendix C Chapter 4 supplementary material

1. PLGA BDP-NAC nanoparticles fabrication protocol (use 1.5mg/ml 50:50 0.20IV PLGA BDP-NAC MPs in Figure 4-6 as an example)

1. Dissolve 50:50 0.20IV PLGA in 10ml acetone at 1.5mg PLGA/ml acetone concentration, wait for it to be fully dissolved
2. Add 1.5mg BDP-NAC to PLGA/acetone solution, mix it well by vertexing
3. Prepare 30ml of 0.5% PF68 in DI water in a 400ml beaker, make sure there is no bubble in it
4. Stir the PF68 solution at a stirring rate of 800rpm with cross-shaped stir bar on a stir plate
5. Transfer 10ml of PLGA/BDP-NAC/acetone solution dropwise with a gel-loading pipette tip to the 30ml stirring PF68 solution
6. Wait 2 hours for solvent evaporation
7. Collect the NPs in 10kDa MWCO filters, centrifuge them at 4000rpm for 30mins to wash the NPs, discard the filtration waste
8. Repeat the wash step with ~10ml of DI water in each 10kDa MWCO filters
9. Collect the NPs in DI water for further analysis

Note: if the NPs is needed for long storage, lyophilize the NPs for three days and store at -20°C

This protocol is developed from Day Lab University of Delaware.

2. Yields of the MPs in Table 4-1

	0 w/v% sucrose	1 w/v% sucrose	2 w/v% sucrose	5 w/v% sucrose	10 w/v% sucrose
Initial mass (mg)	50	90.37	130.05	200.36	350.06
Initial mass (mg)	136.31	179.95	220.30	244.38	390.46
Yield (%)	**272.62**	**199.13**	**169.40**	**121.97**	**111.54**

Table C-1. The 5mg/ml 50:50 0.66IV PLGA empty NPs yields after lyophilization.